# USING GEOLOGIC MAPS AND SEISMIC REFRACTION IN PAVEMENT-DEFLECTION ANALYSIS

*by*

Jeffrey G. Paine

Project Summary Report Number 2990-S

Research Project 7-2990
*Estimating Depth to Bedrock Feasibility Study*

Conducted for the

**TEXAS DEPARTMENT OF TRANSPORTATION**

by the

**BUREAU OF ECONOMIC GEOLOGY**
**and**
**CENTER FOR TRANSPORTATION RESEARCH**
Bureau of Engineering Research
**THE UNIVERSITY OF TEXAS AT AUSTIN**

October 1999

## IMPLEMENTATION RECOMMENDATIONS

1. Create a roadway data base with geologic unit, major rock type, average W7 deflection, and the observed range in W2:W7 deflection ratio as fields. This data base would allow users to enter a highway location and obtain mapped rock type for that location, as well as the expected influence that bedrock type has on Falling-Weight Deflectometer (FWD) deflections. This would give the highway engineer a preliminary check on new FWD data and would provide an approximation of anticipated bedrock rigidity that would aid the deflection-series interpretation.

2. Use existing FWD data to define averages and ranges of FWD response for all mapped geologic units in the state, then use these data in the design and construction of new highway segments. Once a roadway alignment is known, the statistical FWD response for the geologic units mapped along the roadway can be used to suggest bedrock properties, control-test boring locations, and help make highway design decisions.

3. Collect FWD data at closely spaced intervals along roadways over geologic units that are susceptible to sinkhole development or other rapid lateral change in physical properties. W7 deflections should increase and W2:W7 ratios should decrease from a hard limestone substrate to sinkholes where limestone has been removed and voids filled with softer materials.

4. Routinely collect seismic-refraction data along with FWD data. While it is difficult to separate the influences of bedrock rigidity and bedrock depth with FWD data alone, tests with standard and customized seismic-refraction equipment employing an FWD or a small impulsive source show that bedrock depth and rigidity can be estimated from refraction data. These parameters, in turn, will allow better quantitative analysis of deflection series and better assessment of pavement condition.

5. Use available FWD data, or combined FWD–refraction data, to improve geologic maps. This implementation will benefit all users of these maps, including those in transportation, construction, land-use planning, oil and gas exploration, mining, education, and materials exploration. Deflections, bedrock depths, and seismic velocities of bedrock and overburden obtained from a combined FWD–refraction system would allow comparisons of observed values with expected values for mapped rock types, indicate areas where current mapping may need revision, and produce a better understanding of the distribution of geologic units over large areas of the state where surface exposures are limited.

## DISCLAIMERS



Jeffrey G. Paine, Ph.D.
*Research Supervisor*

## ACKNOWLEDGMENTS

The author acknowledges the assistance of Mike Murphy (DES), the Texas Department of Transportation (TxDOT) project director for this study. Other members of the project monitoring committee were D. Chen (DES), S. R. Lambert (DES), and K. Fults (DES). Frank McCullough (Center for Transportation Research) and Mike Murphy provided guidance on the types of geologic information that would be useful in highway design, testing, and performance. James Lee, formerly of TxDOT, arranged access to test sites in Austin and Granite Shoals. TxDOT staff at the Design Division, Pavements Section, provided FWD data and helped modify the FWD for use as a seismic source. Nina Redmond edited the report under the supervision of Susie Doenges. Susan Lloyd did the layout and word processing.

Research performed in cooperation with the Texas Department of Transportation.

## SUMMARY

Geologic maps provide much information about the distribution of rock types at and near the land surface. Deflections of Texas highways measured with the Falling-Weight Deflectometer (FWD) appear to be correlated to bedrock type, particularly at the most distant FWD sensors. To examine this apparent bedrock influence, we compared FWD data with mapped geologic units from six roadway segments in four physiographic regions of Texas. This analysis revealed differences in FWD response among regions that are likely to be related to systematic differences in either bedrock depths or physical properties of geologic units that range from Precambrian to Holocene in age and include many different sedimentary, igneous, and metamorphic rocks. At the W7 detector (6-ft [1.8-m] offset), average normalized deflections are highest for areas where roads are underlain by siliciclastic sedimentary rocks (sandstones, mudstones, and shales) and unconsolidated alluvial sediments. Lowest normalized W7 deflections are measured in areas underlain by Precambrian igneous and metamorphic rocks that include granites, schists, and gneisses and in areas underlain by chemically precipitated sedimentary rocks such as limestone.

Better rock-type discrimination is obtained from ratios calculated from deflections measured at the W2 (1-ft [0.3-m] offset) and W7 detectors than from W7 deflections alone. W2:W7 ratios vary regionally, but observed ratios are highest for rigid rock types such as granites, gneisses, and schists (ratios of 17 to 40), are intermediate for limestones (10 to 27), and are relatively low for sandstones, mudstones, and unconsolidated sediments (6 to 14). These results suggest that (1) existing geologic maps can be used to help analyze FWD sensor response for highway segments, and (2) rock type might be predicted from FWD data, allowing the FWD to be used in such applications as sinkhole detection and geologic mapping.

From FWD data alone, it is difficult to determine whether the relationship between rock type and road deflections is caused by differences in rock properties or bedrock depth. To resolve this ambiguity, we employed the FWD and a modified soil-probe hammer as impulsive sources for seismic-refraction experiments at three test sites in North and Central Texas. These tests, conducted with existing equipment, showed that (1) the FWD can be used as a seismic source for refraction data, but the detectors need to extend farther from the source, (2) refraction data can be acquired with sources and detectors either on road shoulders or directly on pavement, and (3) refraction data can be used to calculate physical properties of fill, soil, and bedrock beneath pavement and to estimate depth to bedrock. The refraction experiments suggest that combined FWD–refraction systems could be used on pavement to aid deflection analysis by

estimating bedrock depth and assist in rock-type identification by measuring compressional velocities for bedrock and overburden.

The success of the refraction experiments in obtaining useful data for pavement analysis led to the design and construction of a refraction system optimized for on-pavement use. This instrument consists of a portable seismic source, a recording array that is shorter, lighter, and has fewer detectors than the previous system, fixed locations for source points and detectors, a foldable series of sections making up the recording array, and a seismograph capable of recording and filtering refraction data, selecting first arrivals, and analyzing refraction data. This instrument was used to acquire refraction data on pavement, select first arrivals, and calculate compressional wave velocities and layer depths.

## TABLE OF CONTENTS

**FIGURES**

**TABLES**

## INTRODUCTION

The purposes of this study are to examine whether (1) existing geologic information can be used to help interpret pavement-deflection data collected with the Texas Department of Transportation's (TxDOT) Falling Weight Deflectometers (FWD's), and (2) seismic-refraction data, perhaps collected in conjunction with FWD data, can be used along with geologic information to estimate bedrock depths and consequently improve FWD analyses. This report summarizes results from a 3-year project, in which we examined the relationship between bedrock type and FWD response, assessed the feasibility of collecting seismic-refraction data on and adjacent to roads, and constructed a seismic-refraction system adapted to pavement use.

Trailer-mounted FWD's consist of a falling weight and a series of seven calibrated detectors at distances of 0, 1, 2, 3, 4, 5, and 6 ft (0, 0.3, 0.6, 0.9, 1.2, 1.5, and 1.8 m) from the falling weight (fig. 1). The height of the weight drop can be selected to produce seismic impulses of varying strength. The vertical detectors, in contact with the pavement as the weight falls, measure pavement deflection following weight impact. The most commonly used FWD data are the maximum deflections at each detector, normalized for drop load. In general, deflections measured close to the source are most affected by pavement condition, and deflections measured at the longest offsets are more affected by deeper layers such as fill, soil, and bedrock (M. Murphy, personal communication, 1997). Physical properties of roadway layers that can be calculated from FWD data also depend on depth to bedrock (depth to "rigid" layer), which is generally not known. Rather than drilling boreholes to measure bedrock depth directly, we wish to determine the precision with which geological and geomorphological information can be used to estimate bedrock depth. We also want to examine whether existing geophysical methods, such as seismic refraction, can be adapted to rapidly and accurately estimate bedrock depths beneath roads.

There is an empirical relationship between rock type and FWD deflections, particularly at the longest offsets. Average W7 deflections (6-ft [1.8-m] source-to-detector distance) calculated by county (fig. 2) resemble a simplified geologic map of the state (fig. 3). The largest W7 deflections are observed along the coast and in the Panhandle, where the geologic units are relatively young; the smallest W7 deflections are observed in Central Texas, where old igneous and metamorphic rocks and younger limestones are mapped. Outcrop trends of individual geologic units match average W7 deflection trends visible over many counties, including (1) the increased average deflections in East Texas on the Miocene Fleming and Oakville Formations and the Pliocene Willis Formation; (2) low deflections on the Cretaceous Trinity, Fredericksburg, and lower Washita Groups in Texas; and (3) increased deflections that follow

the Cretaceous


Figure 1. A Falling-Weight Deflectometer with detectors deployed on pavement.


Figure 2. Average roadway deflection by county measured at Falling-Weight Deflectometer detector W7. Also shown are locations of study areas A though F and refraction test sites R1 (Road D, J. J. Pickle Research Campus), R2 (U.S. Highway 281 near Jacksboro), and R3 (FM 1431 near Granite Shoals).

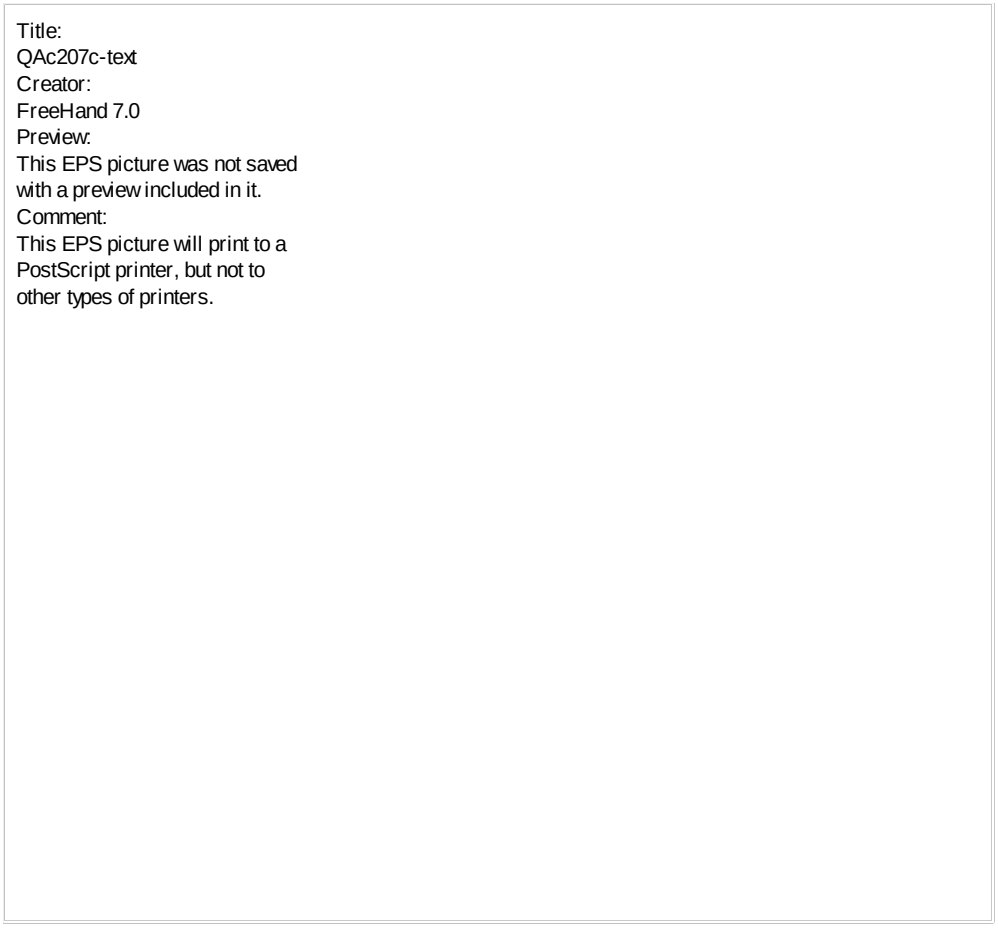


Figure 3. Generalized geologic map of Texas showing outcrop patterns. Adapted from Bureau of Economic Geology (1992).

Austin, Eagle Ford, Woodbine, upper Washita, Navarro, and Taylor Groups in northeast Texas (figs. 2 and 3). Our goals are to determine why this relationship exists, how well it translates to the local scale, and how it might be exploited to both aid pavement-deflection analyses and establish geologic uses of the FWD. We also want to determine whether there is sufficient justification to acquire refraction data along with FWD data.

## PHYSIOGRAPHIC REGIONS AND BEDROCK TYPES

The relationship between far-offset FWD data and geologic units supports the subdivision of Texas into regions that have similar FWD response. Many earth scientists have recognized physiographic regions that reflect differences in elevation, topography, geologic structure, and bedrock types (fig. 4; table 1). These seven principal physiographic regions (Gulf Coastal Plains, Edwards Plateau, Central Texas Uplift, Grand Prairie, Basin and Range, North-Central Plains, and High Plains) provide a framework for grouping rock types that influence FWD response.

Bedrock types differ in each of the seven principal physiographic regions (figs. 3 and 4; table 1). On the Gulf Coastal Plains, unconsolidated and semiconsolidated sands, silts, and clays deposited along rivers and shorelines in the Cenozoic Era (within the last 66 million years [Ma]) form relatively weak highway substrates. Relatively young bedrock is also found in the High Plains, where unconsolidated to moderately cemented eolian (windblown) and alluvial (river-borne) sand and silt formed the Blackwater Draw Formation during the Quaternary Period (less than 2 Ma) and the Ogallala Formation during the Miocene to Pliocene periods (24 to 2 Ma). Limestone and dolomite deposited during the Cretaceous Period (144 to 66 Ma) underlie the Edwards Plateau in Central Texas, forming strong substrates that are resistant to erosion. Sandier, calcareous deposits of similar age underlie the Grand Prairie, the northern extension of the Edwards Plateau. Westward-dipping limestone, sandstone, and shale dating to the late Paleozoic Era (320 to 245 Ma) are found in the North-Central Plains. The oldest rocks in Texas are found in the Central Texas Uplift and the Basin and Range regions. In the Central Texas Uplift, mechanically strong, late Precambrian-era (2,000 to 1,200 Ma) igneous and metamorphic rocks and Paleozoic-era (570 to 245 Ma) sandstone, limestone, and shale crop out. In the Basin and Range, faulting formed a series of basins and ranges. The ranges, cored by strong igneous and metamorphic rocks, are separated by basins that have been filled by younger sedimentary deposits that are generally weaker than the range-forming rocks.

More detailed information on the distribution of geologic units is obtained from geologic maps produced at various scales. The most useful map series for a statewide study is the Geologic Atlas of Texas. This series consists of 38 maps that cover the entire state at a scale of 1:250,000 and have been compiled, published, and updated over the last several decades by the

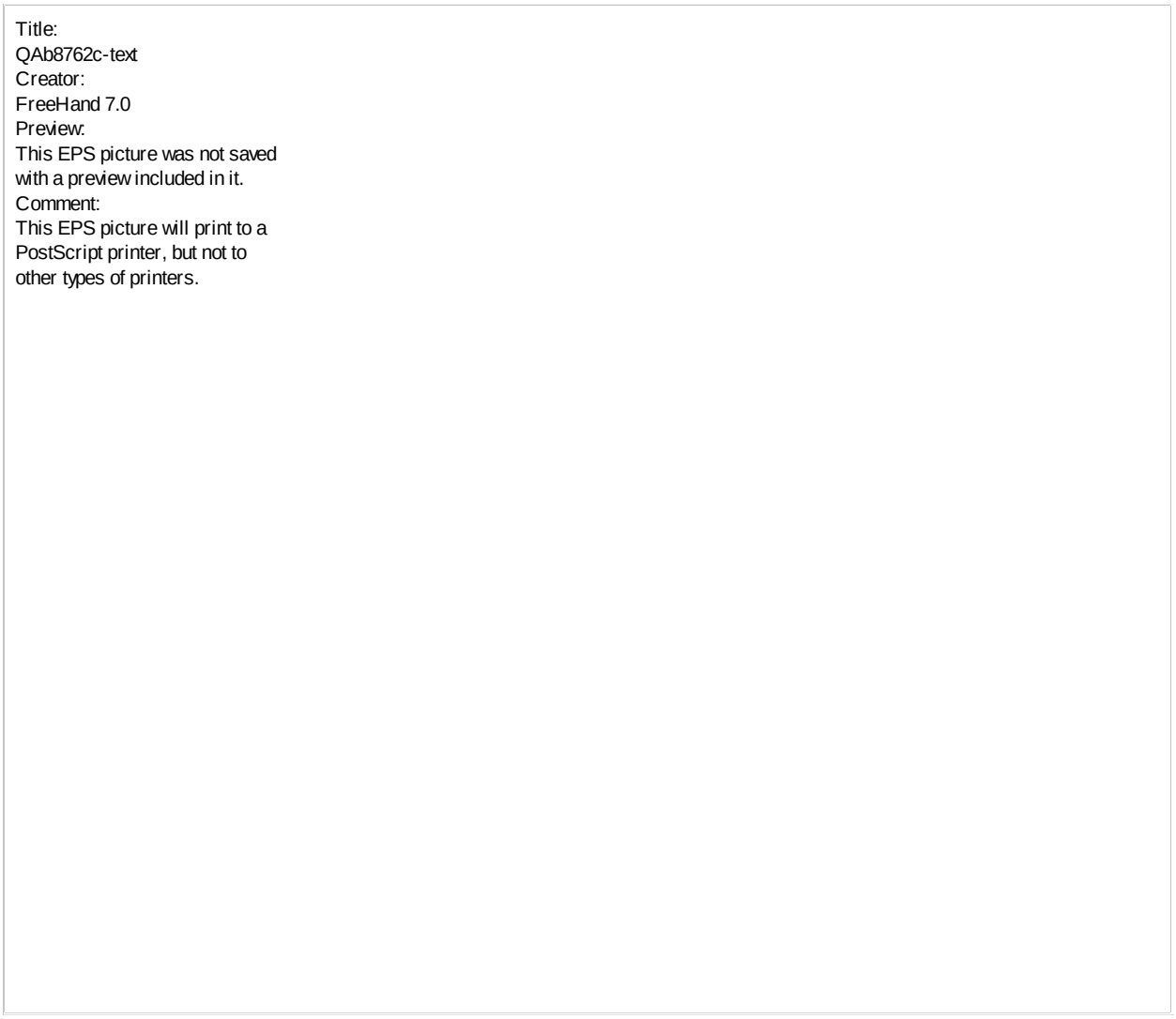


Figure 4. Physiographic regions of Texas. Adapted from Wermund (1996).

Table 1. Principal physiographic regions of Texas. Adapted from Wermund (1996).

| Region | Elevation range | Topography | Geologic structure | Bedrock type |
|---|---|---|---|---|
| Gulf Coastal Plains | 0–100 ft<br>0–30 m | Nearly flat to low rolling terrain | Nearly flat strata | Unconsolidated deltaic sands and muds; chalks and marls |
| Grand Prairie | 450–1,250 ft<br>140–380 m | Plains to low stair-step hills | Eastward dip | Calcareous to sandy |
| Edwards Plateau | 450–3,000 ft<br>140–910 m | Flat upper surface with box canyons | Southward dip | Limestones and dolomites |
| Central Texas Uplift | 800–2,000 ft<br>240–610 m | Knobby plain | Outward dip; faulted | Igneous and metamorphic rocks |
| North-Central Plains | 900–3,000 ft<br>270–910 m | Low north-south ridges | Westward dip | Limestones, sandstones, shales |
| High Plains | 2,200–4,750 ft<br>670–1,450 m | Southeastward-sloping prairies | Gentle southeastward dip | Windblown silt and fine sand |
| Basin and Range | 1,700–8,750 ft<br>520–2,670 m | North-south mountains and basins | Complex folding and faulting | Igneous, metamorphic, and sedimentary rocks |

Bureau of Economic Geology (BEG). Soil surveys, published by the Natural Resources Conservation Service of the U.S. Department of Agriculture, exist for most Texas counties. The information on soil distribution, grain size, soil depth, and surface slope contained in the maps and tables that make up these surveys, more detailed than that shown on geologic maps, may also be useful in the interpretation of FWD data. Soil maps, published at a scale of 1:20,000, show many more units and subdivisions than do most geologic maps but are difficult to place in a statewide or regional context that would lend itself well to FWD analysis.

## INVESTIGATIVE APPROACH

Our approach to understanding the relationship between FWD response and bedrock type and depth was to examine in detail several road segments in different physiographic regions. The six highway segments analyzed are located in the (1) North-Central Plains, (2) Central Texas Uplift, (3) Edwards Plateau, and (4) southern and interior Gulf Coastal Plains. In the first project year, we examined the relationship between existing TxDOT FWD data and mapped geologic units along the highway segments. In year 2, we collected seismic-refraction data on selected roads to investigate the effectiveness of this proven method in directly determining bedrock depths to anticipated maximum depths of about 6 m. In the final year, we acquired additional seismic-refraction data and designed, constructed, and tested a seismic-refraction system specifically for use on pavement.

## METHODS

Methods employed in this study include those that were used to investigate the relationship between existing information on bedrock type and FWD response, and those that were used to augment FWD data with additional geophysical measurements.

### BEDROCK TYPE AND FWD RESPONSE

To determine whether there is a quantifiable relationship between bedrock and FWD response beyond what is apparent from the similarity of the geologic map of Texas and the county average W7 deflection, we selected six highway segments in different parts of the state. For each highway segment, we (1) obtained FWD deflections and locations from TxDOT, (2) normalized FWD response to a common 9,000-lb (4,082-kg) load, (3) plotted FWD locations on U.S. Geological Survey 7.5-minute quadrangle maps (appendix A), (4) determined elevations for each FWD site, and (5) determined what geologic unit underlies the highway at each FWD site from 1:250,000-scale geologic maps published by BEG (appendix A). These data were entered into a data base that includes highway name, reference marker, geologic unit, elevation, and normalized deflection for each FWD site.

We then analyzed the data base to understand better how bedrock influences FWD response. Plots of elevation, rock type, and deflection versus distance along the highway show how deflections relate to different geologic units beneath the highway and to changes in elevation and relief. When the deflection data are sorted by rock type, we can calculate the average deflection series for a given bedrock type, determine how the deflection series vary, and decide whether bedrock types have distinctive deflection series. If deflection series have different slopes, we can calculate deflection ratios for near- and far-offset detectors to further discriminate rock types.

### SEISMIC REFRACTION

Seismic refraction is a well-established geophysical method (Telford and others, 1976; Milsom, 1989) to determine compressional-wave velocity structure at depths as shallow as tens of centimeters to as deep as several kilometers. In the shallow subsurface, seismic refraction is commonly used to measure depth to the water table or to bedrock (rigid layer beneath soil and weathered bedrock). Compressional-wave velocities increase downward in most geologic settings, where relatively dry soil (compressional-wave velocities ranging from 300 to 700 m/s) is underlain by saturated soil at the water table (compressional velocities of about 1,500 m/s) or by unweathered bedrock (compressional velocities commonly more than 2,000 m/s, depending on rock type). These typically abrupt, downward increases in wave velocity refract surface-

generated seismic waves along the interface between the units. The refracted waves generate wavefronts that propagate back to the surface, where they are detected by motion sensors (geophones). The time delay between seismic-source impact and first seismic arrivals at known geophone distances allows calculation of compressional velocities and thicknesses of near-surface layers, which in turn allows estimation of depth to the water table or to bedrock. In general, exploration depth increases with distance between the source and detector. For shallow investigations, the detector spread should extend from within a short distance of the source to four or more times the desired maximum exploration depth. This allows enough arrivals of both the direct wave (traveling in the surface layer only) and the critically refracted wave (traveling along the water table or at the interface between the surface layer and bedrock) to be observed to calculate accurate compressional-wave velocities for these layers.

We recorded seismic-refraction data using forty-eight 40-Hz geophones, a 48-channel seismograph, and two seismic sources (the FWD and a modified soil-probe hammer) at the J. J. Pickle Research Campus at The University of Texas at Austin (PRC), on U.S. Highway 281 southbound at TxDOT's Mobile Load Simulator (MLS) site in North-Central Texas, and on FM 1431 between Marble Falls and Granite Shoals (table 2). Spread length, geophone spacing, and seismic-source selection depend on target depths, ambient seismic noise, ground conditions, and desired lateral resolution. For typical pavement settings, a sledge hammer, a modified soil-probe hammer, or the FWD itself can be suitable sources. We picked the first compressional-wave arrivals using the Seismic Processing Workshop software package. We calculated true seismic velocities, layer thicknesses, and apparent dip angles using the slope-intercept method (Palmer, 1986).

At the Pickle Research Campus site along Road D (site R1, fig. 2), geophones were mounted on 10-cm-long spikes that were driven into the south shoulder near the edge of the pavement (fig. 5). Geophones were spaced at 0.3-m intervals along an east–west recording spread for a total distance of 14.3 m (fig. 6; table 2). The FWD was operated on the pavement, offset north of the recording spread 1.1 to 1.2 m. The soil-probe hammer was operated on the edge of the pavement 0.4 m north of the recording spread, and on the shoulder inline with the recording spread. Seismic pulses from the FWD and the soil-probe hammer were recorded with the sources located at the center and at the east and west ends of the recording spread (fig. 6).

At the Jacksboro site (site R2, fig. 2), the spikeless geophones were threaded onto steel plates that were laid on the pavement surface at 0.5-m intervals (figs. 7 and 8; table 2). The north–south recording spread, covering a distance of 23.5 m, was laid out on the inside, southbound lane of U.S. Highway 281 on the footprint of the MLS. FWD seismic pulses were recorded from source locations offset 0.9 m west of the recording spread; soil-probe hammer

pulses were recorded from locations along the recording spread. For both sources, source points were at the center and north and south ends of the recording spread (fig. 8).

Table 2. Acquisition parameters for seismic-refraction data collected on Road D at the Pickle Research Center (PRC) in Austin, Texas, on U.S. Highway 281 southbound at the Mobile Load Simulator site south of Jacksboro, Texas, and on FM 1431 near Granite Shoals, Texas.

| | PRC | Jacksboro | Granite Shoals |
|---|---|---|---|
| Date acquired | September 23, 1997 | May 28, 1998 | July 1, 1999 |
| Seismic sources | FWD (on pavement) Soil-probe hammer (on pavement and shoulder) | FWD (on pavement) Soil-probe hammer (on pavement) | Soil-probe hammer (on pavement) |
| Source geometry | Center and ends of sensor spread | Center and ends of sensor spread | Center and ends of sensor spread |
| Sensors | 40 Hz (on shoulder) | 40 Hz (on pavement) | 40 Hz (on pavement) |
| Number of sensors | 48 | 48 | 48 |
| Sensor spacing (m) | 0.3 | 0.5 | 0.5 |
| Recording spread (m) | 14.3 | 23.5 | 23.5 |
| Seismograph | Bison 9048 | Bison 9048 | Bison 9048 |
| Recording channels | 48 | 48 | 48 |
| Sample interval (s) | 0.0001 | 0.0001 | 0.0001 |
| Record length (s) | 0.2 | 0.2 | 0.2 |
| Low-cut filter | 4 Hz | 4 Hz | 4 Hz |
| High-cut filter | 1,000 Hz | 1,000 Hz | 1,000 Hz |

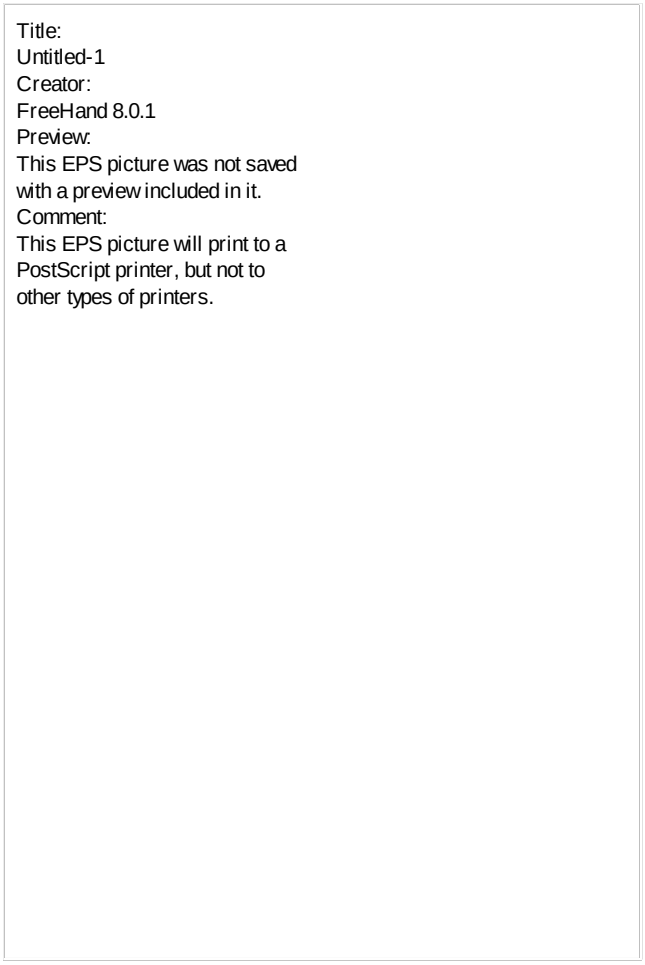


Figure 5. Soil-probe hammer and spike-mounted geophones on the shoulder of Road D at the J. J. Pickle Research Campus, The University of Texas at Austin.

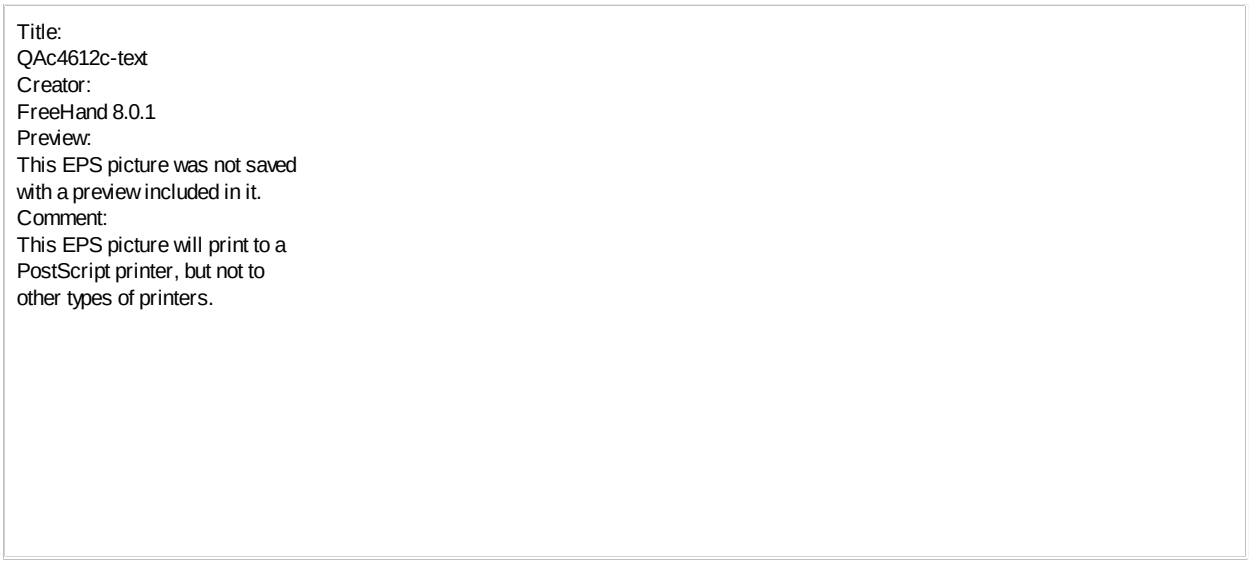


Figure 6. Map of the seismic-refraction test site along Road D at the J. J. Pickle Research Center, The University of Texas at Austin.

Figure 7. Geophones mounted on threaded steel plates and placed on the pavement of southbound U.S. Highway 281 at the Texas Department of Transportation's Mobile Load Simulator site south of Jacksboro, Texas.


Figure 8. Map of the seismic-refraction test site on southbound U.S. Highway 281 at the Texas Department of Transportation's Mobile Load Simulator site south of Jacksboro, Texas.

At Granite Shoals (site R3, fig. 2), geophones mounted on steel plates were laid on the outside, westbound lane at 0.5-m intervals (table 2). The east–west recording spread extended 23.5 m, with seismic pulses recorded from positions at each end and at the center of the spread. No refraction data were recorded using the FWD as a source.

At each site, a short seismograph sample interval of 0.0001 s (table 2) allowed precise first-arrival times to be picked. At a propagation velocity of 500 m/s, a seismic pulse travels 5 cm in 0.0001 s. A longer sample interval, such as 0.001 s typical of many refraction surveys, translates to 0.5 m of wave propagation between samples. Sample intervals this long may cause unacceptable errors in arrival-time picks, which in turn cause erroneous layer depth calculations. Spatial aliasing of the recorded seismic pulse was prevented by having the detector spacing (0.3 to 0.5 m) be much shorter than the compressional-wave wavelengths of 5 to 30 m at a 100-Hz dominant frequency. Recording was initiated by an electronic switch mounted to the seismic source, which was activated when the source struck pavement or the ground. Seismic data were recorded for 0.2 s after source impact.

## RELATIONSHIP BETWEEN BEDROCK TYPE AND FWD RESPONSE

Bedrock units are one of three major rock types: igneous (solidified from molten rock), sedimentary (chemical precipitates or particles deposited by wind, water, or gravity flow), and metamorphic (plastically deformed igneous or sedimentary rock). Physical properties for these major rock types, including density, wave-propagation velocities, and elastic parameters, have been shown in numerous field and laboratory experiments to vary widely (Press, 1966). For geologic maps to be useful in the interpretation of FWD data, FWD deflections should show some relationship to mapped rock type. From the similarity of county deflection averages to a simplified map of Texas, we infer that bedrock type and FWD response are related (figs. 2 and 3). Whether this relationship is caused by a similarity in bedrock depths for a given bedrock type or by a similarity in physical properties of a given bedrock type is unknown.

To determine whether existing maps of bedrock can help interpret FWD data at a local scale, we examined the relationship between bedrock type and FWD response along six highway segments in four physiographic regions (fig. 4). These regions include Precambrian rocks as old as 2 billion years and Holocene sediments deposited at the present, as well as examples of sedimentary, igneous, and metamorphic rocks. Sedimentary bedrock types include (1) unconsolidated gravel, silt, sand, and clay along streams in each of the regions studied, (2) chemically precipitated limestones and dolomites in the Edwards Plateau, Central Texas Uplift, and North-Central Plains, and (3) lithified to semiconsolidated sandstone and shale in each region. Igneous bedrock types include granites that crop out in the Central Texas Uplift. Metamorphic rocks, including gneisses and schists, are also mapped in the Central Texas Uplift.

### NORTH-CENTRAL PLAINS SITE

Compared with the rest of Texas, county average deflections in the North-Central Plains physiographic region are moderate, ranging from 1.1 to 2.0 mils (fig. 2). Lithified sedimentary bedrock types common in this region include Paleozoic limestone, sandstone, and shale (table 1). Land-surface elevation increases from 900 ft (274 m) in the southeast part of the region to 3,000 ft (914 m) in the northwest part. Unconsolidated sediments are common along the major rivers (Colorado, Brazos, Trinity, and Red Rivers) and numerous smaller streams that cross the region. FWD data and bedrock-type information were analyzed for one site in the North-Central Plains.

#### *Site A: Texas 16, Archer and Young Counties*

Site A extends along Texas 16 between reference markers 220 and 264 in Archer and Young Counties. Average W7 deflections are between 1.6 and 2.0 mils for Archer County and 1.1 and 1.5 mils for Young County (fig. 2). Geologic units mapped along this roadway segment

include lithified Paleozoic sandstones, limestones, and mudstones and unconsolidated Quaternary stream deposits (fig. 9; appendix B).

FWD data for 87 locations along this highway segment (appendix C) show a wide range of deflections for each detector (fig. 9). W7 deflections average 0.99 mils (table 3), which is lower than the reported deflection average for Archer and Young Counties. The calculated average for Texas 16 is higher than average deflections calculated for sites in the Central Texas Uplift and Edwards Plateau regions and lower than calculated averages for the Gulf Coastal Plains sites (table 3), in agreement with the map of county-wide average deflections.

For many of the 11 geologic units mapped along this highway segment, FWD data show considerable overlap in observed deflection ranges (fig. 10). For example, W7 deflections over the Markley Mudstone range from 0.8 to more than 2.0 mils; Markley Sandstone deflections range from 0.5 to 2.0 mils (fig. 10b and c). Other rock units with more than a few measured deflections have similarly broad ranges.

Deflection averages calculated for the geologic units mapped at site A decrease from 10 to 40 mils at W1 to between 0.5 and 2 mils at W7 (figs. 10 and 11). Deflection series that have high near-offset deflections also tend to have high far-offset deflections. Geologic units over which relatively small average W7 deflections (<1.0 mil) were measured are the Thrifty-Graham and Kisinger Sandstones at 0.5 mils, the Ranger and Home Creek Limestones at 0.6 to 0.8 mils, and the Gonzales Creek Sandstone at 0.9 mils (fig. 12a). Relatively large average W7 deflections were measured over the Bunger Limestone (1.8 mils), the Markley Mudstone (1.3 mils), and the Ivan Limestone (1.2 mils).

Ratios calculated for average deflections at different detectors can help remove the covariance of near- and far-offset deflections and better reveal bedrock effects. We calculated the W2:W7 ratio (fig. 12b) because W2 should have the largest source- and pavement-related deflection component and W7 should have the largest bedrock-related deflection. Ratios calculated for the North-Central Plains geologic units range from 7.96 to 14.01, increasing for units that have large W2 deflections for a given W7 deflection. With all other factors equal, rigid geologic units should have higher W2:W7 ratios than less rigid ones. In this analysis, the Home Creek Limestone, Kisinger Sandstone, and Thrifty-Graham Mudstone have low ratios (less rigid); the Markley Sandstone, Ranger Limestone, and Thrifty-Graham Sandstone have relatively high ratios (more rigid). When compared with geologic units at other sites in other physiographic regions, these ratios are lower than those calculated for the Central Texas Uplift and Edwards Plateau but are higher than those in the Gulf Coastal Plains.

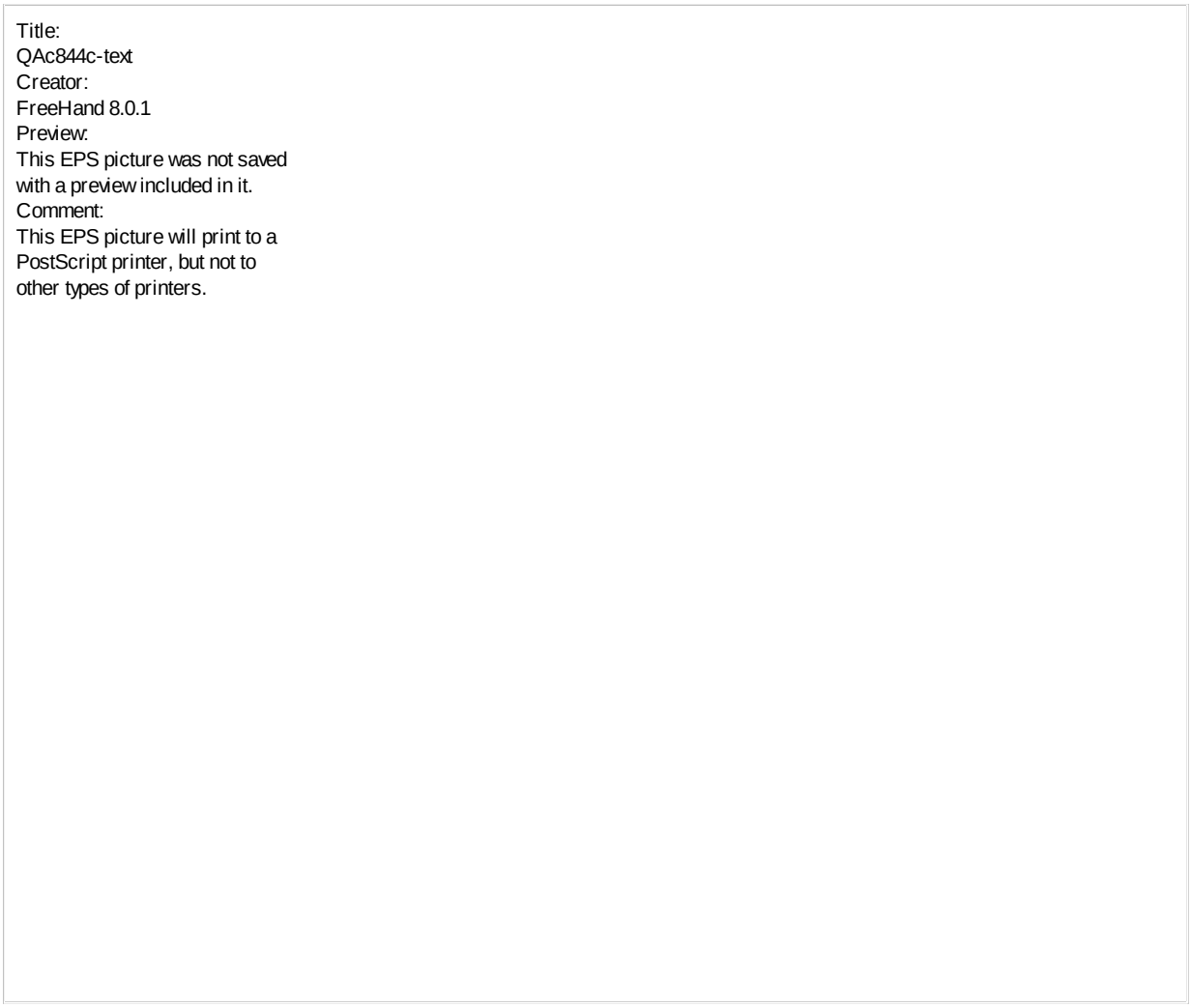


Figure 9. Geologic units, elevation, and W1 through W7 deflections along Texas 16 between reference markers 220 and 265, Archer and Young Counties, North Texas.

Table 3. Deflection statistics (normalized to 9,000-lb [4,082-kg] load) for sites A through F (fig. 2).

Site A: Texas 16, Archer and Young Counties, n = 87.

| Statistic | W1 | W2 | W3 | W4 | W5 | W6 | W7 |
|---|---|---|---|---|---|---|---|
| Average | 18.68 | 10.48 | 5.22 | 2.89 | 1.87 | 1.33 | 0.99 |
| Standard deviation | 8.07 | 4.60 | 2.38 | 1.30 | 0.83 | 0.59 | 0.45 |
| Maximum | 46.12 | 22.96 | 11.43 | 6.57 | 4.45 | 3.29 | 2.56 |
| Minimum | 6.87 | 2.86 | 1.23 | 0.59 | 0.39 | 0.26 | 0.21 |

Site B: Texas 16, Llano and Gillespie Counties, n = 69.

| Statistic | W1 | W2 | W3 | W4 | W5 | W6 | W7 |
|---|---|---|---|---|---|---|---|
| Average | 34.72 | 15.19 | 5.31 | 2.73 | 1.71 | 1.23 | 0.93 |
| Standard deviation | 13.73 | 6.52 | 2.34 | 1.20 | 0.73 | 0.53 | 0.41 |
| Maximum | 79.12 | 30.76 | 12.00 | 6.05 | 3.80 | 2.65 | 1.96 |
| Minimum | 4.67 | 2.11 | 0.85 | 0.77 | 0.48 | 0.32 | 0.23 |

Site C: Texas 71, Burnet County, n = 30.

| Statistic | W1 | W2 | W3 | W4 | W5 | W6 | W7 |
|---|---|---|---|---|---|---|---|
| Average | 16.09 | 7.08 | 2.94 | 1.61 | 1.03 | 0.76 | 0.57 |
| Standard deviation | 6.20 | 3.56 | 1.68 | 1.02 | 0.68 | 0.51 | 0.41 |
| Maximum | 35.96 | 16.85 | 7.51 | 4.34 | 2.94 | 2.06 | 1.59 |
| Minimum | 7.56 | 2.47 | 1.03 | 0.48 | 0.30 | 0.18 | 0.09 |

Site D: U.S. 290, Blanco and Hays Counties, n = 52.

| Statistic | W1 | W2 | W3 | W4 | W5 | W6 | W7 |
|---|---|---|---|---|---|---|---|
| Average | 11.02 | 5.30 | 2.20 | 1.15 | 0.72 | 0.52 | 0.40 |
| Standard deviation | 3.39 | 1.63 | 0.80 | 0.50 | 0.36 | 0.28 | 0.22 |
| Maximum | 20.19 | 9.47 | 4.27 | 2.55 | 1.67 | 1.26 | 1.04 |
| Minimum | 4.45 | 2.30 | 0.70 | 0.34 | 0.13 | 0.06 | 0.05 |

Site E: Texas 71, Bastrop County, n = 34.

| Statistic | W1 | W2 | W3 | W4 | W5 | W6 | W7 |
|---|---|---|---|---|---|---|---|
| Average | 21.25 | 12.07 | 6.37 | 3.77 | 2.51 | 1.88 | 1.49 |
| Standard deviation | 6.71 | 5.29 | 3.37 | 2.07 | 1.32 | 0.95 | 0.74 |
| Maximum | 38.57 | 23.83 | 14.35 | 9.07 | 6.04 | 4.52 | 3.49 |
| Minimum | 13.49 | 5.11 | 2.20 | 0.78 | 0.46 | 0.40 | 0.32 |

Site F: Texas 16, Jim Hogg and Zapata Counties, n = 89.

| Statistic | W1 | W2 | W3 | W4 | W5 | W6 | W7 |
|---|---|---|---|---|---|---|---|
| Average | 34.28 | 15.24 | 5.90 | 3.32 | 2.32 | 1.77 | 1.41 |
| Standard deviation | 16.90 | 6.77 | 2.47 | 1.37 | 0.94 | 0.71 | 0.54 |
| Maximum | 84.44 | 36.97 | 13.51 | 6.92 | 4.80 | 3.53 | 2.69 |
| Minimum | 6.66 | 4.00 | 1.58 | 1.00 | 0.79 | 0.61 | 0.46 |


Figure 10. Average and individual deflections for rock types mapped along Texas 16 in Archer and Young Counties.

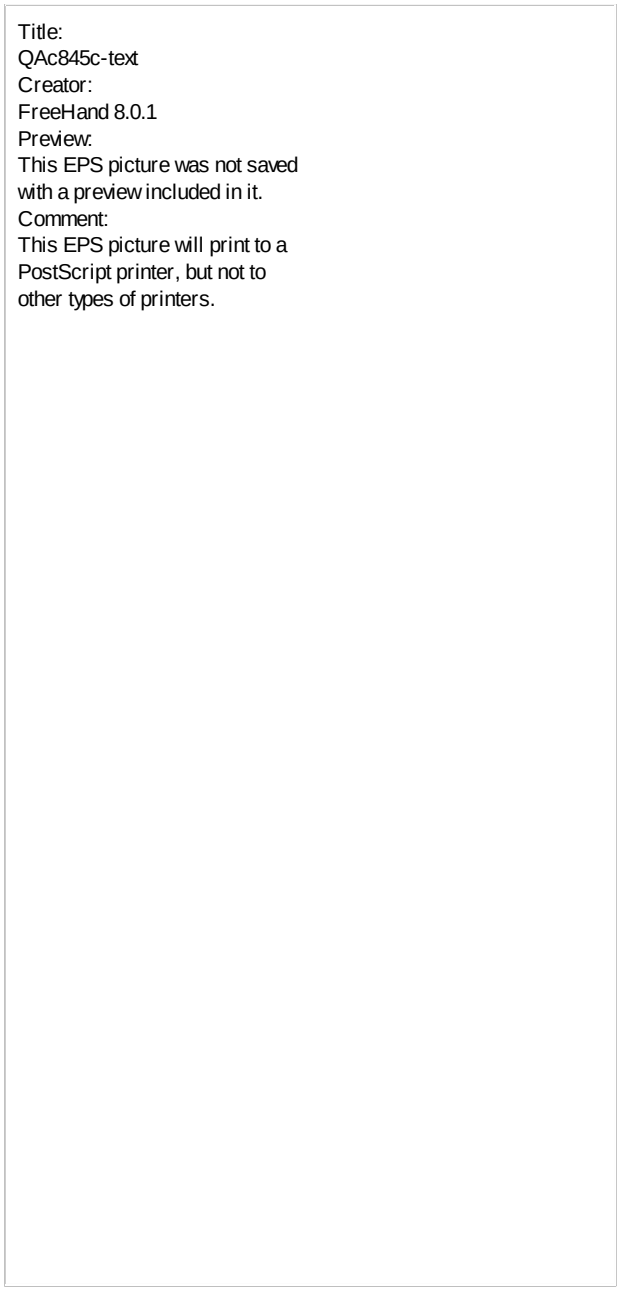


Figure 11. Average deflections for all rock units mapped along Texas 16 in Archer and Young Counties.

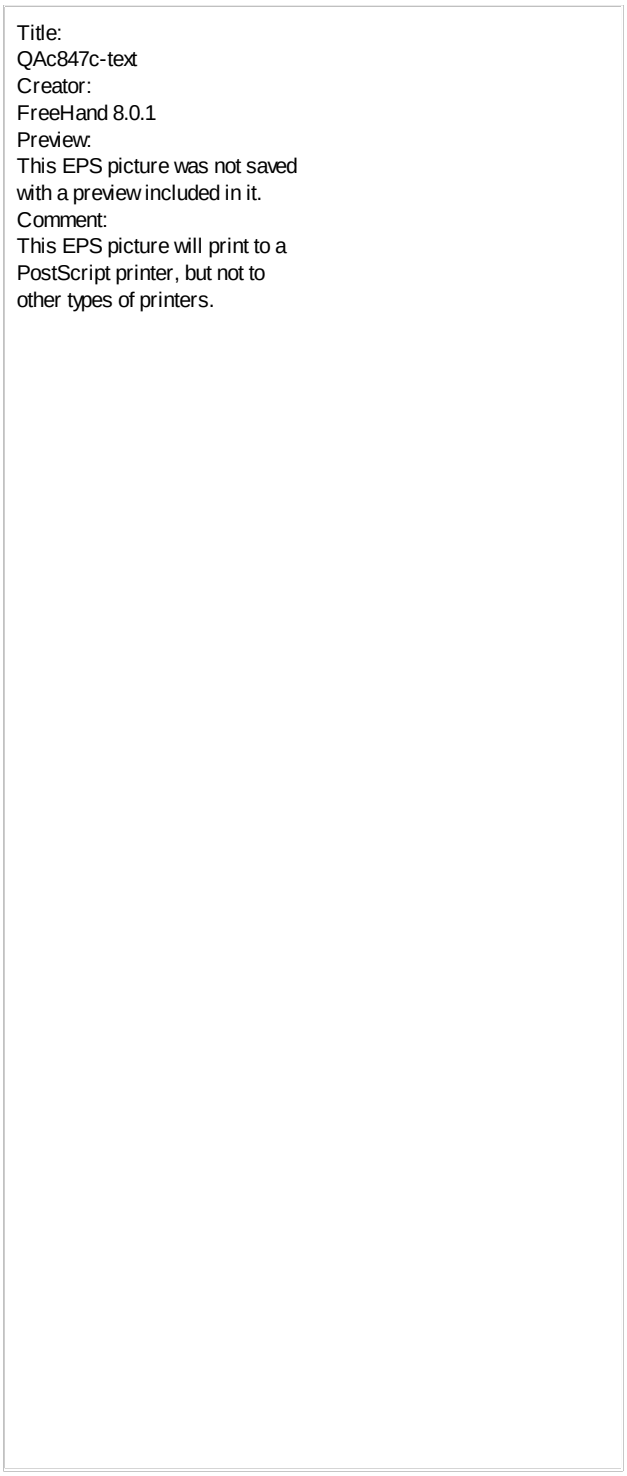


Figure 12. (a) Average W7 deflection and (b) W2:W7 deflection ratio by rock type along Texas 16, Archer and Young Counties.

## CENTRAL TEXAS UPLIFT SITES

The Central Texas Uplift, underlain by Precambrian igneous and metamorphic rocks, Paleozoic and Mesozoic sedimentary rocks, and unconsolidated Quaternary sediments (table 1), covers the smallest area of any physiographic region (fig. 4). County average deflections in this region of typically rigid bedrock types are the lowest in the state, ranging from less than 1 to 1.5 mils (fig. 2). Two study sites, B and C, are located in this region (fig. 4).

### *Site B: Texas 16, Llano and Gillespie Counties*

This segment of Texas 16 begins at reference marker 450 south of Llano and extends about 38 mi (61 km) to reference marker 488 north of Fredericksburg. It is mostly underlain by Precambrian metamorphic (Packsaddle Schist and Valley Spring Gneiss) and igneous (Town Mountain Granite) rocks and the Cretaceous Hensell Sand (fig. 13). A few occurrences of younger granites, Cambrian Hickory Sandstone, Cretaceous Fort Terrett Limestone, and Quaternary stream deposits are mapped along the highway (fig. 13; appendix B). Younger geologic units are found at the relatively high elevations on the south part of the segment; older igneous and metamorphic rocks are found at relatively low elevations on the north part of the segment (fig. 13). Average W7 deflections for both Llano and Gillespie Counties are less than 1.0 mil (fig. 2), reflecting the abundance of rigid bedrock in the Central Texas Uplift.

We analyzed FWD data from 69 sites along this highway segment (table 3; appendix C). This segment has the highest average W1 deflection of any of the study sites (34.7 mils) but the third-lowest average W7 deflection (0.93 mils). When the data are grouped by geologic unit (fig. 14), they show that (1) sites with large near-offset deflections generally also have large far-offset deflections, and (2) there is more variation within a geologic unit than there is between average deflections of each rock type. Although average W7 deflections calculated for the Hensell Sand are higher than those for the Town Mountain Granite and the Valley Spring Gneiss, the range in individual W7 deflections observed for these rock types is similar: 0.4 to 2 mils for the Hensell Sand, 0.3 to 1.1 mils for the Town Mountain Granite, and 0.3 to 1.8 mils for the Valley Spring Gneiss (fig. 14).

Statistically, Precambrian igneous and metamorphic rocks have low average W7 deflections that range from 0.53 mils for younger granites to 0.87 mils for the Packsaddle Schist (figs. 15 and 16a). Higher average W7 deflections, ranging from 1.11 to 1.24 mils, are calculated for Cretaceous and younger sedimentary units. W7 averages for geologic units at site B are similar to those calculated for geologic units in the North-Central Plains.

The W2:W7 ratio provides better discrimination of rock type for site B. Very high ratios are calculated for the rigid rock units (fig. 16b): between 17 and 40 for granites, metamorphic rocks,

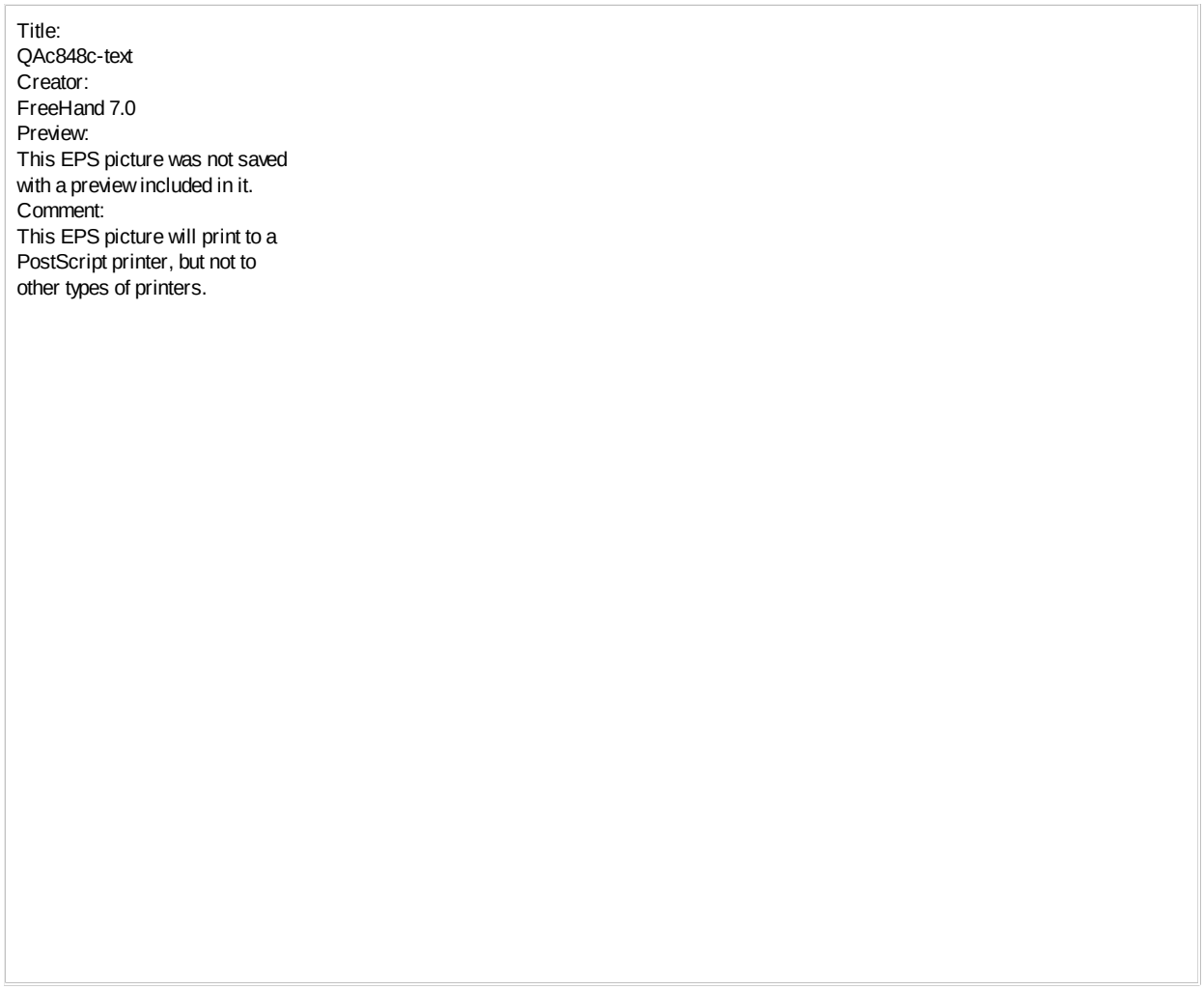


Figure 13. Geologic units, elevation, and W1 through W7 deflections along Texas 16 between reference markers 450 and 490, Llano and Gillespie Counties, Central Texas.


Figure 14. Average and individual deflections for rock types mapped along Texas 16 in Llano and Gillespie Counties.

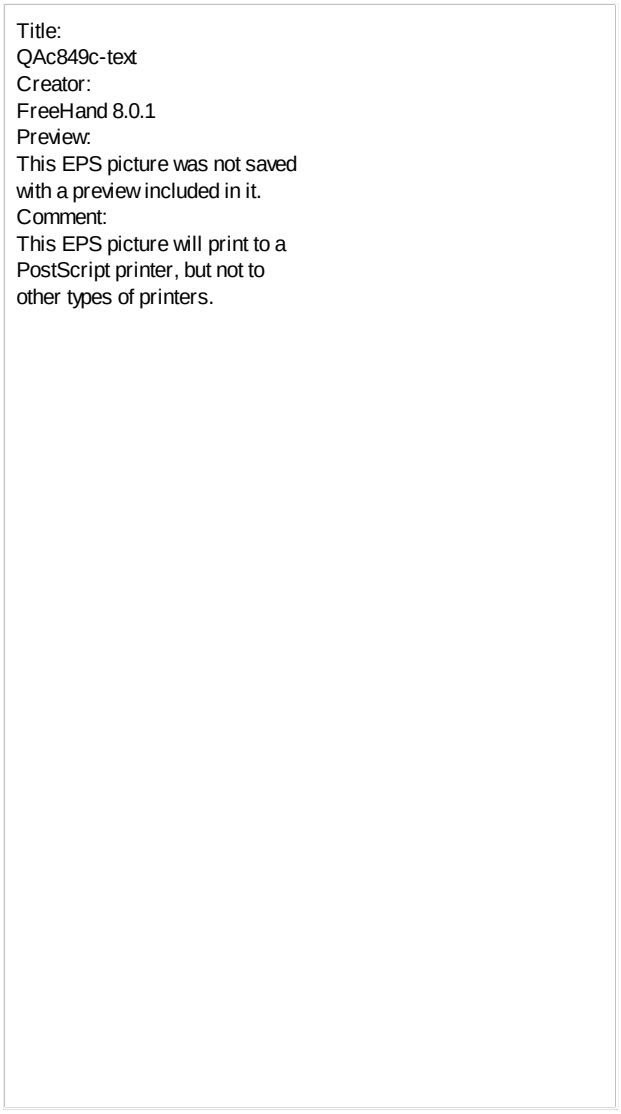


Figure 15. Average deflections for all rock units mapped along Texas 16 in Llano and Gillespie Counties.

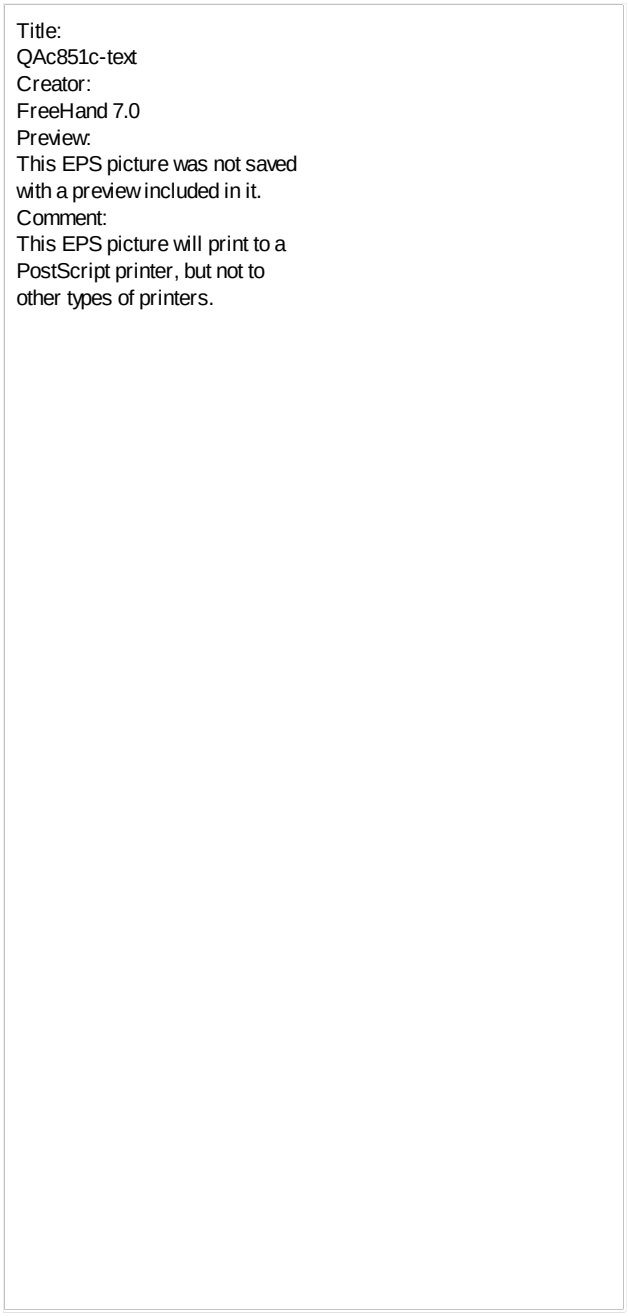


Figure 16. (a) Average W7 deflection and (b) W2:W7 deflection ratio by rock type along Texas 16, Llano and Gillespie Counties.

and the Fort Terrett Limestone. Lower ratios are calculated for the younger sedimentary units, ranging from 13 to 14 for the Hickory Sandstone and Hensell Sand, and 11 for Quaternary stream deposits. Ratios for the most common units encountered along Texas 16 are higher than those observed in the North-Central Plains and Gulf Coastal Plains and are similar to ratios calculated for the Edwards Plateau.

***Site C: Texas 71, Burnet County***

This 14-mi-long (23-km) segment extends from reference markers 528 to 542 in eastern Burnet County. Along the west part of this segment, Paleozoic limestones are mapped that are extensively exposed within the Central Texas Uplift (fig. 17). Cretaceous sands and limestones are common along the east part of this segment, which represents a transitional zone from typical Central Texas Uplift units to typical Edwards Plateau units. Average W7 deflection for Burnet County is less than 1 mil, the lowest category (fig. 2).

FWD data from 30 locations along this highway segment (table 3; appendix C) indicate that average deflections at each offset are the second-lowest of the six study sites. Average W7 deflection is 0.57 mils, which falls within the indicated county-average category (fig. 2). Most of the FWD measurements were acquired over the Ordovician Honeycut Limestone, for which individual W7 deflections ranged from less than 0.1 to 0.8 mils (fig. 18). The average W7 deflections for all but two rock types fall within this range, including Quaternary stream deposits, Cretaceous upper Glen Rose Limestone and Hensell Sand, and Ordovician Gorman Limestone (figs. 19 and 20a). Two units that had higher average W7 deflections than the range observed for the Honeycut Limestone were the Cretaceous Sycamore Sand (1.5 mils) and the Pennsylvanian–Permian Marble Falls Limestone (1.1 mils). Average W7 values for all other units were below 0.7 mils.

W2:W7 ratios (fig. 20b) proved to be a better discriminant of rock types than W7 values alone. High ratios (between 13 and 27), indicating a rapid decrease in deflection as offset increases and probably a relatively stiff or shallow bedrock, were calculated for the Honeycut Limestone, the upper Glen Rose Limestone, and the Gorman Limestone. Intermediate ratios (9 to 10) were calculated for the small number of examples over the Marble Falls Limestone, the Sycamore and Hensell Sands, and Quaternary stream deposits. A low ratio of about 5 was calculated for the one example of lower Glen Rose Limestone mapped along the segment. The most common geologic unit along the highway, the Honeycut Limestone, has a ratio that is similar to that of other rigid units in the Central Texas Uplift and Edwards Plateau regions and is higher than those in the North-Central Plains and Gulf Coastal Plains regions.

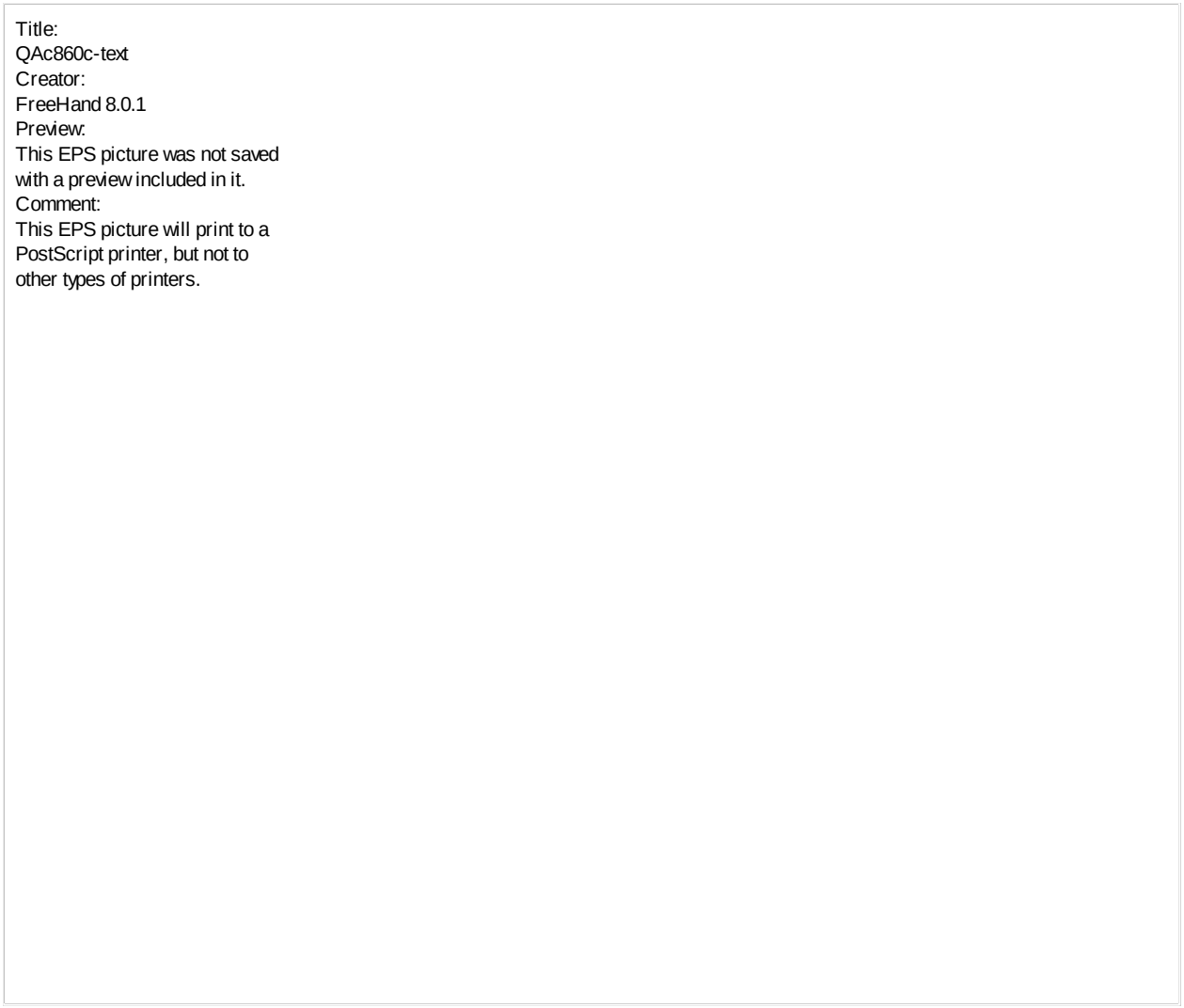


Figure 17. Geologic units, elevation, and W1 through W7 deflections along Texas 71 between reference markers 528 and 542, Burnet County, Central Texas.

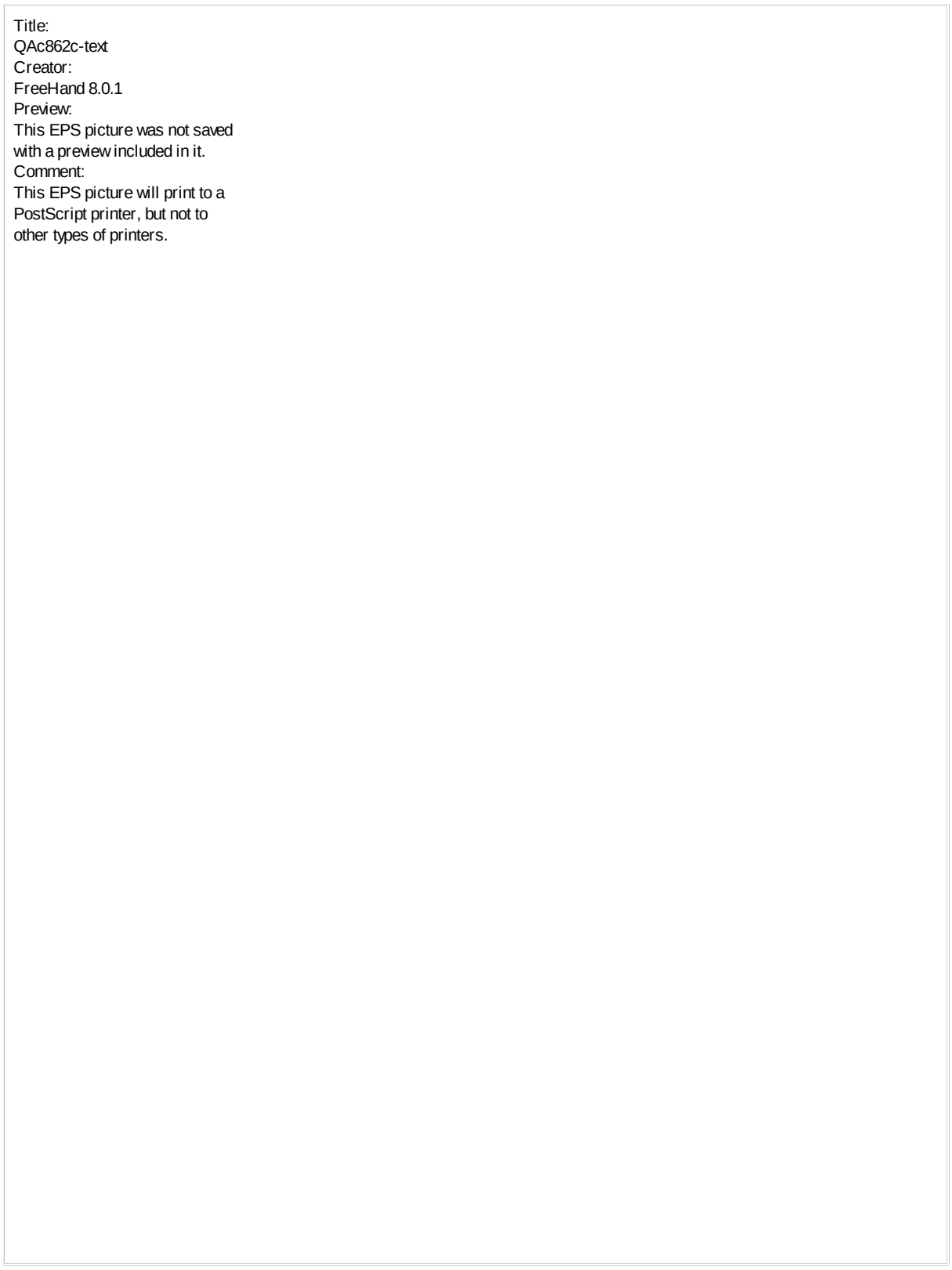


Figure 18. Average and individual deflections for rock types mapped along Texas 71 in Burnet County.


Figure 19. Average deflections for all rock units mapped along Texas 71 in Burnet County.

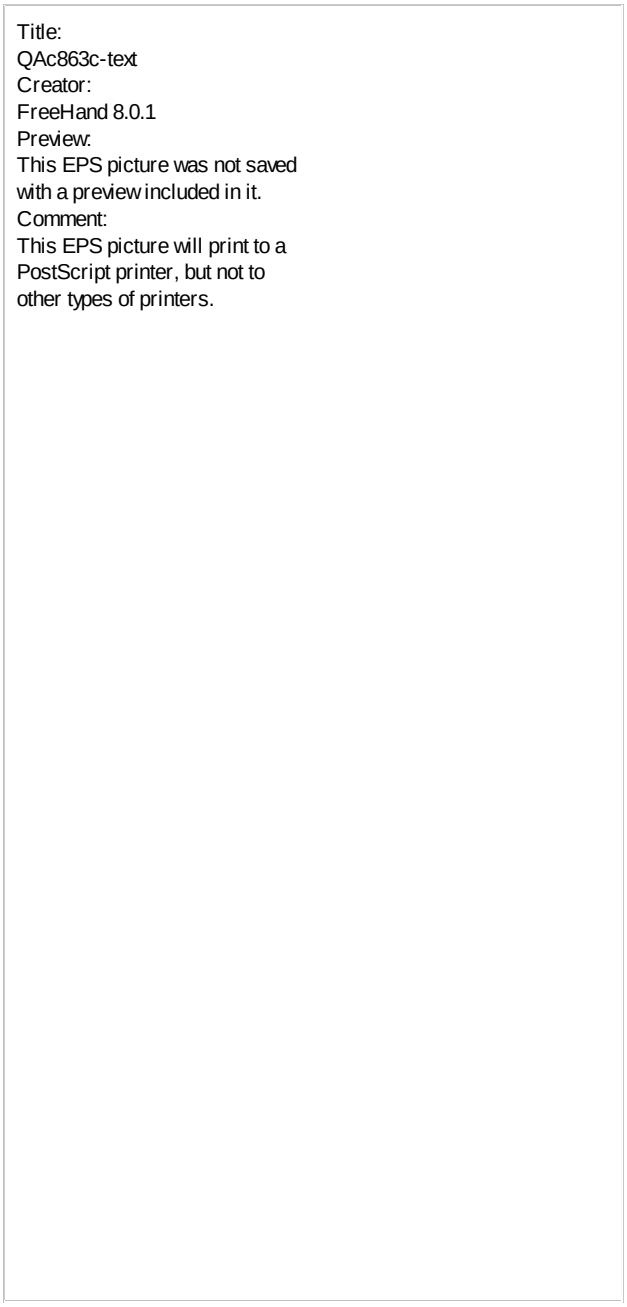


Figure 20. (a) Average W7 deflection and (b) W2:W7 deflection ratio by rock type along Texas 71, Burnet County.

## EDWARDS PLATEAU SITE

Average W7 deflections for counties within the Edwards Plateau region are below 1.5 mils (figs. 2 and 4), similar to those in the Central Texas Uplift counties and the lowest in the state. Relatively rigid Cretaceous limestones and dolomites are the most common bedrock types across the Edwards Plateau (table 1). Young, unconsolidated gravel, sand, and clay are common along numerous streams and rivers that dissect the plateau (fig. 3). One study site is located in the central part of the Edwards Plateau.

### *Site D: U.S. 290, Blanco and Hays Counties*

This segment of U.S. 290 extends about 27 mi (43 km) across eastern Blanco and northern Hays Counties between reference markers 536 and 563. Average W7 deflections for these counties are very low (each is below 1.0 mils, fig. 2). Only four geologic units are mapped: Cretaceous lithified sedimentary rocks that include the upper and lower Glen Rose and Fort Terrett Limestones and unconsolidated Quaternary stream deposits (appendix B). Upper and lower Glen Rose Limestones are the most common geologic units; the lower Glen Rose is found in the west part of the segment (reference markers 526 to 541, fig. 21), and the upper Glen Rose crops out at the higher elevations common in the east part of the segment (reference markers 542 to 563). Younger, unconsolidated deposits are found in local topographic lows.

FWD measurements acquired at 52 sites have the lowest average deflections of the six sites at all offsets (table 3; appendix C). Average deflections for the W5, W6, and W7 detectors are each below 1.0 mil. Deflections observed at detector W7 for the upper Glen Rose Limestone, the most common geologic unit along this segment, range from less than 0.1 to 0.9 mils. This range matches Blanco and Hays County averages and includes W7 deflections for each of the other geologic units (fig. 22).

Upper and lower Glen Rose Limestones have similar deflection averages for each offset (fig. 23) and have very low W7 averages (0.36 to 0.38 mils, fig. 24a). Deflections for the one Fort Terrett Limestone example are even lower than the Glen Rose units for detectors W5, W6, and W7. Highest deflections are observed for the Quaternary stream deposits, although W7 values for this unit are quite low (0.6 mils) relative to similar deposits in other regions, perhaps because of roadway stiffness.

Calculations of W2:W7 ratios for these geologic units appear to remove the road-stiffness effect (fig. 24b). The Fort Terrett and upper and lower Glen Rose Limestones all have high ratios (19 to 24) that are comparable to those of rigid geologic units in the Central Texas Uplift. The W2:W7 ratio for Quaternary stream deposits is near 10, which is within the range of 7 to 12 observed for similar deposits in other regions.

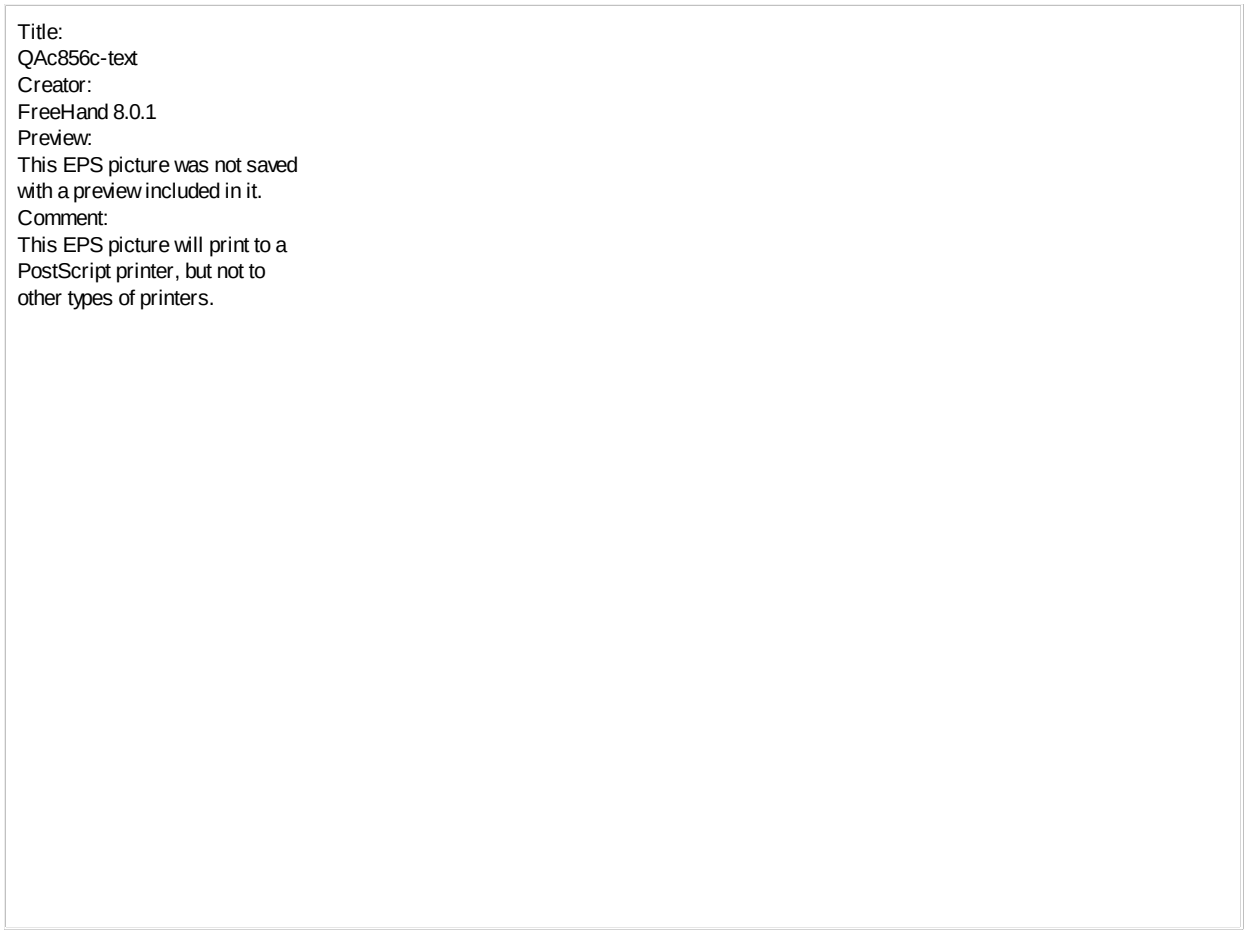


Figure 21. Geologic units, elevation, and W1 through W7 deflections along U.S. 290 between reference markers 536 and 563, Blanco and Hays Counties, Central Texas.

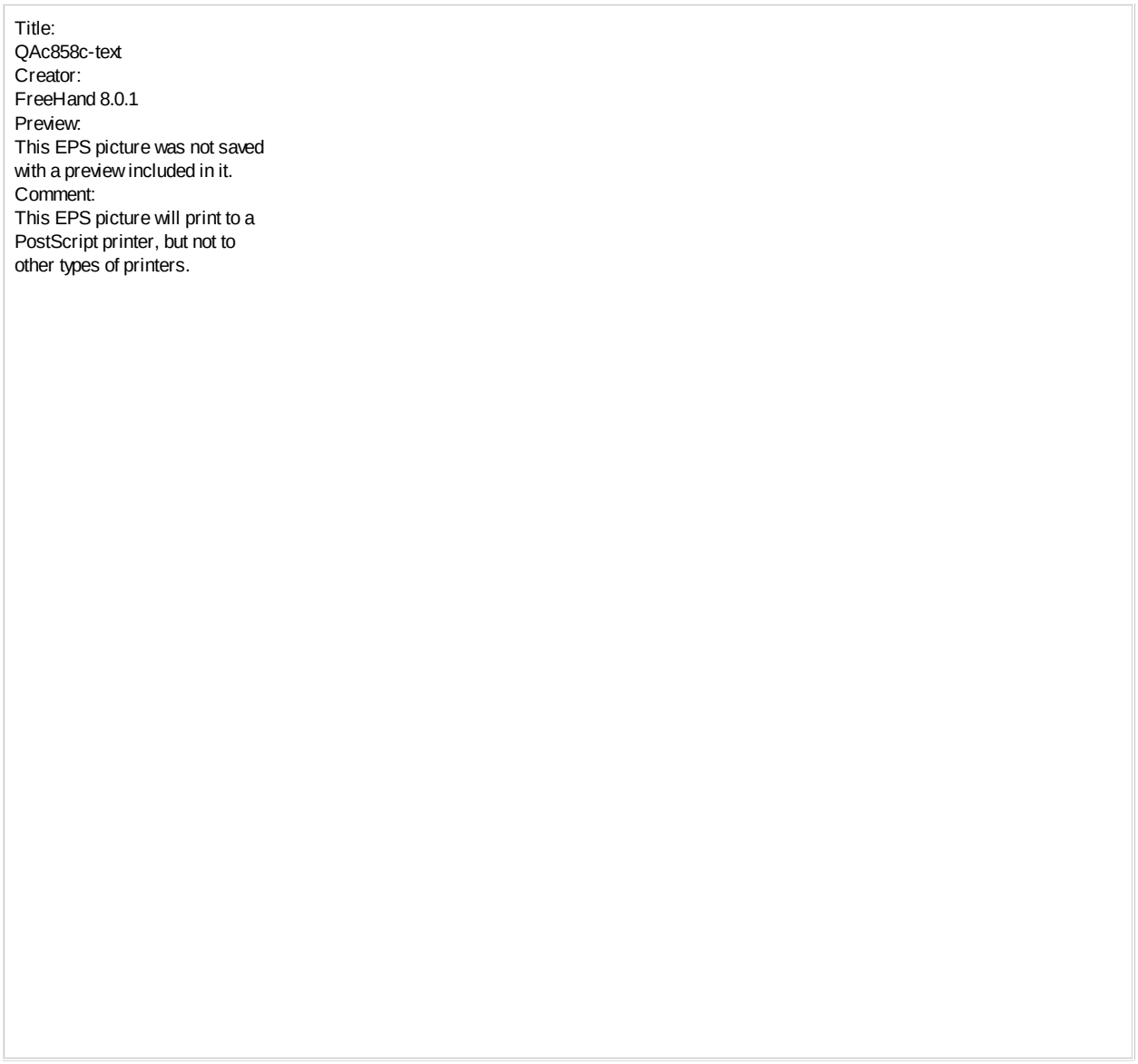


Figure 22. Average and individual deflections for rock types mapped along U.S. 290 in Blanco and Hays Counties.

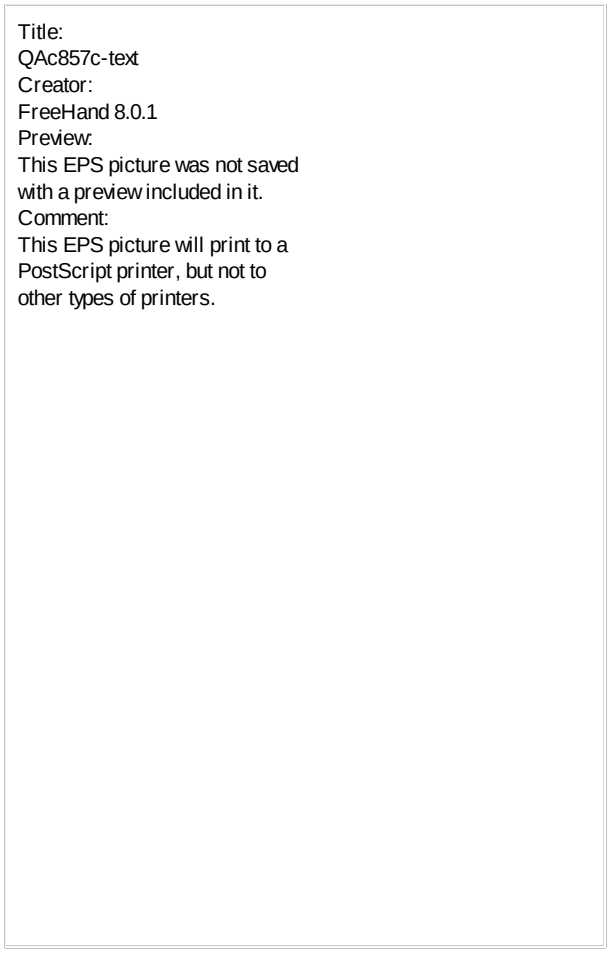


Figure 23. Average deflections for all rock units mapped along U.S. 290 in Blanco and Hays Counties.

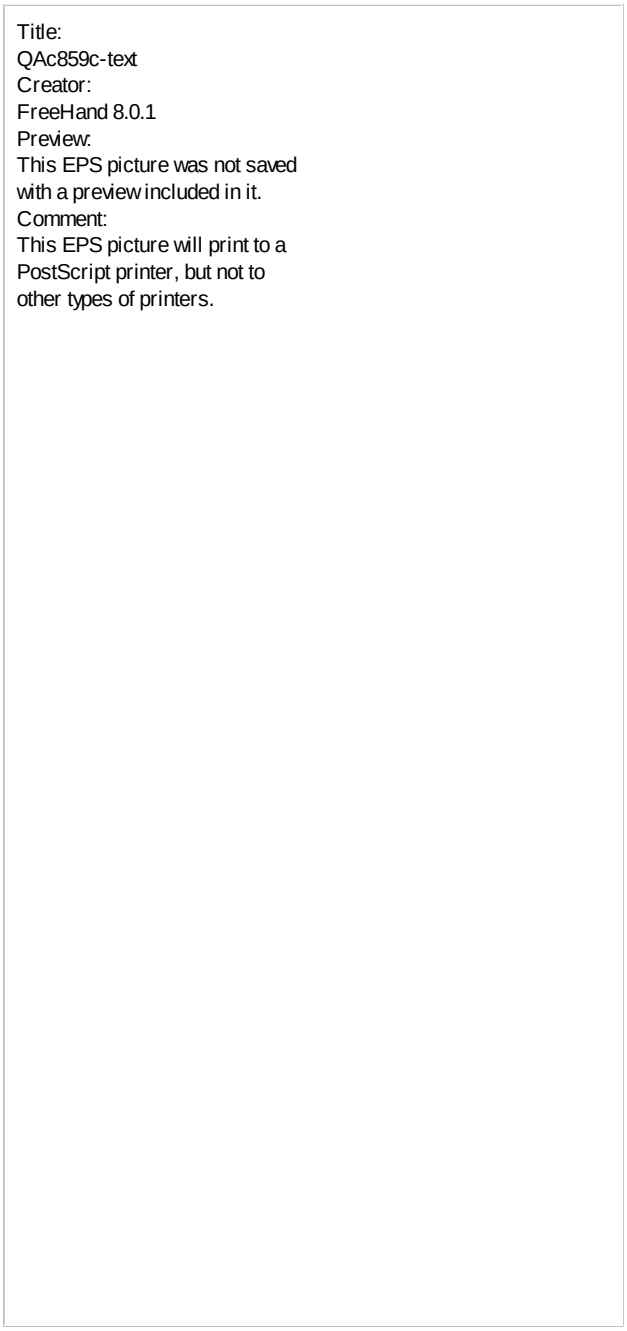


Figure 24. (a) Average W7 deflection and (b) W2:W7 deflection ratio by rock type along U.S. 290, Blanco and Hays Counties.

## GULF COASTAL PLAINS SITES

The Texas coastal plain, which slopes toward the Gulf of Mexico from the Edwards Plateau (fig. 4), is the largest and geologically youngest of the major physiographic regions. Bedrock types in this region are all Cenozoic sedimentary deposits that are variably lithified (table 1). This region has the highest county average W7 deflections in the state, ranging from 1.1 to more than 2.5 mils (fig. 2). The two sites studied in this region (sites D and E, fig. 4) are located on the central and south parts of the upper coastal plain.

### *Site E: Texas 71, Bastrop County*

Site E is an 8-mi-long (13-km) segment of Texas 71 between reference markers 590 and 598 on the central part of the upper Gulf Coastal Plains (fig. 4). Average W7 deflections for Bastrop County (between 1.1 and 1.5 mils) represent the low end of the range observed for all Coastal Plain counties (fig. 2). Geologic units mapped along this segment are old relative to deposits closer to the Gulf of Mexico (fig. 3). They include Cretaceous clay and marl, Eocene mudstones, sandstones, and unconsolidated clay and sand, and unconsolidated Quaternary gravel, sand, and clay (fig. 25; appendix B).

Average deflections calculated from FWD measurements along both sides of the roadway at 17 locations (34 deflection series) are higher for the W3 to W7 detectors than they are for any other study site (table 3). Average W7 deflection is 1.49 mils, which is in the same range calculated for Bastrop County (fig. 2). There are large variations in deflections measured at individual detectors for some geologic units (W7 deflection is between 0.5 and 4 mils for the Hooper Mudstone, fig. 26) and relatively small variations in other geologic units (W7 deflection ranges from 0.9 to 1.5 mils for the Simsboro Sand).

Most geologic units have large average deflections relative to geologic units in other physiographic regions (figs. 27 and 28a). The largest W7 deflections, above 2 mils, were recorded at locations mapped as Cretaceous clay and marl units and Quaternary stream deposits. Intermediate W7 deflections of 1.1 to 1.9 mils were observed over the Midway Group, Hooper Mudstone, Simsboro Sand, and Quaternary gravel found at the highest topographic positions along the roadway (fig. 25). The smallest W7 deflections were measured over the Calvert Bluff Mudstone, which is the most rigid unit at site E.

Ratios calculated from average W2 and W7 deflections also suggest that the Calvert Bluff Mudstone is the most rigid of the geologic units mapped at this site (fig. 28b). The W2:W7 ratio for this unit is 15, well below that of the most rigid units in the Central Texas Uplift and Edwards Plateau regions but comparable to those of similar lithified sedimentary rocks in the

North-

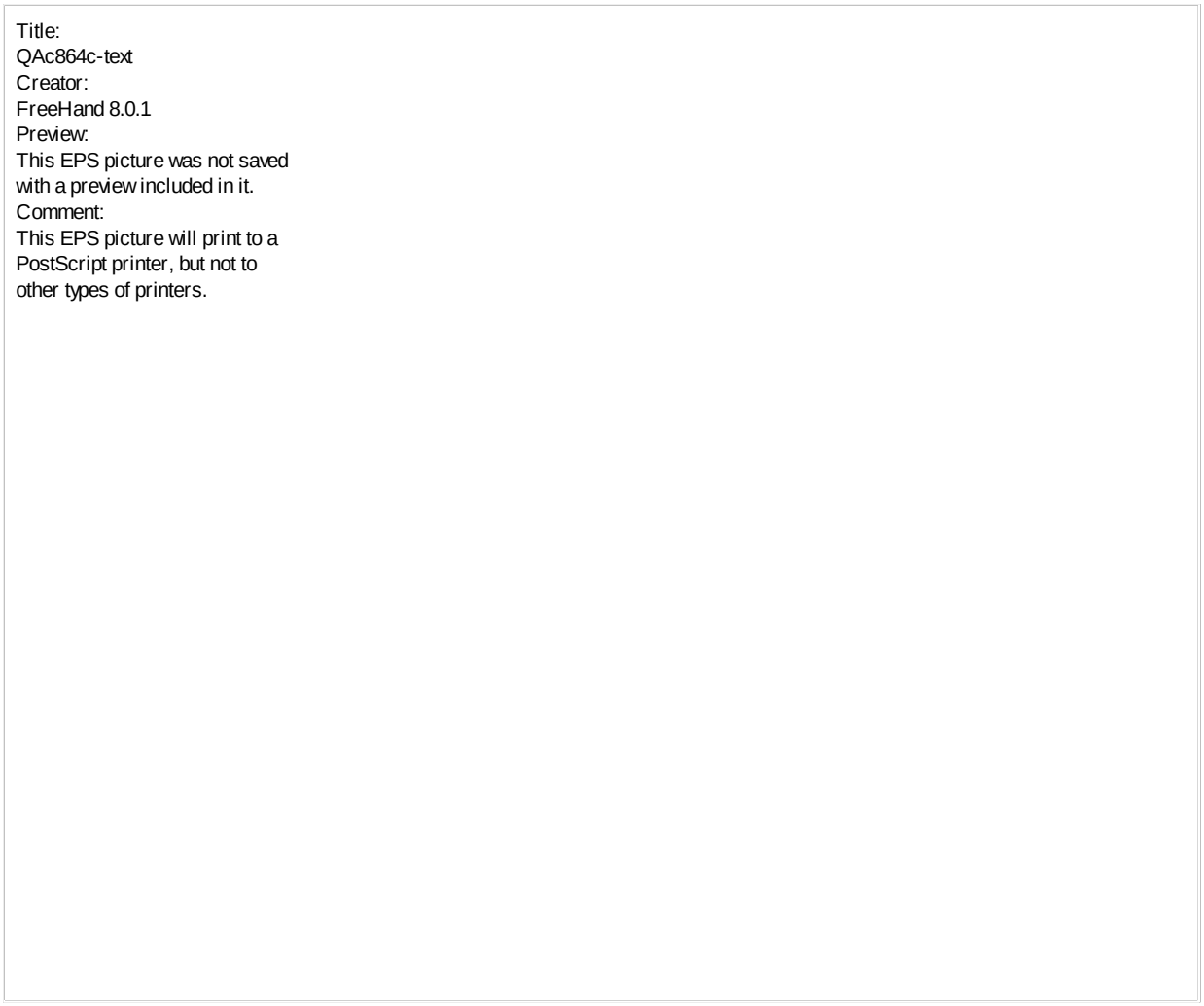


Figure 25. Geologic units, elevation, and W1 through W7 deflections along Texas 71 between reference markers 590 and 598, Bastrop County, southeast Texas.


Figure 26. Average and individual deflections for rock types mapped along Texas 71 in Bastrop County.

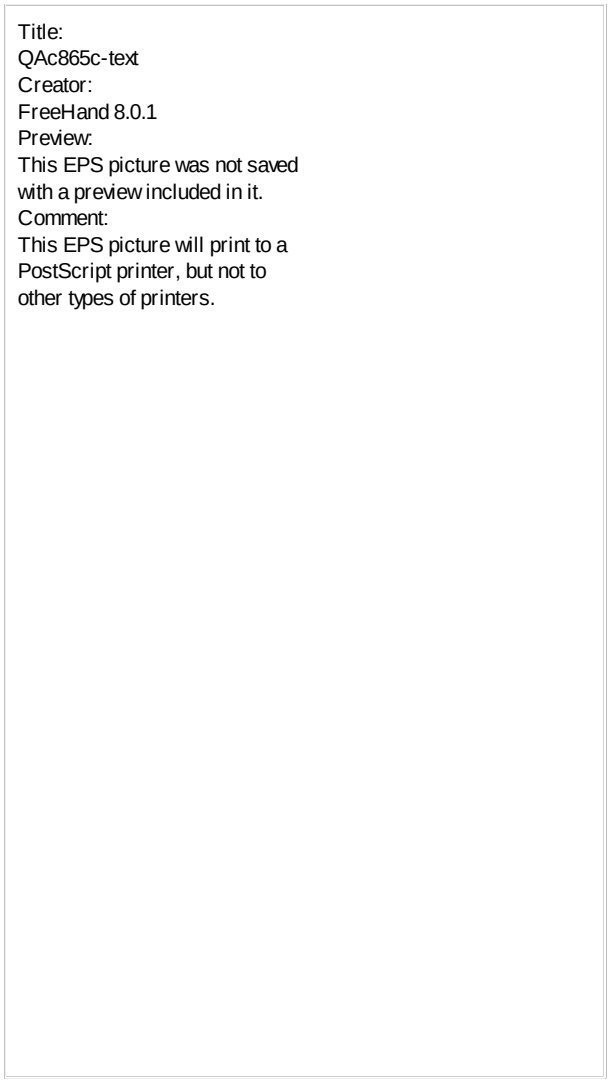


Figure 27. Average deflections for all rock units mapped along Texas 71 in Bastrop County.

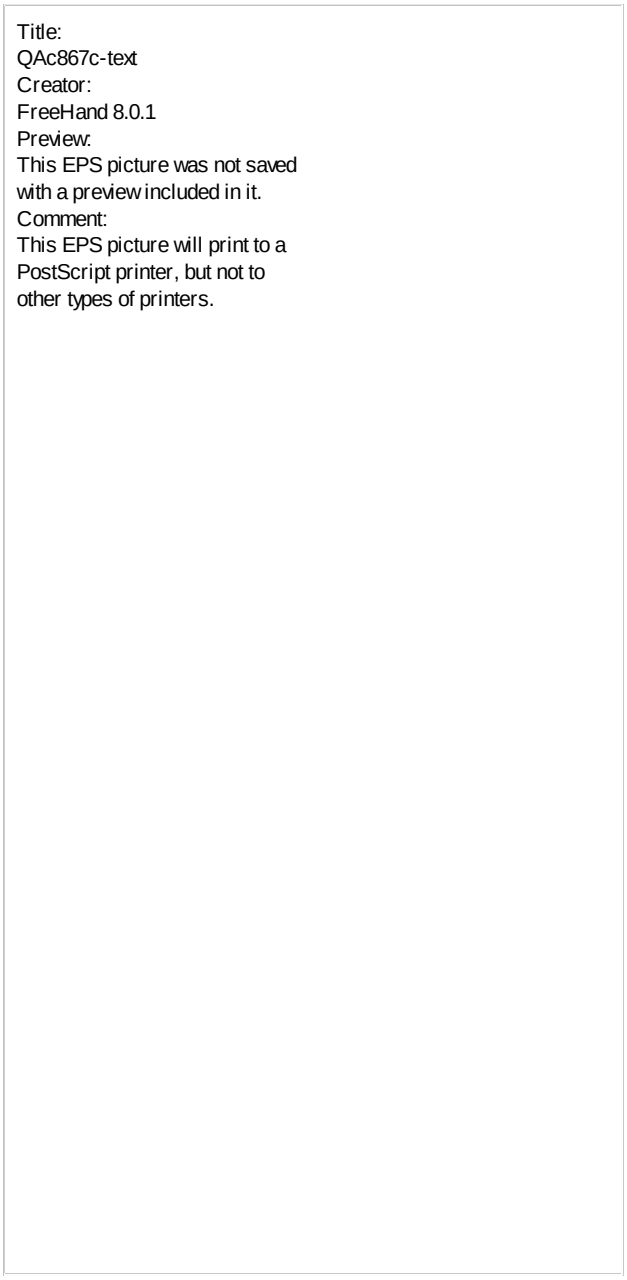


Figure 28. (a) Average W7 deflection and (b) W2:W7 deflection ratio by rock type along Texas 71, Bastrop County.

Central Plains. Ratios for all other geologic units at site E are below 10, indicating materials with low rigidity or deep bedrock (fig. 28b).

***Site F: Texas 16, Jim Hogg and Zapata Counties***

Site F is located in the Rio Grande Valley on the south part of the Gulf Coastal Plains (fig. 4). Average W7 deflections for the counties crossed by this segment of Texas 16 are moderate to high, ranging from 1.1 to 1.5 mils for Jim Hogg County and 1.6 to 2.0 mils for Zapata County (fig. 2). Geologic units mapped along this roadway are variably lithified Cenozoic sedimentary deposits that include Eocene sandstone and clay formations, Miocene to Oligocene mudstones, Pliocene clay, and younger Quaternary wind- and stream-deposited sediments
(fig. 29; appendix B).

Average deflections calculated from FWD data from 89 locations between reference markers 758 and 804 are either the highest or second-highest values calculated for the 6 study segments (table 3). Average W7 deflection is 1.41 mils, a value that is within the deflection range reported for these counties (fig. 2). Individual deflections at all detectors are relatively high, particularly between reference markers 775 and 795, where Catahoula and Frio mudstones and Jackson Group sandstones are mapped (fig. 29). Ranges of individual deflections are large; despite differences in the average deflections for each geologic unit, many individual deflections collected over one rock type fall within a deflection range recorded for another rock type (fig. 30). W7 deflections measured over Jackson Group sandstones range from 0.8 to nearly 3.0 mils, a range that is similar to that measured for Catahoula and Frio mudstones and Laredo sandstones. Lower, but overlapping, W7 deflections are observed for the Goliad Formation (0.5 to 2 mils) and the Quaternary sand sheet (0.7 to 2 mils).

Average deflections for each geologic unit are relatively high at all offsets (fig. 31). The highest average W7 deflections (1.66 to 1.78 mils) are found over unconsolidated Quaternary stream deposits, Jackson sandstones, and Catahoula and Frio mudstones; the lowest average W7 deflections, just above 1 mil, are calculated for segments over areas where Quaternary windblown sands and the Pliocene Goliad Formation are mapped (fig. 32a).

Ratios of W2 to W7 deflections occupy a narrow range between 7.9 and 13.1 (fig. 32b). These relatively low values are similar to ratios calculated over stream deposits in other physiographic regions, indicating that much of the Coastal Plains is underlain by materials of low rigidity. Ratios below 10, indicating the weakest material, were calculated for Quaternary stream deposits, the Yegua Clay, and the Laredo Sandstone. The Pliocene Goliad Formation (W2:W7 = 13) is the most rigid sedimentary deposit at this site.

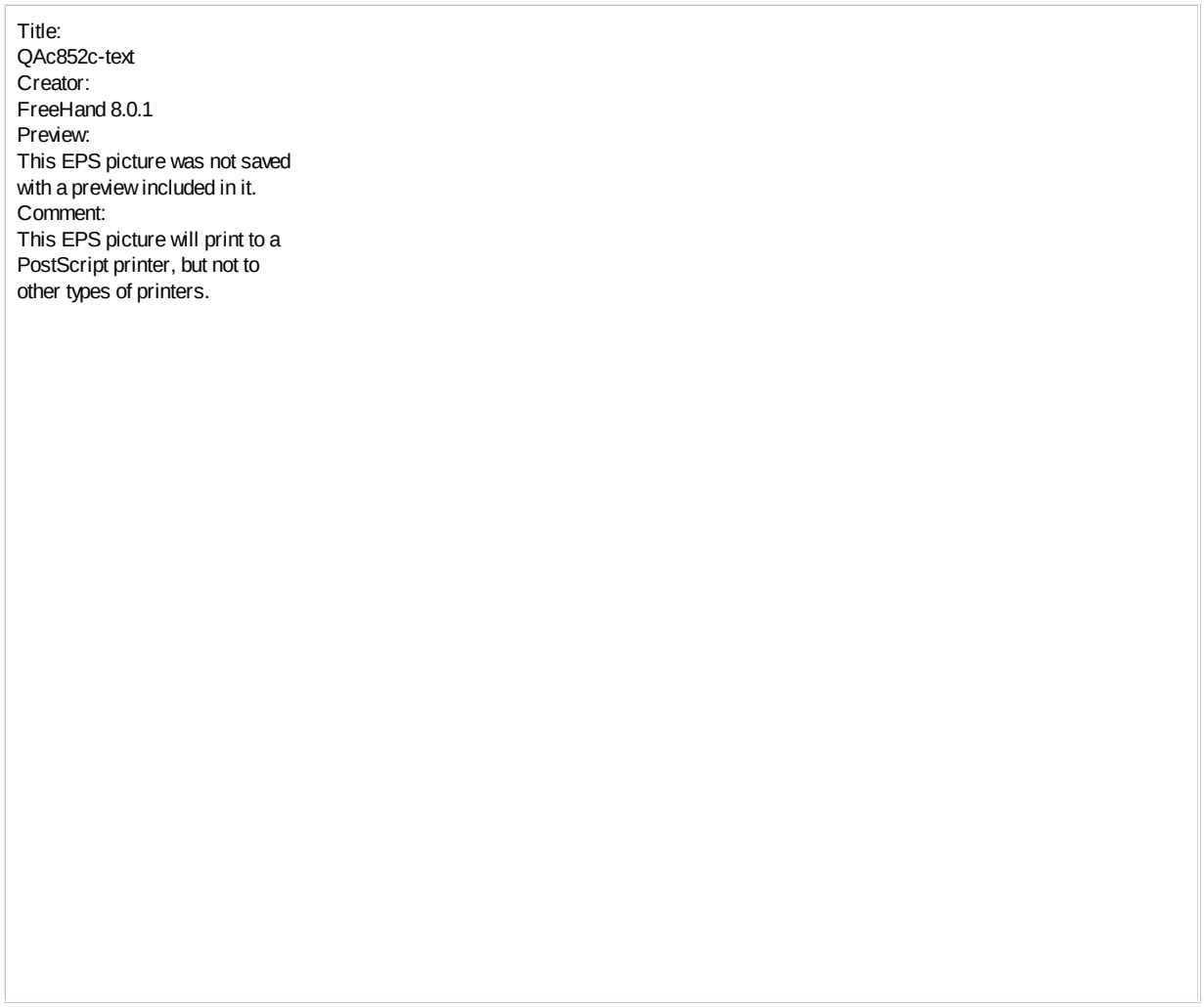


Figure 29. Geologic units, elevation, and W1 through W7 deflections along Texas 16 between reference markers 758 and 804, Jim Hogg and Zapata Counties, South Texas.


Figure 30. Average and individual deflections for rock types mapped along Texas 16 in Jim Hogg and Zapata Counties.


Figure 31. Average deflections for all rock units mapped along Texas 16 in Jim Hogg and Zapata Counties.

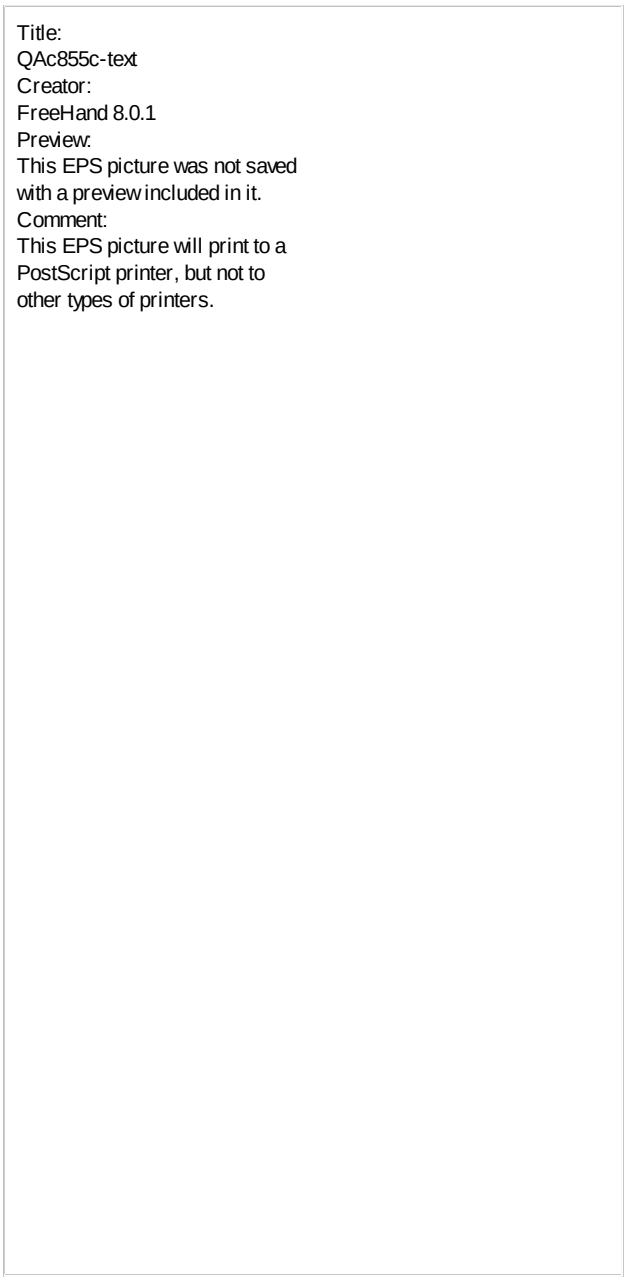


Figure 32. (a) Average W7 deflection and (b) W2:W7 deflection ratio by rock type along Texas 16, Llano and Gillespie Counties.

## COMBINED SITE RESPONSE

Average FWD response for principal rock types can be examined by grouping individual geologic units into these basic types regardless of physiographic region. Principal rock types mapped in the Central Texas Uplift, North-Central Plains, Edwards Plateau, and Gulf Coastal Plains regions are (1) unconsolidated sedimentary deposits, (2) sandstones, (3) mudstones, (4) limestones, (5) granites, and (6) metamorphic gneisses and schists. Each geologic unit mapped at FWD sites along the six test segments can be classified as one of these principal geologic types.

W7 averages and W2:W7 ratios for each individual rock type define ranges of observed values for the principal rock types (fig. 33). FWD response along roadways built over igneous and metamorphic rock types such as granite, gneiss, and schist have low average W7 deflections (0.5 to 0.9 mils) and high to very high W2:W7 ratios (more than 17) compared with other rock types. Siliciclastic sedimentary units such as sandstone and mudstone have similarly low W2:W7 ratios between 9 and 15, but sandstone tends to have smaller average W7 deflections than does the less consolidated mudstone. Unconsolidated sediments, including Quaternary alluvium and older uncemented sand and gravel, exhibit a wide range of W7 deflections (0.6 to 2.3 mils) along with very low W2:W7 ratios (6 to 14) that are similar to those observed for lithified siliciclastic rocks. Although sandstone, mudstone, and unconsolidated sedimentary deposits have similar W2:W7 ratios, average W7 deflections, which are generally highest for unconsolidated deposits and lowest for sandstones, provide a basis for discriminating these types.

FWD response along highways underlain by limestone is perhaps the most variable of all the principal rock types (fig. 33). Some limestone units have the lowest observed W7 deflections (below 0.5 mils) and high W2:W7 ratios (15 to 27); other limestone units have W7 deflections as much as 1.8 mils and W2:W7 ratios as low as 5, values that are comparable to those of siliciclastic units. These higher W7 deflections and lower W2:W7 ratios probably indicate either common clay-rich units within larger sections of limestone, weathered limestone, or greater depth to bedrock.


Figure 33. Average W7 deflection and W2:W7 deflection ratio for individual rock types mapped along the Texas 16, U.S. 290, and Texas 71 test sites.

## BEDROCK DEPTHS FROM SEISMIC REFRACTION

We collected seismic-refraction data at three sites (fig. 2) to prove the concept of collecting refraction data in highway settings, to investigate the usefulness of the data in determining bedrock depth to support deflection analysis, and to optimize equipment and acquisition parameters to balance operational simplicity with the collection of interpretable data. Knowing bedrock depths at a given site enables one to address the ambiguity of whether bedrock type or depth is the source of the correlation between geologic unit and road deflection.

### PICKLE RESEARCH CAMPUS SITE

We acquired seismic-refraction data in September 1997 along Road D on the J. J. Pickle Research Campus (PRC) at The University of Texas at Austin (table 2). Road D is an asphalt-pavement road laid on an unknown thickness of road base over residual sediments and lower Cretaceous limestone of the Austin Group (Garner and Young, 1976).

Several seismic wave types are evident in a field record collected at PRC using the FWD as a seismic source (fig. 34). Types of ground motion detected by the geophones during the first 60 ms following impact of the FWD weight with the pavement include (1) high-amplitude, low-frequency, and slowly propagating surface waves (lower left of field record, less than 280 m/s propagation velocity); (2) a direct wave, which is the first recorded signal at geophones that are less than 4 m from the source; (3) a critically refracted arrival, representing the first recorded signal at geophones greater than 4 m from the source (3,000 m/s propagation velocity), and (4) a reflected wave that has a hyperbolic shape, arriving at approximately 20 ms at the source location and approximately 30 ms at the maximum offset. Spectral analyses of ground motion detected by near-source geophones indicate that the FWD produces an impulse with frequencies between about 20 and 200 Hz, which is a useful range for shallow seismic investigations.

In refraction analysis, the direct arrival represents a compressional wave traveling from the source to the geophone without appreciable refraction through a surface layer. The surface layer has a wave velocity equal to the propagation velocity calculated from the direct wave's arrival time at each detector. The critically refracted wave represents a compressional wave that travels through the surface layer and is refracted along the interface between the surface layer and an underlying, higher velocity material (bedrock in this instance). The refracted wave travels at the velocity of the underlying material, generating wavefronts as it propagates along the boundary. The refraction-generated wavefronts subsequently reach the surface and are recorded by the geophones. To calculate the depth of the layer that refracts the compressional wave, we pick the arrival times of the direct and critically refracted waves, calculate an apparent velocity for the direct and refracted waves, and extrapolate the arrival time of the refracted arrival to a position

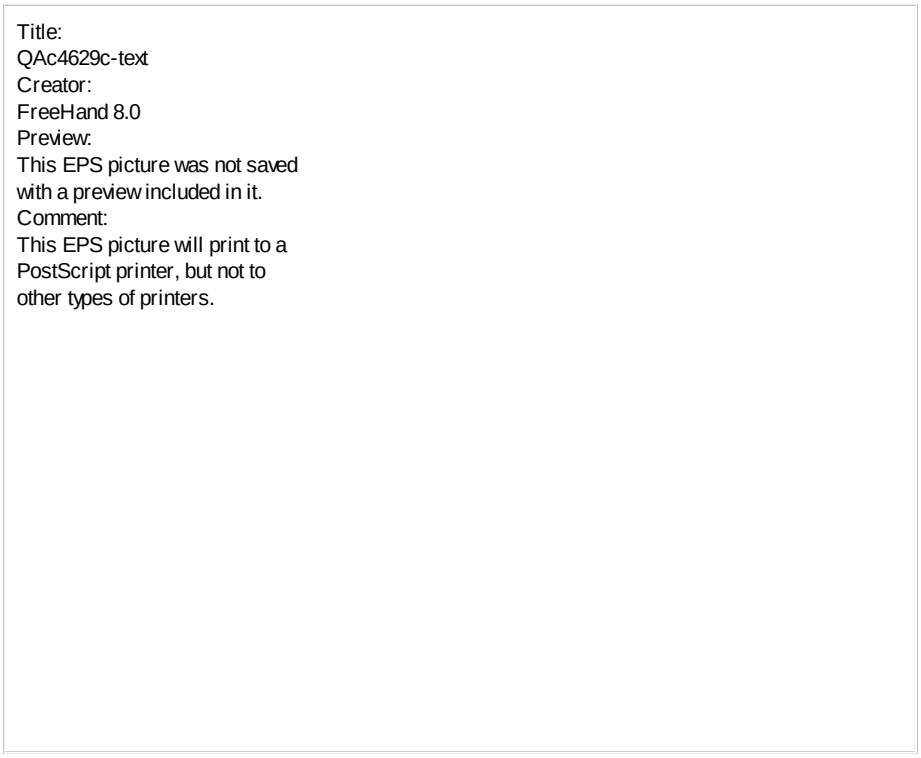


Figure 34. Seismic response recorded with a 48-geophone spread using the FWD as a seismic source. Visible phases include the direct arrival, a critically refracted arrival from the underlying rigid layer, long-wavelength, low-frequency surface waves, and reflected compressional waves. Data recorded on a flexible-pavement road on the J. J. Pickle Research Campus, The University of Texas at Austin.

beneath the source (zero offset). Because we were uncertain how well the beginning of the seismic record matches the impact of the FWD with the pavement, we did not calculate layer depths using the FWD source.

***Refraction Experiment PRC SPH1***

In this refraction test, both the soil-probe hammer source and the 48 geophones were located on the south shoulder of PRC Road D (fig. 6; tables 2 and 4). Displays of filtered and amplified seismic energy from impulses at the west and east ends and the center of the recording spread

(fig. 35) reveal the presence of a slowly propagating direct arrival at geophones nearest the source and a faster, critically refracted arrival at geophones farther from the source. First-arrival times for each trace can be plotted against distance from the source and segregated into arrivals measured when the source was west of the geophone (arbitrarily assigned the forward direction, fig. 36) and when the source was east of the geophone (the reverse direction).

In the forward direction, arrivals can be grouped by offset range into two linear segments (fig. 36). The group located closest to the source (between 0 and about 6 m forward offset) is interpreted to be arrivals from the direct wave. Arrivals at greater offsets belong to the compressional wave that is critically refracted by a higher velocity layer at some depth beneath the surface, which may be bedrock or some other rigid layer. If a line is fit to these arrival times, the inverse of its slope (in m/s) is the apparent velocity of the critically refracted wave. Extrapolating this line to an offset distance of 0 gives the intercept time, which is used along with the direct and refracted velocities to calculate the depth of the refractor. Arrivals in the reverse direction can be interpreted similarly, but calculated velocities and intercept times may differ from those calculated in the forward direction.

Rather than qualitatively choosing arrival-time layer assignments by viewing a time-versus-distance plot (fig. 36), velocity-versus-distance and intercept-time-versus-distance relationships allow rigorous definition of layer assignments for forward- and reverse-propagation directions (figs. 37 and 38). By calculating best-fit velocities progressively (gradually increasing the offset range included in the calculation), the effect of changing the layer assignments can be quantified and the optimal offset range can be chosen (figs. 37a and 38a). Similarly, the effect of changing offset ranges on calculated intercept times can be assessed (figs. 37b and 38b). Ideally, cutoff distances between arrivals assigned to the direct wave and arrivals assigned to the critically refracted wave can be consistently chosen in this manner.

In the forward direction, calculated velocities for arrivals between the source and increasingly distant geophones (fig. 37a) increase to about 500 m/s by 1-m offset and remain near that velocity to an offset distance of 3 m. Including arrival times from more distant

geophones in the velocity calculation causes the velocities to progressively increase with distance, suggesting

Table 4. Summary of refraction data collected at the J. J. Pickle Research Campus (PRC) and the Jacksboro site. Velocity, depth, and apparent dip calculated using the slope-intercept method (Palmer, 1986).

| | Pickle Research Campus | | Jacksboro | Granite Shoals |
|---|---|---|---|---|
| Forward direction | West to east | | South to north | West to east |
| Shot sequence | PRC SPH1 | PRC SPH2 | Jacksboro SPH1 | Granite Shoals |
| Source surface | Shoulder | Pavement | Pavement | Pavement |
| Sensor surface | Shoulder | Shoulder | Pavement | Pavement |
| Layer 1 velocity (m/s) | | | | |
| Forward | 499.5 | 602.2 | 584.5 | 533.4 |
| Reverse | 506.8 | 475.2 | 556.0 | 450.7 |
| Calculated | 503.1 | 531.2 | 569.9 | 488.6 |
| Layer 2 velocity (m/s) | | | | |
| Forward | 3,795.6 | 3,475.6 | 2,083.7 | 2492.3 |
| Reverse | 2,911.4 | 3,042.4 | 3,546.3 | 4661.8 |
| Calculated | 3,294.5 | 3,244.4 | 2,620.6 | 3244.6 |
| Intercept time (s) | | | | |
| Forward | 0.0089 | 0.0074 | 0.0066 | 0.0096 |
| Reverse | 0.0087 | 0.0073 | 0.0109 | 0.0117 |
| Layer 1 thickness (m) | 2.26 | 2.00 | 1.92 | 2.36 |
| Apparent dip (degrees) | 1.2 west | 0.6 west | 3.3 north | 2.6 west |

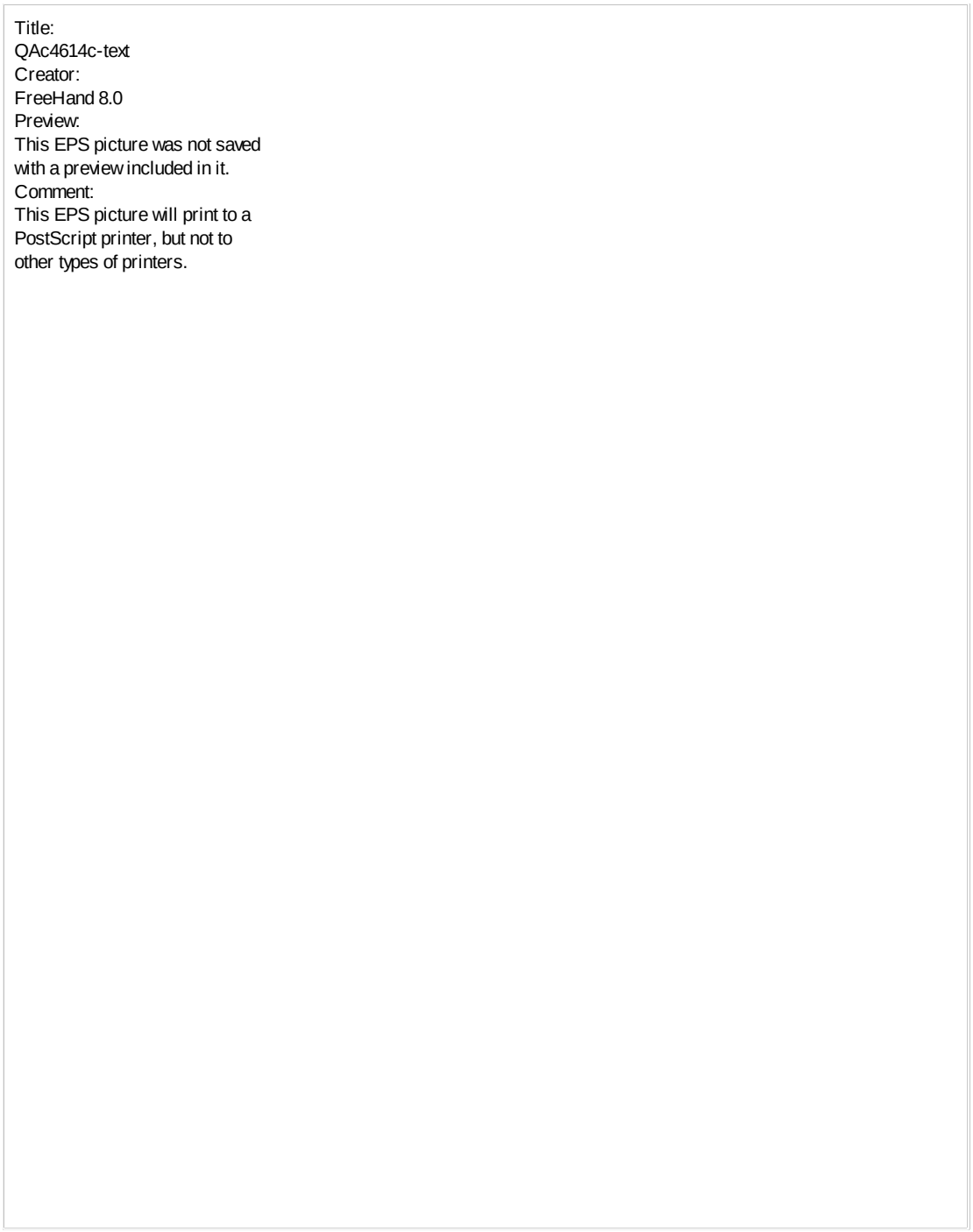


Figure 35. Field records from refraction test PRC SPH1 (site R1, fig. 2) using a soil-probe hammer as a seismic source. Source was located on the shoulder of Road D at the (a) west end, (b) east end, and (c) center of the recording spread. Records displayed with a 125-Hz low-cut filter and time-varying gain (20-ms window) applied. Geophone spacing is 0.3 m.

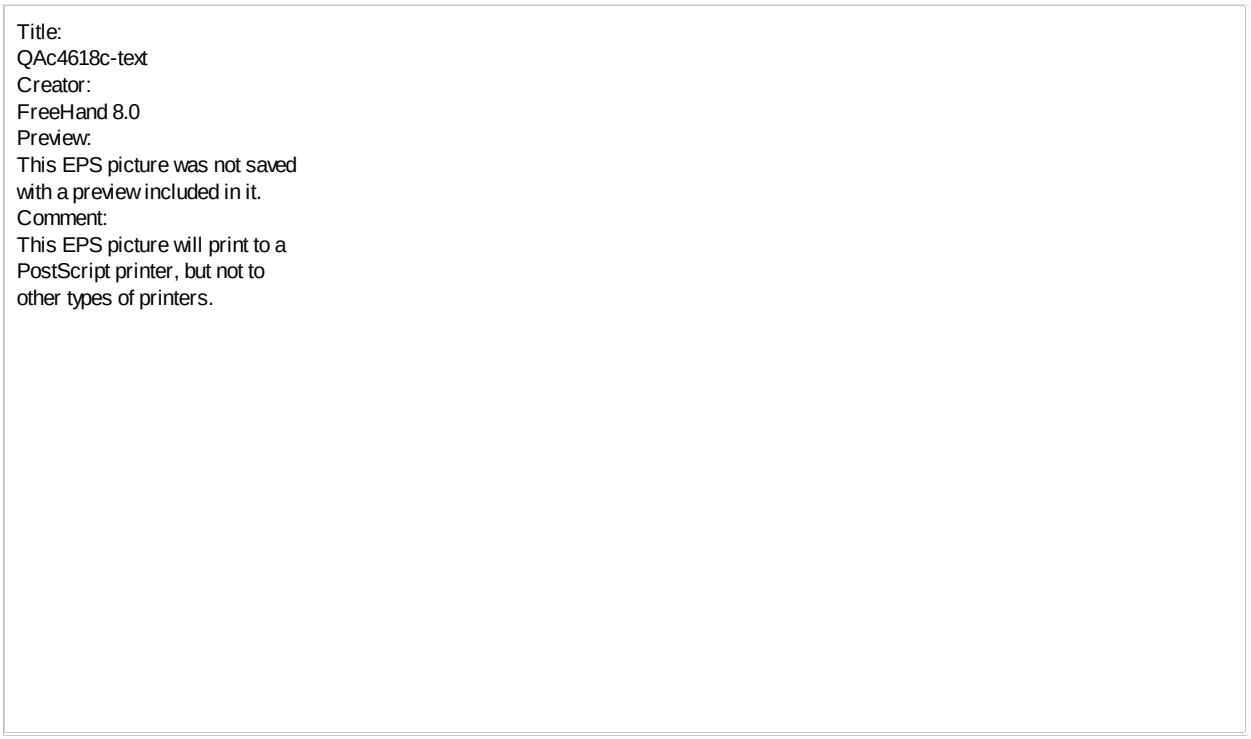


Figure 36. First-arrival times for refraction test PRC SPH1 for forward- (eastward-) and reverse- (westward-) propagating waves.

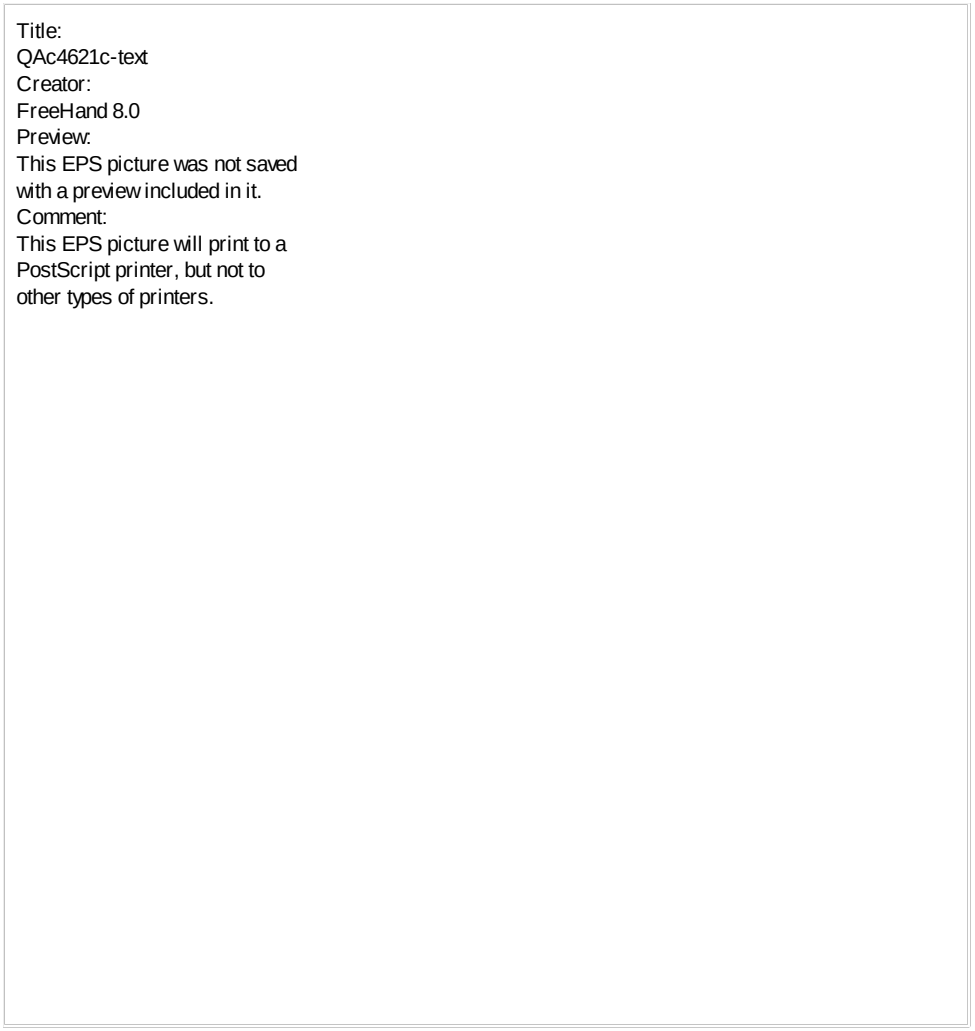


Figure 37. (a) Apparent velocity and (b) zero-offset time for forward data from refraction test PRC SPH1. Velocities and intercepts calculated by assigning arrivals from various offset ranges to the direct or refracted arrival. Velocities and intercepts (black boxes) calculated from arrivals at geophones located between the source and progressively increasing source–receiver distances are used to pick the optimal velocity and offset range for arrivals assigned to the direct wave. Velocities and intercepts (open boxes) calculated from arrivals at geophones located between the maximum source–receiver distance and progressively decreasing source–receiver distances are used to pick the optimal velocity, intercept time, and offset range for arrivals assigned to the critically refracted wave.


Figure 38. (a) Apparent velocity and (b) zero-offset time for reverse data from refraction test PRC SPH1. Velocities and intercepts calculated by assigning arrivals from various offset ranges to the direct or refracted arrival.

that only arrivals between the source and 3 m belong to the direct arrival. This interpretation is confirmed by calculating zero-offset intercept times (fig. 37b), which begin increasing from the expected value of 0 s when arrivals from geophones at source–receiver distances greater than 3 m are included in the calculation. By assigning all arrivals at offsets of 3 m or less to the direct wave, a layer 1 velocity of 500 m/s is calculated (table 4).

To make layer 2 assignments in a two-layer setting such as that evident from the PRC SPH1 shot records and arrival times (figs. 35 and 36), velocity and intercept time can be calculated using arrival times from geophones between the maximum source–receiver distance and those progressively closer to the source. For PRC SPH1 forward data, calculated velocities reach a maximum when arrivals at geophones at distances greater than about 6 m are included in the calculation (fig. 37a). Calculated intercept times increase with increasing minimum source–receiver distance (fig. 37b), suggesting that arrivals at geophones less than about 6 m from the source belong to the direct wave or an intermediate refractor. Using arrival times from geophones at distances greater than 6 m results in a calculated apparent velocity of 3,796 m/s and an intercept time of 0.0089 s (table 4) for the forward data.

For seismic energy propagating from east to west (reverse data), time and distance plots (fig. 36) suggest a crossover distance separating direct from refracted arrivals of near 6 m. Calculated velocities for arrivals at geophones located nearest the source increase to 500 m/s by a distance of 1 m from the source, remaining at that velocity to a maximum source–receiver distance of 5 m (fig. 38a). Intercept times, which should be zero for direct-wave arrivals, begin increasing as source–receiver distances increase beyond 5 m (fig. 38b). Non-zero intercepts for the reverse data suggest either a slight delay (<0.001 s) between the source impact and the onset of recording, or the presence of a very shallow, low-velocity refractor. The velocity calculated for layer 1 in the reverse direction is 507 m/s, only slightly higher than that calculated for the forward direction (table 4).

The apparent velocity of the critically refracted arrival reaches a plateau when arrivals from geophones beyond 7 m from the source are included in the velocity calculation (fig. 38a). Higher velocities calculated for greater threshold distances suggest that arrivals from deeper, higher velocity layers have been included in the analysis. Using 7 m as the cutoff distance, the apparent velocity of the critically refracted wave is 2,911 m/s. Its extrapolated intercept time is 0.0087 s (table 4).

To use the slope-intercept method (Palmer, 1986) to calculate refractor depth beneath the shoulder of Road D, we must know apparent velocities for the direct and critically refracted arrivals in the forward and reverse directions and the intercept times for the critically refracted arrivals. Using the values mentioned above, we calculate the true direct-wave velocity (layer 1) to be 503 m/s, the true layer 2 velocity to be 3,295 m/s, and the thickness of layer 1 to be 2.26 m

(table 4). The interface between layers 1 and 2 has an apparent dip of 1.2° westward. Calculated depths to layer 2 are 2.27 m below at the west end and 2.21 m at the east end of the recording spread (fig. 39a).

***Refraction Experiment PRC SPH2***

The site and acquisition parameters are the same for this experiment as they were for PRC SPH1 (tables 2 and 4), except that the soil-probe hammer was offset from the receiver spread on the paved road rather than being on the unpaved shoulder (fig. 6). The geophones remained embedded in the shoulder.

Filtered and amplified ground motion recorded by the geophones with the source located at the west end, east end, and center of the recording spread (fig. 40) is similar to that recorded for experiment PRC SPH1. Recorded wave types include surface waves and direct, critically refracted, and reflected compressional waves. The first ground motion reaches the geophones within 15 ms of the impact of the source on the pavement. These first arrivals in the forward- and reverse-propagation directions are assigned to the direct wave between the source position and a point about 8 m from the source, and to the critically refracted wave at source–receiver distances longer than about 8 m (fig. 41). A line extending through the arrivals assigned to the direct wave passes near the intersection of the axes, whereas a line extending through the critically refracted arrivals has a nonzero intercept time.

Apparent velocities and intercept times necessary for calculating layer velocities and thicknesses were determined using velocity and intercept plots. For forward data, in which the source is west of the recording geophones, apparent velocities remain near 500 m/s and intercept times near 0 s when geophones between the source and a distance as great as 6 m are included in the calculation (fig. 42a and b). Including geophones at greater distances causes the calculated apparent velocity and intercept time to increase, suggesting that the direct wave is the first arrival only out to a distance of about 6 m. When the minimum source–receiver distance is progressively increased, calculated apparent velocities increase from about 1,000 m/s using all geophones to about 3,500 m/s using geophones greater than 7 m from the source (fig. 42a). Intercept times are between 0.007 and 0.008 s where minimum distances are between 6 and 10 m (fig. 42b), suggesting that arrivals at 7 m and greater source–receiver distance can be attributed to the first critically refracted wave.

For reverse data, in which the source is east of the recording geophones, apparent velocities reach 500 m/s using arrival times measured at geophones between the source and a distance of 1.5 m (fig. 43a). Apparent velocities gradually increase when geophones beyond a 2-m source–receiver distance are included in the calculation. Intercept times calculated for the near-source geophones reach a minimum of near -0.001 s when geophones closer than 2 m from the

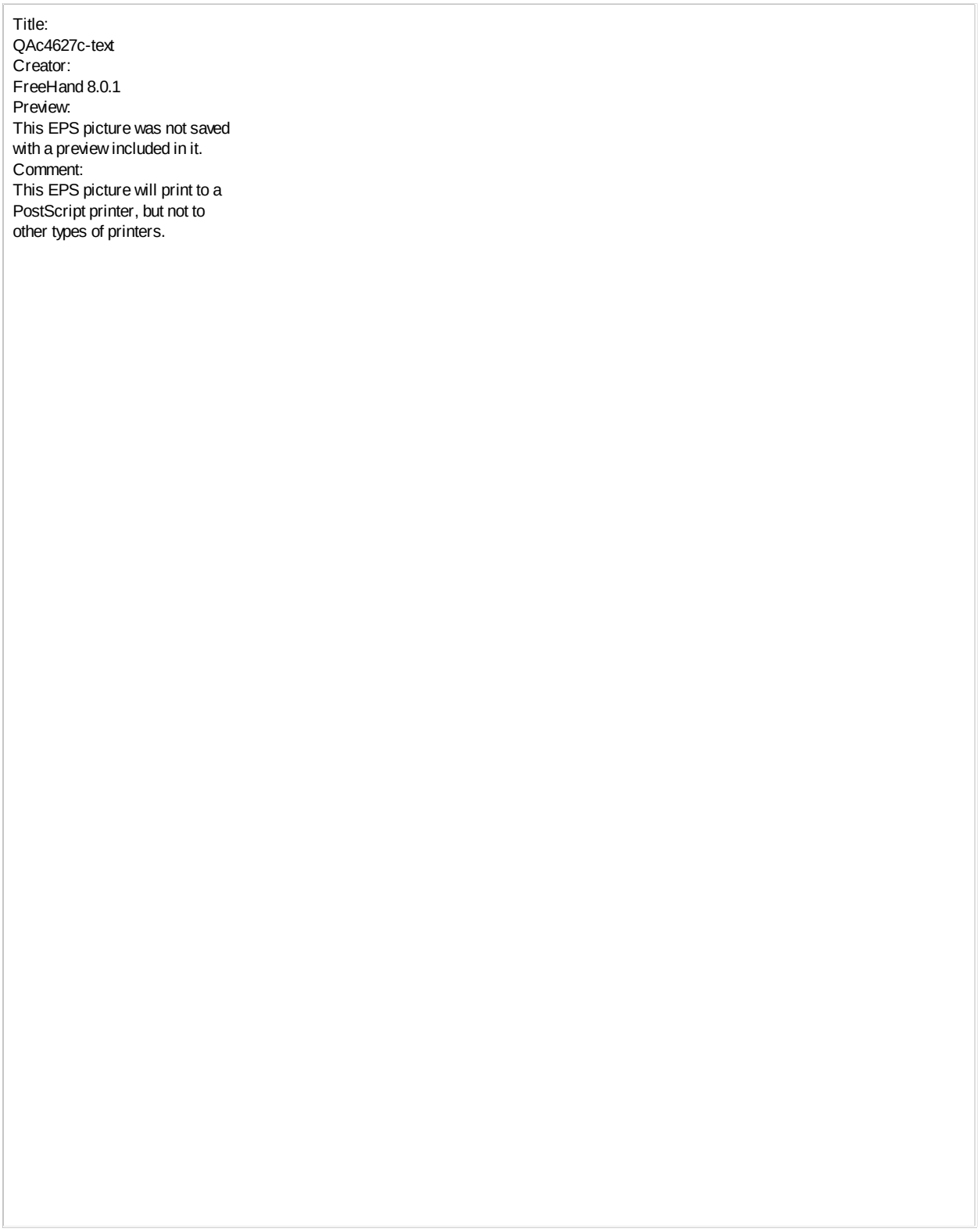


Figure 39. Calculated layer velocities and thicknesses and apparent dips of layer interfaces for refraction tests (a) PRC SPH1, (b) PRC SPH2, and (c) Jacksboro SPH1.


Figure 40. Field records from refraction test PRC SPH2 (site R1, fig. 2) using a soil-probe hammer as a seismic source. Source was located on the pavement of Road D at the (a) west end, (b) east end, and (c) center of the recording spread. Records displayed with a 125-Hz low-cut filter and time-varying gain (20-ms window) applied. Geophone spacing is 0.3 m.

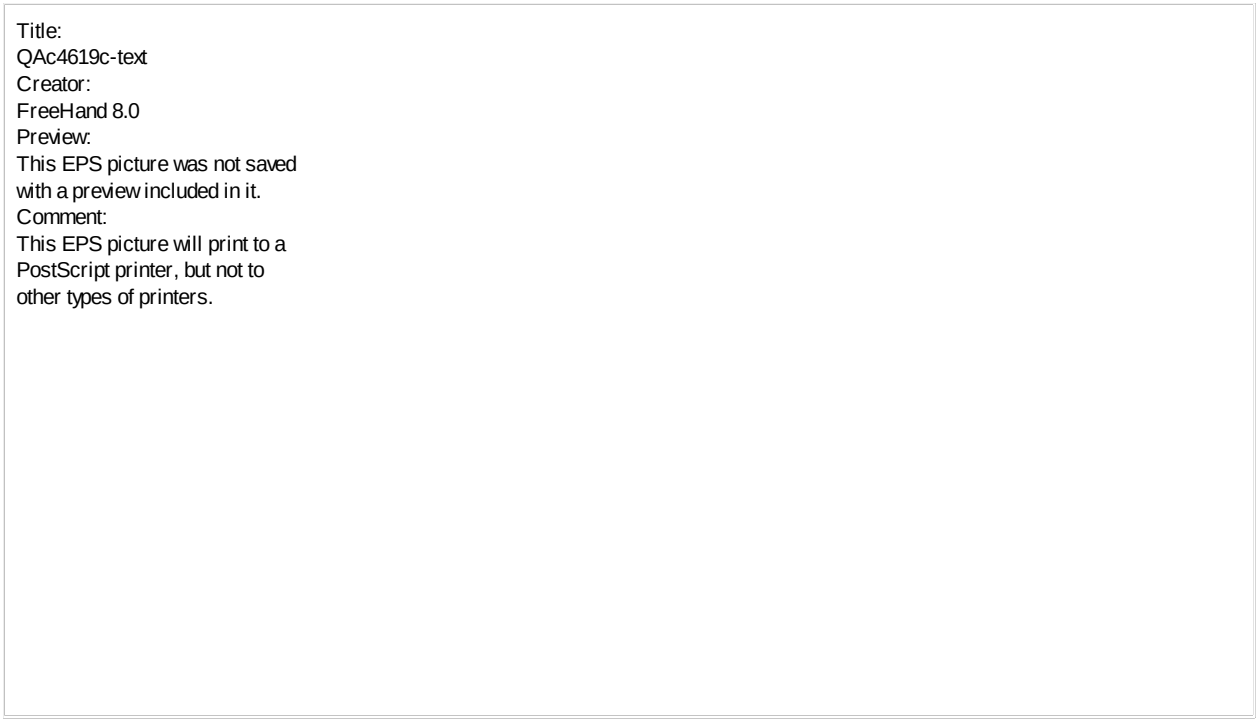


Figure 41. First-arrival times for refraction test PRC SPH2 for forward- (eastward-) and reverse- (westward-) propagating waves.

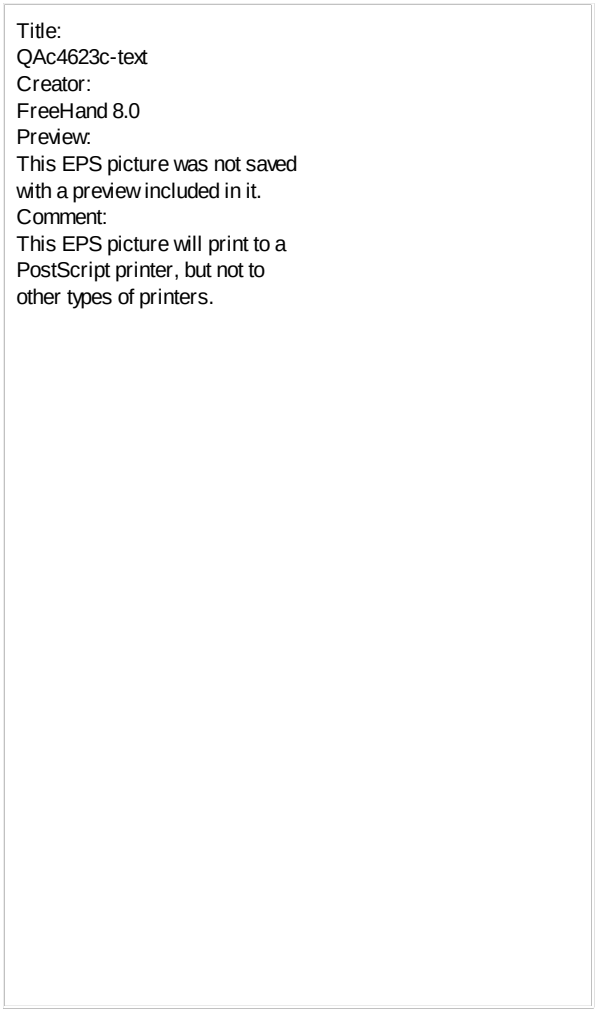


Figure 42. (a) Apparent velocity and (b) zero-offset time for forward data from refraction test PRC SPH2. Velocities and intercepts calculated by assigning arrivals from various offset ranges to the direct or refracted arrival.

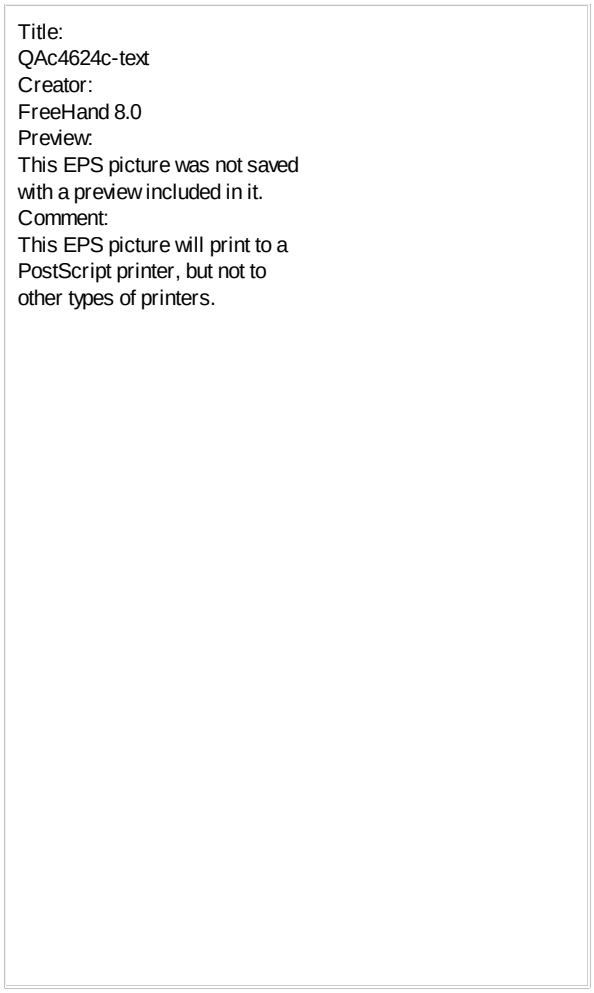


Figure 43. (a) Apparent velocity and (b) zero-offset time for reverse data from refraction test PRC SPH2. Velocities and intercepts calculated by assigning arrivals from various offset ranges to the direct or refracted arrival.

source are included (fig. 43b), suggesting either inconsistent arrival picks or a late recording onset. Using arrival times at all geophones, the calculated apparent velocity is near 1,000 m/s (fig. 43a). Apparent velocities and intercept times increase as the minimum source–receiver distance increases, reaching a minor plateau at about 3,000 m/s and between 0.007 and 0.008 s when geophones at distances greater than 7 to 9 m are included (figs. 43a and b).

The velocity calculated for the direct arrival is 531 m/s, which is the velocity of layer 1 (table 4). Because the interface between layers 1 and 2 has a small apparent dip to the west, the apparent layer 2 velocity is higher in the forward direction (eastward propagation) than it is in the reverse direction (westward propagation). Layer 2 velocity, which represents the propagation speed of the critically refracted wave, is calculated to be 3,244 m/s, similar to that obtained in experiment PRC SPH1 (table 4). Using the intercept times of 0.0074 s at the west end of the spread and 0.0073 s at the east end of the recording spread, depths to layer 2 are 1.99 m at the west end and 1.97 m at the east end (fig. 39b).

### *Interpreted Strata*

Measured layer 1 compressional-wave velocities of about 500 m/s are within the 300 to 900 m/s range reported for dry, unconsolidated material (Press, 1966; Wylie, 1969), suggesting that layer 1 consists largely of road base and residual or surficial sediments above the bedrock contact. Higher velocities measured for layer 2, reaching nearly 3,250 m/s, are consistent with those expected for relatively soft limestone (Press, 1966) such as the Cretaceous Austin Chalk. The Austin Chalk is the mapped geologic unit at the site (Garner and Young, 1976) and is exposed in nearby ditches.

## JACKSBORO MLS SITE

In May 1998, we acquired seismic-refraction data on U.S. Highway 281 south of Jacksboro, Texas (figs. 2 and 6; table 2). Data were acquired with seismic sources and geophones on the southbound inner-lane pavement at a former location of TxDOT's MLS. Geologic maps of the site show the Pennsylvanian Ranger Limestone as the surface geologic unit (Hentz and Brown, 1987); a thin veneer of surficial sediments mantles the Ranger Limestone in fields adjacent to the highway. An FWD and the soil-probe hammer were both tested as on-pavement sources, but the FWD did not produce a sharp trigger impulse for the seismograph. This caused unacceptably large errors in establishing zero time.

### *Effect of Digital Filtering*

Data quality is generally similar at the Jacksboro and PRC sites (compare figs. 44d and 35a). Noise levels are somewhat higher at the Jacksboro site because of increased road traffic and poorer coupling between the ground and the geophones, but data quality is sufficient to detect direct and critically refracted arrivals. Accurate picking of arrival times is enhanced by digitally filtering and amplifying the recorded signals (fig. 44). Low-frequency and high-amplitude surface waves dominate the field record without filtering or amplification (fig. 44a), but direct and critically refracted arrivals are apparent in the record. Application of time-varying gain balances the amplitude along each segment of a geophone trace and makes first breaks easier to see (fig. 44b), yet low-frequency seismic noise visible in the early part of the record makes accurate picking of arrival times difficult. Applying a digital filter that removes seismic energy with frequencies below 125 Hz removes much of the low-frequency noise, revealing the presence of a weaker, earlier arrival than the critically refracted arrival evident in the unfiltered record (fig. 44c). Balancing the amplitude of the filtered record using time-varying gain does not greatly aid the picking of first arrivals but does reveal the presence of reflected seismic energy later in the field record (fig. 44d). Filtered and amplified field records were used for refraction analysis at the Jacksboro site, where vertical ground motion was detected after seismic impulses were generated at the south end, north end, and center of the recording spread (fig. 45).

### *Refraction Analysis*

First-arrival times picked for the forward and reverse end shots and for the reverse part of the center shot form two groups, each with a linear trend (fig. 46). For the forward data, in which the seismic source was south of the recording geophones, near-source geophones (5 m or less from the source) record direct seismic waves that have an apparent velocity of about 585 m/s (table 4; fig. 47a) and intercept the time axis at 0 s (fig. 47b). Including geophones at longer source–receiver distances results in increasing apparent velocities and nonzero intercept times. The critically refracted wave is the first arrival at source–receiver distances greater than approximately 7 m. Including all geophones 7 m and farther from the source in the velocity and intercept calculation, the apparent velocity of the critically refracted wave is 2,084 m/s (fig. 47a; table 4) and its intercept time is 0.0066 s (fig. 47b).For the reverse data, in which the source was north of the recording geophones, apparent velocity decreases as the maximum included source–receiver distance increases to about 6 m, remains relatively constant to a maximum included distance of about 9 m, and increases as geophones beyond a 9-m source–receiver distance are included (fig. 48a). Over this same distance range, intercept times decrease to near zero

when arrival times at geophones at source– receiver distances less than 5 to 9 m are included


Figure 44. Effect of digital filtering and amplification on a field record from the Jacksboro MLS site (site R2, fig. 2) using a soil-probe hammer as a seismic source. Record displayed with (a) neither digital filtering nor time-varying gain; (b) time-varying gain (20-ms window) but no digital filtering; (c) 125-Hz low-cut filter without time-varying gain; and (d) 125-Hz low-cut filter and time-varying gain (20-ms window) applied. Geophone spacing is 0.5 m.

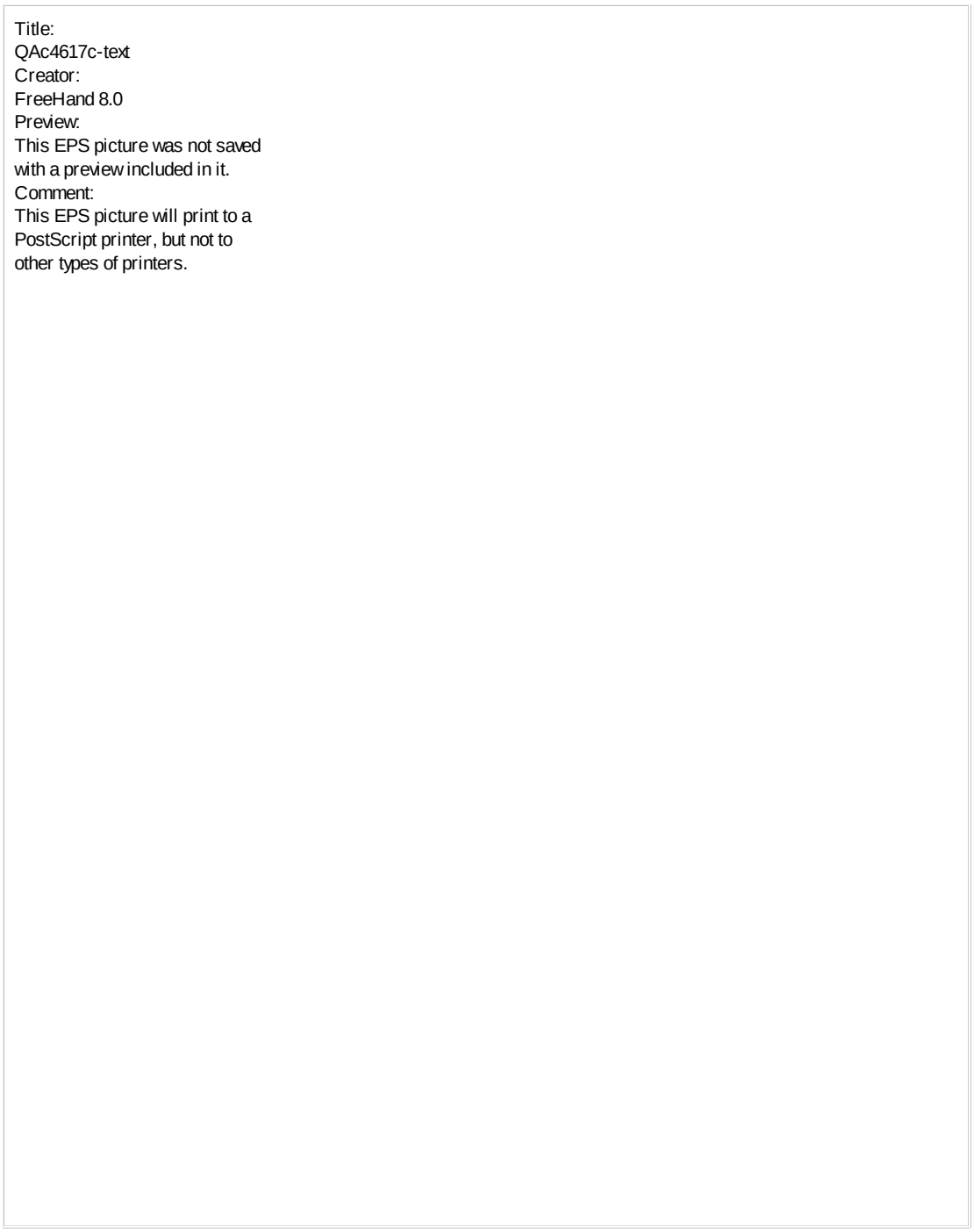


Figure 45. Field records from refraction test Jacksboro SPH1 using a soil-probe hammer as a seismic source. Source and geophones were located on the pavement of U.S. Highway 281. Source was at the (a) south end, (b) north end, and (c) center of the recording spread. Records displayed with a 125-Hz low-cut filter and time-varying gain (20-ms window) applied. Geophone spacing is 0.5 m.

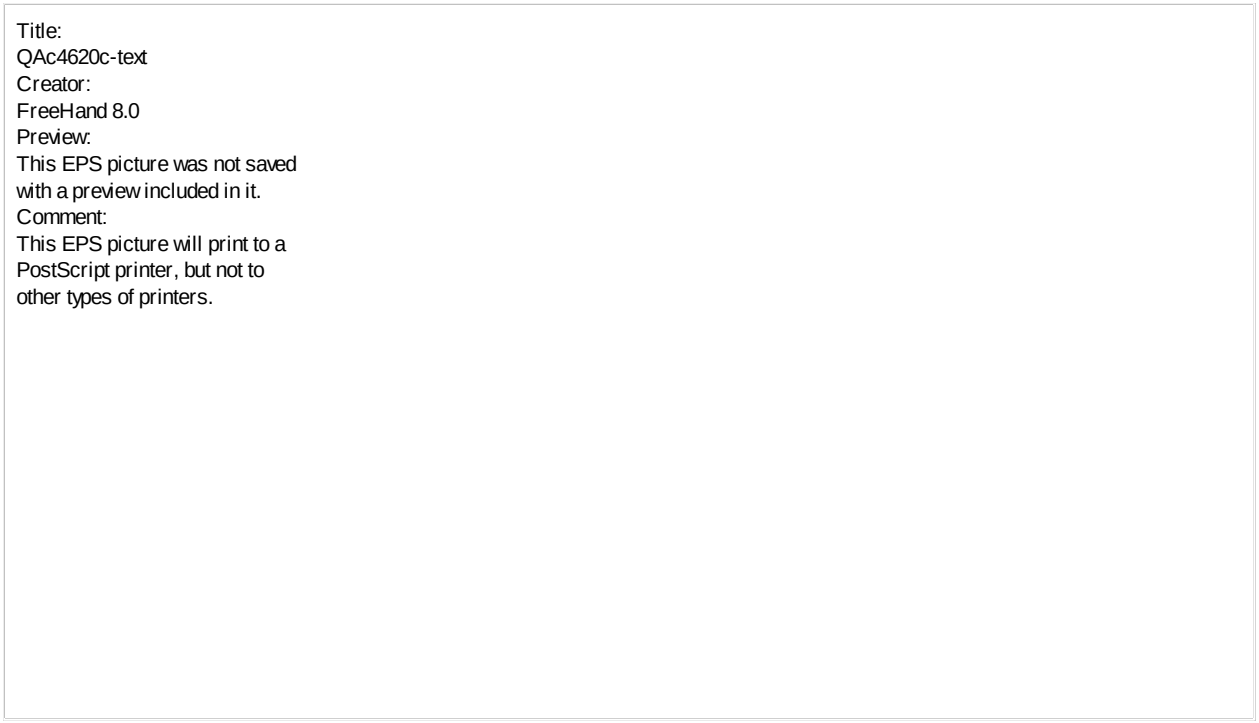


Figure 46. First-arrival times for refraction test Jacksboro SPH1 for forward- (northward-) and reverse- (southward-) propagating waves.

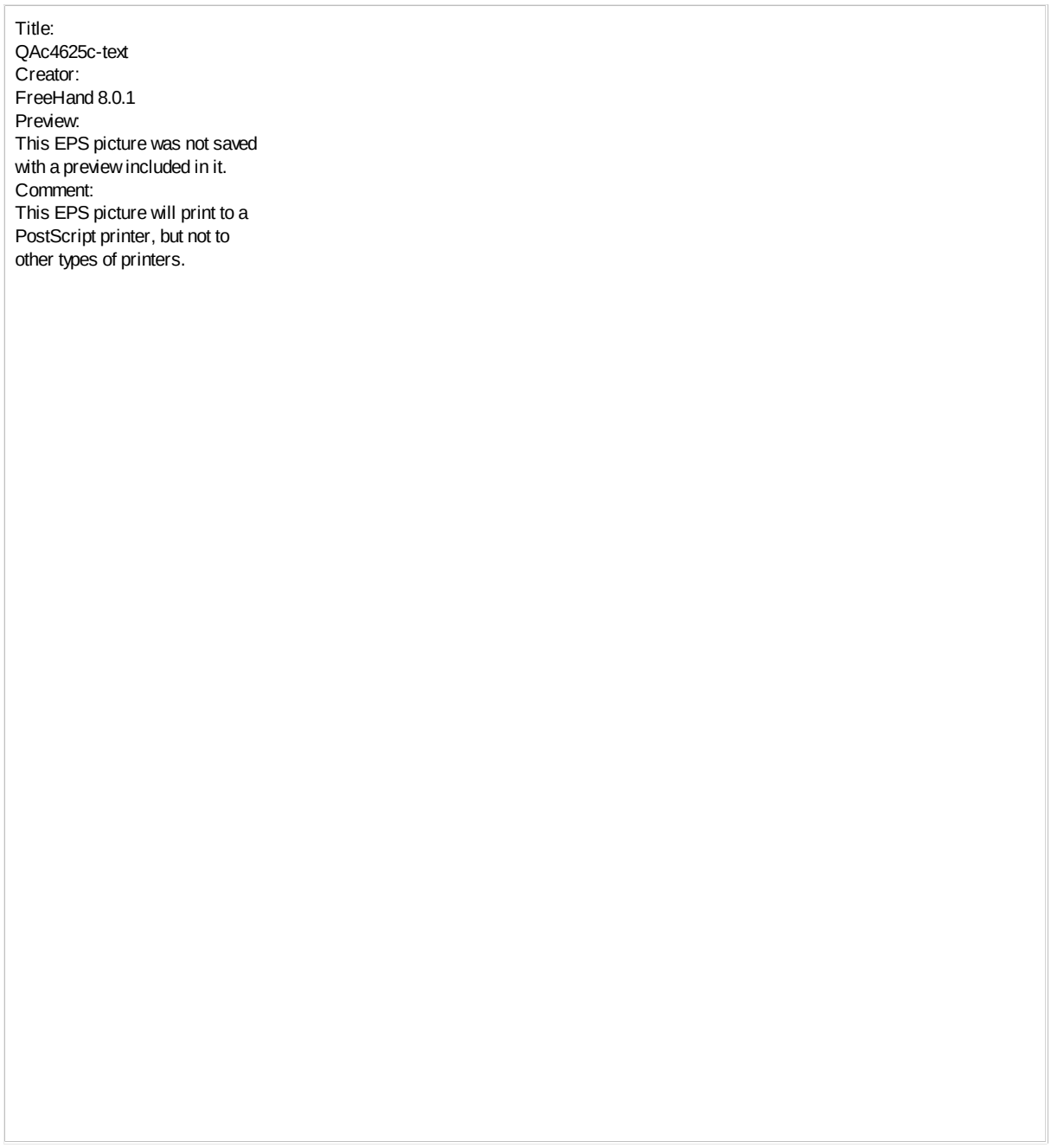


Figure 47. (a) Velocity and (b) intercept plots for forward data from refraction test Jacksboro SPH1. Velocities and intercepts calculated by assigning arrivals from various offset ranges to the direct or refracted arrival.

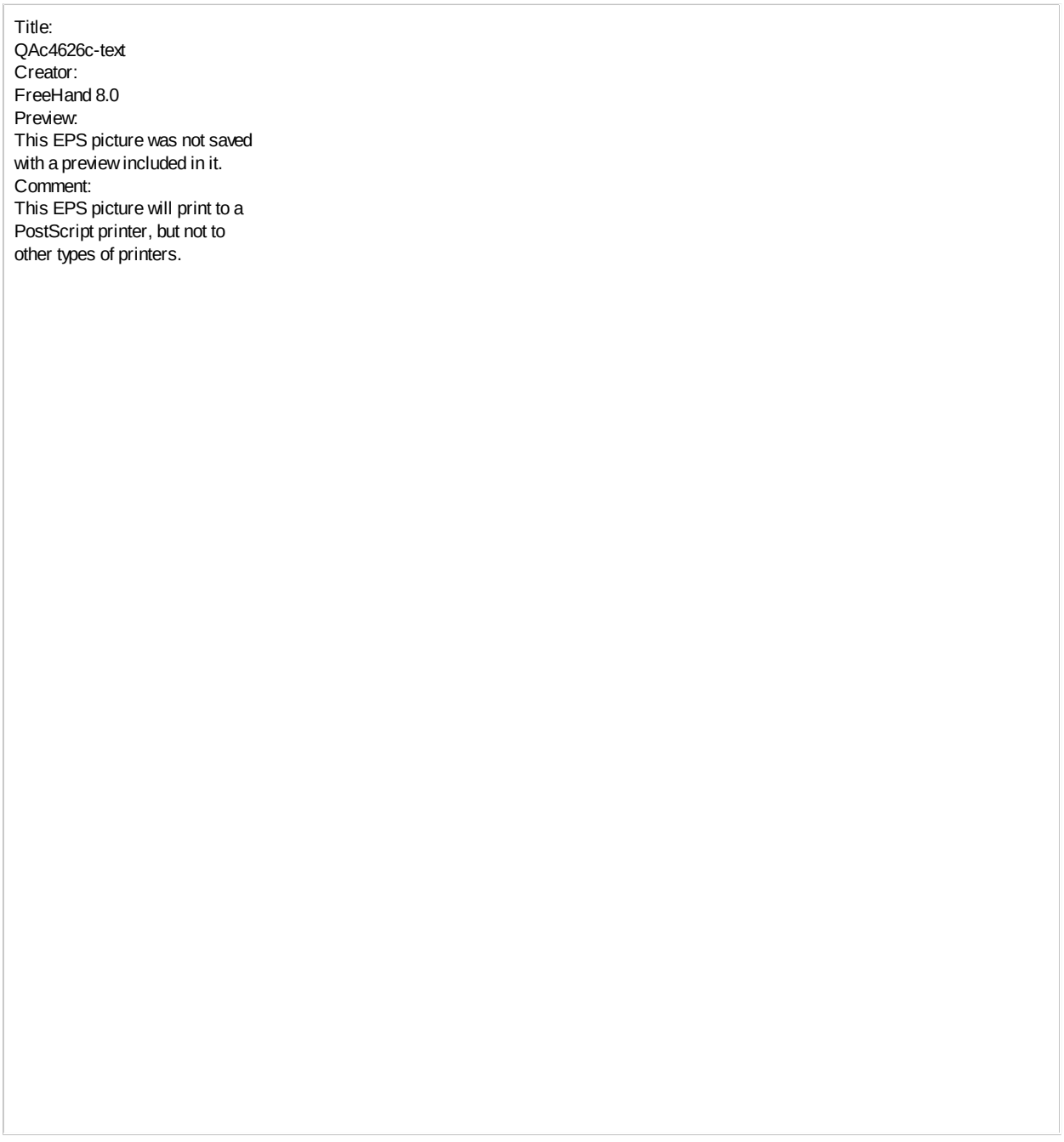


Figure 48. (a) Velocity and (b) intercept plots for reverse data from refraction test Jacksboro SPH1. Velocities and intercepts calculated by assigning arrivals from various offset ranges to the direct or refracted arrival.

(fig. 48b). The optimal maximum distance for arrivals attributed to the southward-propagating direct wave is 7 m, resulting in an apparent direct-wave velocity of 556 m/s (table 4).

As the minimum source–receiver distance decreases for reverse data, apparent velocity and intercept times reach a plateau when arrival times at geophones located at least 7 m from the source are included (fig. 48a and b). Using 7 m as the minimum source-receiver distance for inclusion in the calculation, apparent velocity of the arrivals attributed to the southward-propagating, critically refracted wave is 3,546 m/s and the intercept time is 0.0109 s (table 4).

True velocities derived from the forward and reverse data (table 4) are 570 m/s for the direct wave (layer 1) and 2,621 m/s for the critically refracted wave (layer 2). The interface between

layers 1 and 2 has an apparent dip of about 3° northward and a depth of 1.92 m calculated using the slope–intercept method (Palmer, 1986). Using the true velocities and the intercept times at each end of the recording spread, we obtain layer 2 depth estimates of 1.9 m at the south end and 3.2 m at the north end (fig. 39c).

### *Interpreted Strata*

Layer 1 velocities at the Jacksboro site are relatively low, similar to those determined at the PRC site (table 4). These velocities are typical of dry, unconsolidated soil and sediment commonly found overlying more rigid bedrock in many geologic settings. At the Jacksboro site, layer 1 probably represents road base, underlying surface deposits, and perhaps weathered bedrock. Layer 2 velocities at the Jacksboro site, though lower than those measured at the PRC site, are within the range reported for soft limestone (Press, 1966). This interpretation is consistent with the geologic map of the area, which shows the Pennsylvanian Ranger Limestone to be the bedrock unit (Hentz and Brown, 1987).

## GRANITE SHOALS SITE

Refraction data were collected on the westbound, outside lane of FM 1431 between Marble Falls and Granite Shoals in southwestern Burnet County (site R3, fig. 2 and table 2). The mapped bedrock unit is the Town Mountain Granite (Barnes, 1981), a Precambrian igneous intrusive rock that is quarried nearby. Reversed refraction data were collected using the soil-probe hammer. Traffic on this road was heavy compared with that at other sites during the refraction survey, resulting in a higher level of ambient seismic noise.

### *Refraction Analysis*

Despite the heavy traffic during data acquisition, digitally filtered field records from Granite Shoals show the presence of direct and refracted first arrivals for the forward, reverse,

and center shots (fig. 49). Picked first arrivals are attributable to the direct wave out to a source-receiver

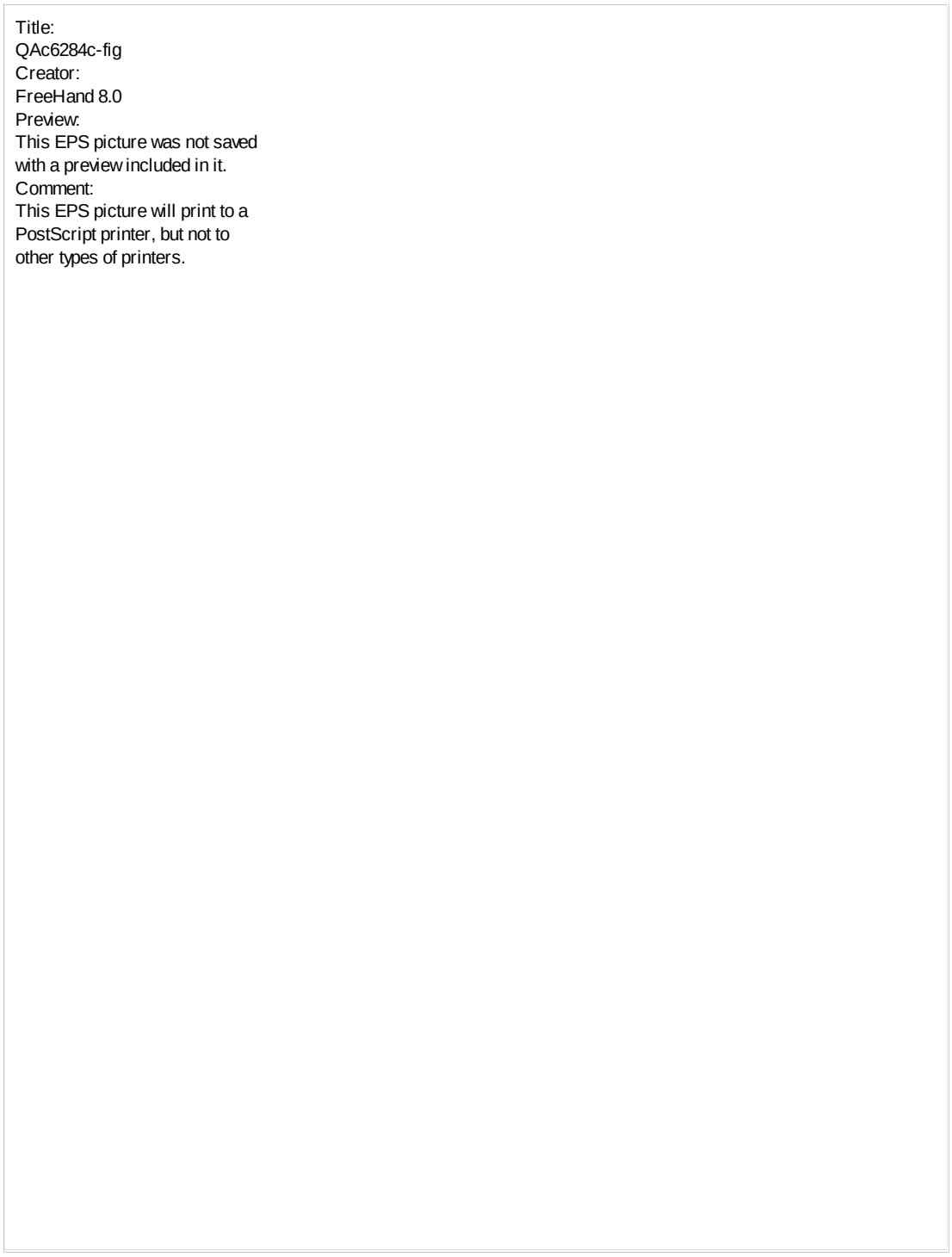


Figure 49. Field records from a refraction test near Granite Shoals (site R3, fig. 2) using a soil-probe hammer as a seismic source. Source and geophones were located on the pavement of FM 1431. Source was located at the (a) east end, (b) west end, and (c) center of the recording spread. Records displayed with a 125-Hz low-cut filter and time-varying gain (20-ms window) applied. Geophone spacing is 0.5 m.

distance of about 5 m in both the forward and reverse directions (fig. 50), where a faster-propagating refracted wave becomes the first-arriving seismic energy. Velocities and intercepts calculated using arrivals at progressively longer distances from the source gradually increase beyond about 5 m in both directions as well (figs. 51 and 52), further suggesting that these arrivals belong to the direct wave. Direct-wave velocities calculated from these arrivals average 489 m/s (table 4).

Arrivals at geophones farther than 5 to 10 m from the source show gradually increasing apparent velocities, suggesting a transition from soil to bedrock beneath the road. Velocities and intercepts calculated for the critically refracted wave are relatively consistent when geophones farther than about 12 to 16 m from the source are used (figs. 51 and 52). The apparent velocities are significantly higher in the eastward-propagating direction (4,662 m/s, table 4) than they are in the westward-propagating direction (2,492 m/s). Intercept times are near 0.01 s in both directions.

The true velocity for the layer in which the critically refracted wave travels is calculated to be 3,245 m/s. This layer is estimated to be about 2.4 m below the pavement and has an apparent dip of about 3° to the west (table 4).

***Interpreted Strata***

Layer 1 velocities of nearly 500 m/s at the Granite Shoals site are within the range observed at the other refraction test sites and can be similarly interpreted as a combination of road base, soil, and weathered bedrock. Below 2.4 m at this site, these materials are underlain by more rigid bedrock with substantially higher compressional wave velocities of more than 3,000 m/s. These velocities are below the range of 4,000 to 6,000 m/s reported for granite (Milsom, 1989), yet granite is the bedrock type at this site. Possible explanations for the lower measured seismic velocity include the presence of fractures and weathering.

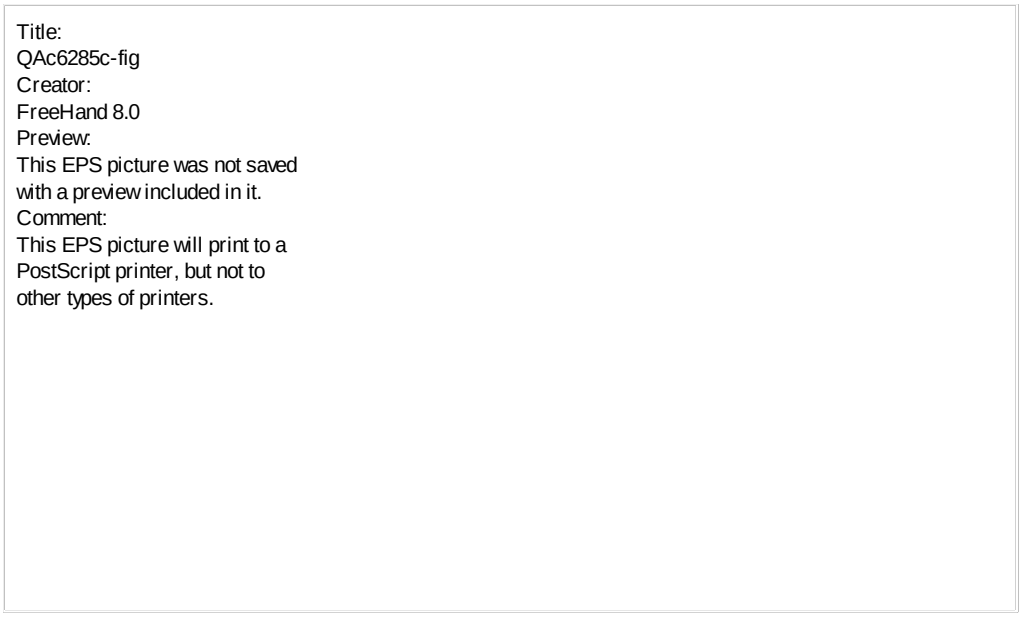


Figure 50. First-arrival times for the Granite Shoals refraction test for forward- (westward-) and reverse- (eastward-) propagating waves.


Figure 51. (a) Velocity and (b) intercept plots for forward data from the Granite Shoals refraction test. Velocities and intercepts calculated by assigning arrivals from various offset ranges to the direct or refracted arrival.

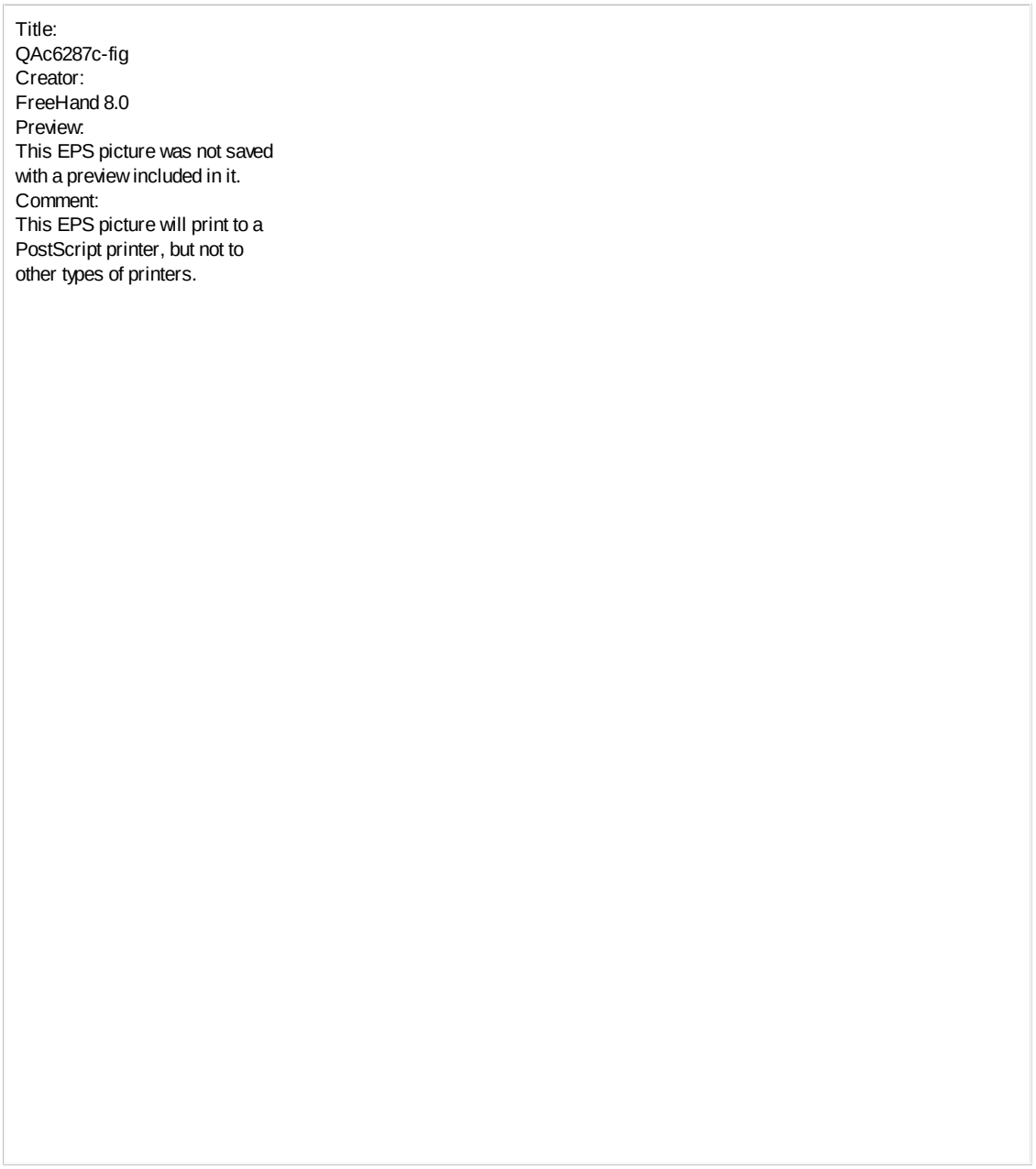


Figure 52. (a) Velocity and (b) intercept plots for reverse data from the Granite Shoals refraction test. Velocities and intercepts calculated by assigning arrivals from various offset ranges to the direct or refracted arrival.

## SEISMIC REFRACTION BEDROCK ANALYZER

The success of the refraction method in detecting bedrock beneath pavement, measuring compressional velocities of fill and bedrock, and estimating depth to bedrock led us to consider how the method might be optimized for use on paved roads. Logistical shortcomings of the system employed in the refraction tests described above included the following:

- Heaviness: each of 48 geophones was attached to a steel plate;
- Difficult deployment: because the refraction system was designed for use in a variety of environments, the geophone spacing was not fixed and required the spacings to be measured at each site;
- Unnecessary connection and disconnection of cables: each geophone must be attached to the recording cable before data can be recorded and must be detached before transport to the next site; and
- Excessive length of the recording array: because the desired exploration depth is about 6 m, a recording array of about four times that distance is required to ensure detection of a refracted arrival in most environments.

These and other attributes of the system that made it useful in a wide variety of geological environments restricted its practicality in this specific application. During the third project year, we designed and built a refraction system (the Seismic Refraction Bedrock Analyzer, or SRBA) that is lighter, uses fewer parts, is easier to deploy, has a fixed recording spread, and can be used to acquire seismic-refraction data on roads more rapidly.

### DESIGN

Principal design goals for the SRBA were to make it quicker and easier to deploy, easier to use, and easier to transport. The system consists of a movable seismic source, the recording array, and the seismograph (figs. 53 and 54). The chosen source is the soil-probe hammer of the type used in the refraction tests (fig. 5), which is easily carried by one person, operates on a variety of surfaces, and delivers a consistent and adequate amount of seismic energy for the refraction geometries used in most pavement applications.

Because a 24-m-long recording spread is unwieldy and impractical for routine highway use, we shortened the spread to half its original length and reduced the number of geophones from 48 to 24, keeping the geophone spacing constant at 0.5 m (fig. 53). The seismic source is portable, allowing it to be moved beyond the ends of the recording spread. This allows source-receiver separations equivalent to that achieved with the longer recording array. Using a 12-m-long recording array and four source points (one at each end of the spread and one 12 m beyond each end of the spread), reversed refraction data are recorded to source offsets of 24 m, the same

offset

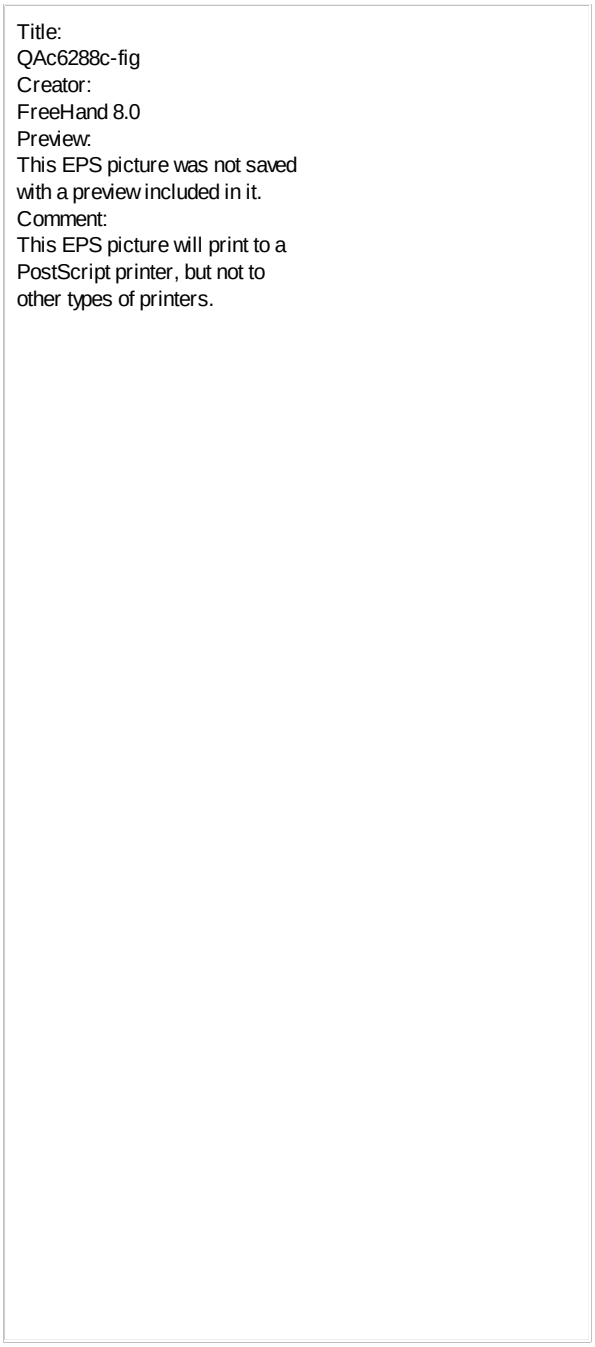


Figure 53. Schematic layout of the Seismic Refraction Bedrock Analyzer as deployed on pavement behind a Falling-Weight Deflectometer trailer.

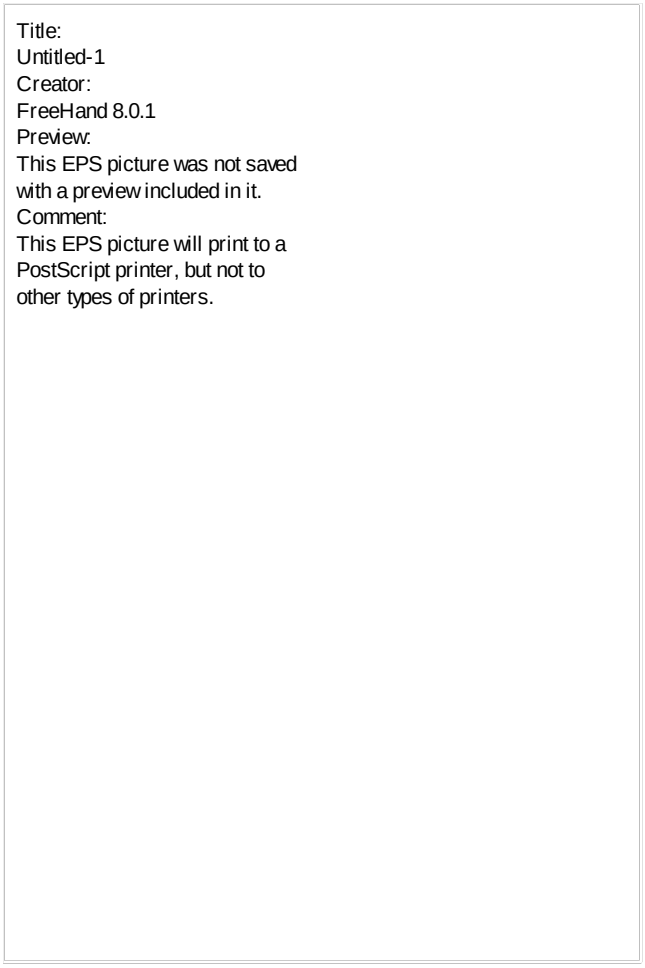


Figure 54. Photograph of Seismic Refraction Bedrock Analyzer deployed on pavement. The battery and seismograph are in the foreground. The soil-probe hammer is at the front end of the recording spread containing 24 geophones.

range obtained with the longer array. Further, sites with shallow bedrock at which critically refracted waves are recorded at shorter offsets will not require acquisition of the longer shots.

Rather than deploy each geophone individually on the pavement, the 24 geophones are mounted on a series of four semirigid PVC racks (fig. 55) that are each 3 m long. The connector cable is also mounted to the rack and connected to the geophones. The four geophone racks can be folded for carrying and stowing (figs. 55 and 56). Each geophone occupies a hole in the rack that allows it to move up or down a few centimeters to allow for slight pavement irregularities (fig. 57).

The seismograph used in the SRBA is the Geometrics SmartSeis, a 24-channel seismograph having sampling intervals as small as 10 μs and built-in first-arrival picking and refraction analysis software. These capabilities allow in-field processing of seismic-refraction data and interpretation of bedrock depth and subpavement velocity layering. The seismograph is powered by either a 12-V automotive battery or power supply.

## TESTING

We tested the SRBA on Road D at the PRC in Austin, Texas (site R1, figs. 2 and 54). Refraction data were acquired with both the soil-probe hammer source and the recording spread on the pavement. Good quality data were recorded for all shots (fig. 58), including the shots at the east end of the recording spread (fig. 58a), 12 m east of the east end (fig. 58b), 12 m west of the west end (fig. 58c), and at the west end (fig. 58d). Because bedrock is relatively shallow at this site, the critically refracted wave associated with bedrock is visible on the field records acquired with the source at the ends of the recording spread (figs. 58a and d). The longer-offset data, though not needed at this site, also show a clear refracted first arrival (figs. 58b and c) in both propagation directions, indicating that the source provides sufficient seismic energy to produce a detectable refracted arrival at the longer offsets.

The digital filtering capabilities of the seismograph allowed first arrivals to be picked semi-automatically on the seismograph display. Direct-wave arrivals were assigned to layer 1; refracted arrivals were assigned to layer 2. Refraction analysis software integrated with the acquisition software calculated compressional velocities of layers 1 and 2 (417 and 2,038 m/s) and depths to layer 2 beneath each of the 24 geophones in the recording spread (fig. 59). Calculated bedrock depths averaged about 1.4 m.

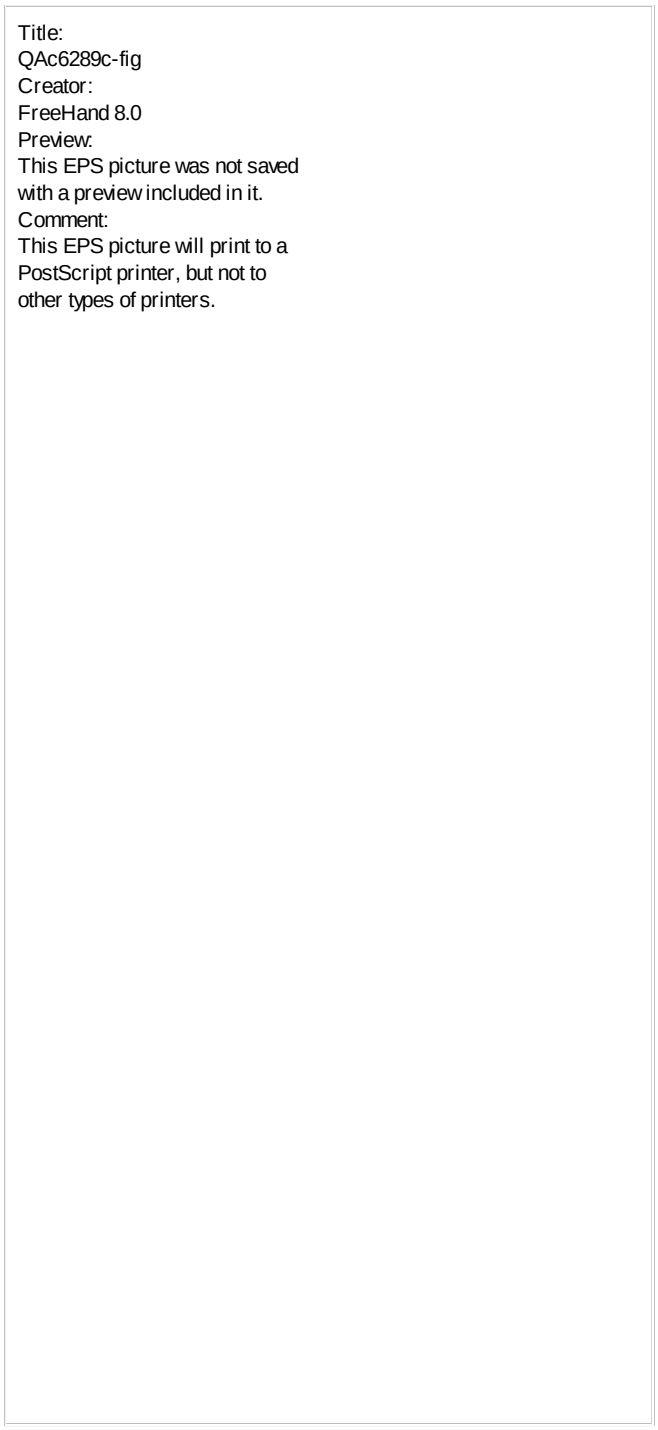


Figure 55. Schematic of recording array (left) as deployed and (right) folded for transport.

Figure 56. Photograph of recording array folded for transport.

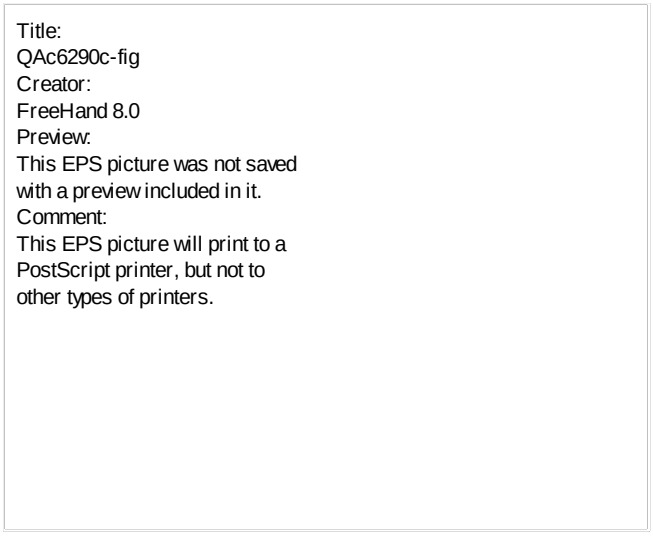


Figure 57. Cross section of recording array showing one geophone installed through PVC pipe rail and resting on aluminum tripod base. Surface irregularities can be accommodated by free vertical movement of the geophone between the tripod base and geophone lip.

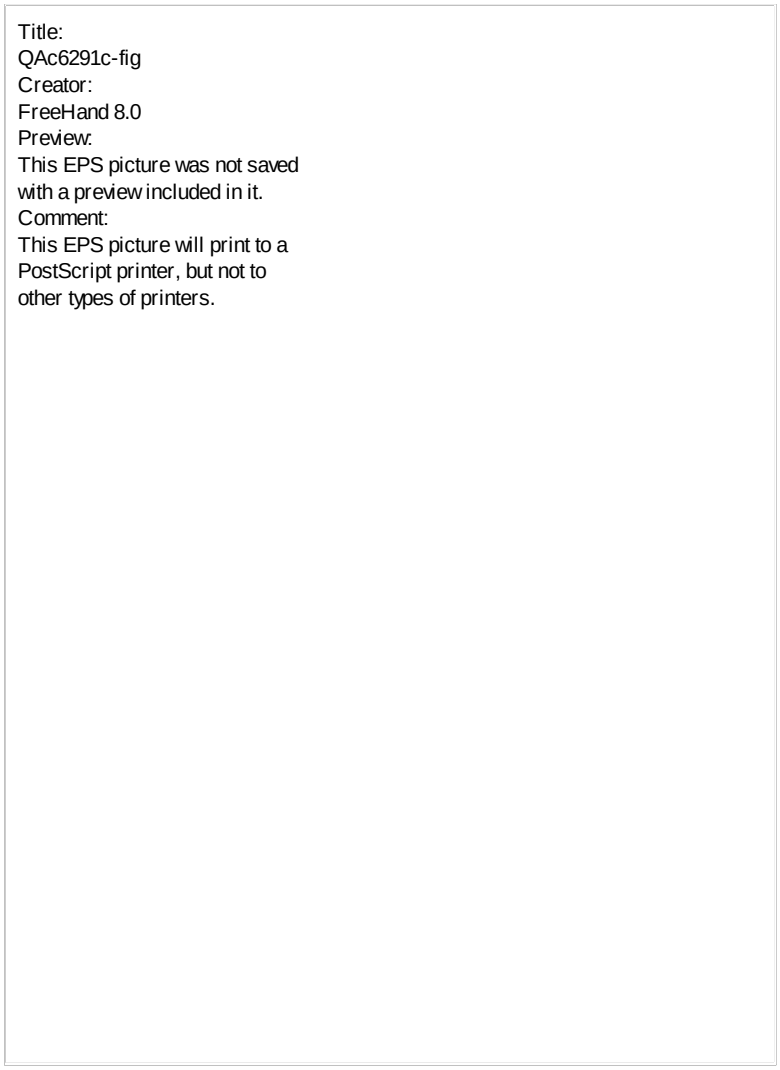


Figure 58. Field records acquired using Seismic Refraction Bedrock Analyzer at the J. J. Pickle Research Campus, The University of Texas at Austin (site R1, fig. 2). Source and recording array were located on the pavement of Road D. Source was (a) at the east end of the recording spread, (b) 12.5 m east of the east end of the recording spread, (c) 12.5 m west of the west end of the recording spread, and (d) at the west end of the recording spread. Records displayed with a 125-Hz low-cut filter and time-varying gain (20-ms window) applied. Geophone spacing is 0.5 m.

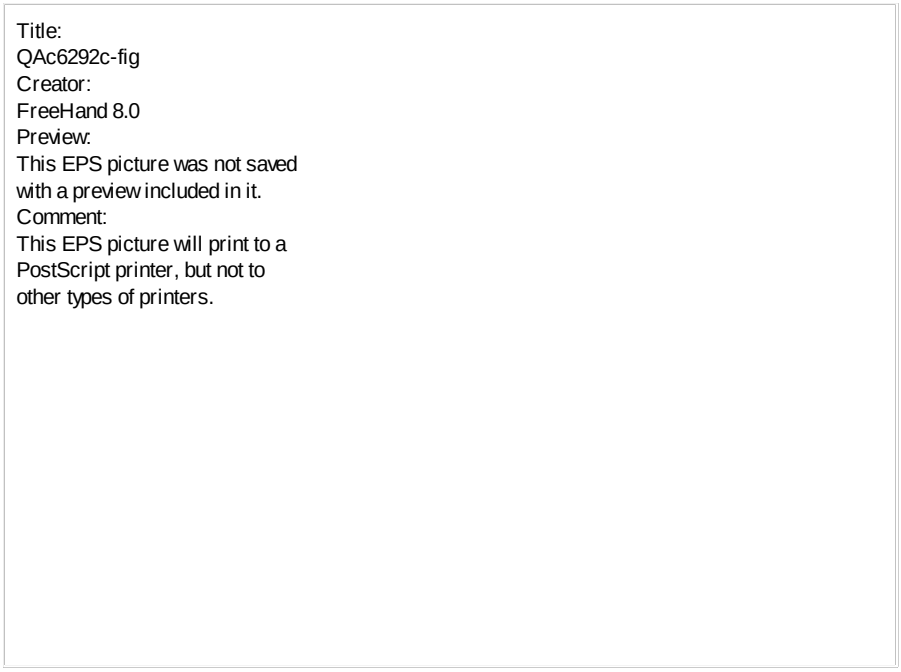


Figure 59. Cross section beneath Road D at the J. J. Pickle Research Campus, The University of Texas at Austin, showing locations of source points and recording array, interpreted depths to bedrock beneath the array, and approximate compressional-wave velocities of layer 1 (soil and road material) and layer 2 (bedrock).

## DISCUSSION

The relationship between bedrock and FWD response at long offsets that is suggested by average deflections by county is supported by more detailed analysis of FWD response along individual highway segments in four of the major physiographic regions of Texas. Although we can show that more rigid rock types such as limestones and igneous and metamorphic rocks have statistically lower deflections at the outermost detector than do less rigid sedimentary rock types, there is enough scatter in FWD deflections for a given rock type to make it difficult to predict rock type reliably from the outermost deflections alone. Better discrimination of rock types is obtained by comparing deflection ratios that tend to normalize road construction differences; in this study, W2:W7 ratios were highest for rigid rock types and lowest for materials with low characteristic stiffness, such as sandstones, mudstones, and unconsolidated sediments.

To develop a method that resolves the ambiguity of whether lower W7 deflections and higher W2:W7 ratios for highways over rigid rocks versus highways over soft rocks are due to differences in material properties of the mapped geologic units or to systematic differences in depth to bedrock among rock types, we collected seismic-refraction measurements at three sites in North and Central Texas. These tests show that refraction data can be collected on pavement, the FWD can serve as a seismic source, and estimates of bedrock depth and interpretations of bedrock type can be made using the refraction data. Arrival-time measurements acquired at three test sites have been converted to estimates of compressional-wave velocities for the surface layer and underlying bedrock, apparent dip of the bedrock surface, and bedrock depth. The success of this method allows direct comparison of observed deflection, depth to bedrock, and mapped geologic unit at a site, enabling determination of the relative influence of bedrock rigidity and bedrock depth on FWD response. It may be that bedrock rigidity accounts for the differences in average deflection calculated for the outermost FWD detector, and that site-to-site variations in bedrock depth over a given rock type account for the large variance observed for that rock type along a roadway.

Because measurements might be made on roads and because calculations of true velocities and layer dips require source operation at both ends of the recording spread, the source chosen for refraction measurements should be nondestructive, rapidly operated, and easily moved. In our tests, a modified soil-probe hammer met these requirements, provided a reliable zero-time break for the seismograph to begin recording, and provided sufficient seismic energy for the relatively short source–receiver distances that are typical of most highway investigations. Longer spreads appropriate for bedrock depths greater than 4 or 5 m might require a stronger seismic impulse. The FWD provides a stronger seismic impulse and produces interpretable direct and critically

refracted arrivals, but we have had difficulty obtaining a reliable zero-time break to begin seismograph recording. This is a problem that might be solved by using more sensitive trigger switches or FWD-mounted electronic switches.

As is evident from the PRC and Jacksboro data, accurate first-arrival picks are required to calculate bedrock depth accurately. Differing first arrivals may be interpreted by varying the display parameters of the seismic record, causing different bedrock depths to be calculated from the same record. At these two sites, using a digital low-cut filter to remove seismic noise below 125 Hz and a short-window (20 ms), time-varying gain produced the most interpretable seismic record. Records without these display adjustments might induce an interpreter to select later, stronger arrivals as a first arrival and inaccurately choose an arrival time for a geophone where seismic noise interferes with the first arrival.

Difficulties encountered employing the standard refraction method on highways include deployment of the array of seismic detectors, operation of the seismic source, and accurate first-arrival picks on the seismic records. Geophones with attached spikes offer the best coupling with the surface, but they can only be used on road shoulders where it may be difficult to insert the spikes fully into hard-packed material. Plate-mounted geophones can be laid rapidly and directly on pavement, but the surface coupling may be degraded. At the three sites tested, plate-mounted geophones yielded acceptable data for refraction analysis.

Many of the shortcomings encountered with the standard refraction method and existing seismic equipment were overcome by designing and building a seismic-refraction system optimized for pavement use. Because the surface type and depth range of interest are known, the instrument can use fixed detector arrays that are shorter than those used in the refraction tests. Where conditions warrant, deeper investigations can be made by moving the source farther from the recording spread rather than by using a longer spread.

## CONCLUSIONS

This study of the relationship between three data types—geologic maps, measurements of pavement deflection under load, and seismic-refraction data—yielded the following conclusions:

- FWD deflections at the outermost sensors correlate to mapped geologic units at the county average scale,
- at six test highway segments in four major physiographic regions, there is a statistical relationship between mapped geologic unit and FWD response,
- variance in FWD response within individual geologic units is large, making interpretation of geologic unit from FWD response alone uncertain,
- ratios of inner- and outer-detector deflections, such as W2:W7, partly normalize roadway construction differences and allow better rock-type discrimination than that obtained from W7 data alone,
- in general, highway segments constructed over relatively rigid bedrock units such as limestone, granite, and metamorphic rocks exhibit low average W7 deflections and high W2:W7 ratios, whereas highways constructed over softer bedrock units such as mudstone, sandstone, and unconsolidated sediments have high average W7 deflections and low W2:W7 ratios,
- from FWD data and mapped geologic units alone, we cannot determine whether the influence that bedrock type has on FWD response is due to bedrock rigidity or to systematic changes in bedrock depth among geologic units,
- seismic-refraction data can be collected on pavement to measure wave velocities in fill and bedrock and estimate bedrock depth, and
- the seismic refraction method can be optimized for use on pavement by using fixed detector arrays, plate-mounted geophones, portable seismic sources, and commercially available seismographs with integrated data collection, processing, and analysis capabilities.

## REFERENCES


Barnes, V. E., 1981, Llano sheet: The University of Texas at Austin, Bureau of Economic Geology, Geologic Atlas of Texas, scale 1:250,000.

Brewton, J. L., Owen, F., Aronow, S., and Barnes, V. E., 1976a, Laredo sheet: The University of Texas at Austin, Bureau of Economic Geology, Geologic Atlas of Texas, scale 1:250,000.

Brewton, J. L., Owen, F., Aronow, S., and Barnes, V. E., 1976b, McAllen-Brownsville sheet: The University of Texas at Austin, Bureau of Economic Geology, Geologic Atlas of Texas, scale 1:250,000.

Brown, L. F. J., Goodson, J. L., Harwood, P., and Barnes, V. E., 1972, Abilene sheet: The University of Texas at Austin, Bureau of Economic Geology, Geologic Atlas of Texas, scale 1:250,000.

Bureau of Economic Geology, 1992, Geology of Texas: The University of Texas at Austin, Bureau of Economic Geology, scale 1:6,336,000.

Garner, L. E., and Young, K. P., 1976, Environmental geology of the Austin area; an aid to urban planning: The University of Texas at Austin, Bureau of Economic Geology Report of Investigations No. 86, 39 p.

Hentz, T. F., and Brown, L. F., Jr., 1987, Wichita Falls-Lawton sheet: The University of Texas at Austin, Bureau of Economic Geology, Geologic Atlas of Texas, scale 1:250,000.

Milsom, John, 1989, Field geophysics: New York, Open University Press, Milton Keynes, Geological Society of London Handbook, 182 p.

Palmer, Derecke, 1986, Refraction seismics: the lateral resolution of structure and seismic velocity, *in* Helbig, Klaus, and Treitel, Swen, eds., Seismic exploration: London, Geophysical Press, Handbook of Geophysical Exploration, v. 13, 269 p.

Press, Frank, 1966, Seismic velocities, *in* Clark, S. P., Jr., ed., Handbook of physical constants: Geological Society of America Memoir 97, p. 195–218.

Proctor, C. V., Jr., Brown, T. E., McGowen, J. H., Waechter, N. B., and Barnes, V. E., 1974, Austin sheet: The University of Texas at Austin, Bureau of Economic Geology, Geologic Atlas of Texas, scale 1:250,000.

Telford, W. M., Geldart, L. P., Sheriff, R. E., and Keys, D. A., 1976, Applied geophysics: Cambridge, Cambridge University Press, 841 p.

Wermund, E. G., Jr., 1996, Physiographic map of Texas: The University of Texas at Austin, Bureau of Economic Geology, scale 1:6,336,000.

Wylie, K. M., 1969, Seismic analysis: The Testing World, no. 22, p. 4–5.

# APPENDIX A: TOPOGRAPHIC[1] AND GEOLOGIC[2] MAPS OF THE STUDY SITES

[1] U.S.G.S. 7.5-minute quadrangle map, 1:24,000 scale
[2] BEG geologic atlas map, 1° x 2°, 1:250,000 scale

Site A: Texas 16, reference markers 220 to 264, Archer and Young Counties.

| Topographic Maps | Reference Markers |
|---|---|
| Darnell Branch | 220 to 228 |
| Markley | 229 to 236 |
| Loving | 237 to 239 |
| Lake Eddleman | 240 to 249 |
| Graham | 249 to 258 |
| Ross Mountain | 259 to 261, 264 to 265 |
| Palo Pinto | 262 to 263 |

| Geologic Maps | Reference Markers |
|---|---|
| Wichita Falls–Lawton | 220 to 261, 264 to 265 |
| Abilene | 262 to 263 |

Site B: Texas 16, reference markers 450 to 488, Llano and Gillespie Counties.

| Topographic Maps | Reference Markers |
|---|---|
| Llano South | 450 to 457 |
| Oxford | 458 to 466 |
| Willow City | 468 to 477 |
| Fredericksburg East | 478 to 487 |

| Geologic Maps | Reference Markers |
|---|---|
| Llano | 450 to 490 |

Site C: Texas 71, reference markers 528 to 542, Burnet County.

| Topographic Maps | Reference Markers |
|---|---|
| Marble Falls | 528 to 533 |
| Round Mountain | 533 to 534 |
| Spicewood | 535 to 543 |

| Geologic Maps | Reference Markers |
|---|---|
| Llano | 528 to 543 |

Site D: U.S. 290, reference markers 536 to 563, Blanco and Hays Counties.

| Topographic Maps | Reference Markers |
|---|---|
| Monument Hill | 535 |
| Yeager Creek | 536 to 543 |
| Henly | 544 to 553 |
| Dripping Springs | 554 to 560 |
| Signal Hill | 561 to 563 |

| Geologic Maps | Reference Markers |
|---|---|
| Llano | 535 to 560 |
| Austin | 561 to 563 |

Site E: Texas 71, reference markers 590 to 598, Bastrop County.

| Topographic Maps | Reference Markers |
|---|---|
| Webberville | 590 to 592 |
| Utley | 593 to 596 |
| Bastrop SW | 597 to 598 |

| Geologic Maps | Reference Markers |
|---|---|
| Austin | 590 to 598 |

Site F: Texas 16, reference markers 758 to 804, Jim Hogg and Zapata Counties.

| Topographic Maps | Reference Markers |
|---|---|
| McCambell Ranch | 758 to 761 |
| Armstrong Ranch | 762 to 766 |
| San Pablo Ranch | 767 to 774 |
| Randado | 775 to 783 |
| Escobas | 784 to 792 |
| Arroyo Huisache | 793 |
| Arroyo Veleño | 794 to 802 |
| Zapata | 803 to 804 |

| Geologic Maps | Reference Markers |
|---|---|
| Laredo | 758 to 792 |
| McAllen–Brownsville | 793 to 804 |

# APPENDIX B: AGE, LITHOLOGY, CONSTITUENTS, AND THICKNESS OF GEOLOGIC UNITS

Site A: Texas 16 between reference markers 220 and 264, Archer and Young Counties, Wichita Falls–Lawton (Hentz and Brown, 1987) and Abilene (Brown and others, 1972) geologic atlases.

| Geologic unit | Symbol | Age | Major lithology | Minor lithology | Constituents[1] | Thickness (ft) | Notes |
|---|---|---|---|---|---|---|---|
| Alluvium | Qal | Quaternary | unconsolidated | | sd, st, cl, gr | <30 | |
| Markley | IPPm | Pennsylvanian–Permian | mudstone | | st, cl | | |
| Markley | IPPm-SS14 | Pennsylvanian–Permian | sandstone | conglomerate | sd, gr | 15 to 50 | |
| Markley | IPPm-SS12 | Pennsylvanian–Permian | sandstone | conglomerate, mudstone | sd, gr | 30 to 60 | |
| Markley | IPPm-SS11 | Pennsylvanian–Permian | sandstone | conglomerate | sd, gr | 10 to 30 | |
| Markley | IPPm-SS10 | Pennsylvanian–Permian | sandstone | conglomerate, mudstone | sd, gr | 10 to 50 | |
| Thrifty, Graham | IPtg | Pennsylvanian–Permian | mudstone | | st, cl | | |
| Ivan Limestone | IPi | Pennsylvanian–Permian | limestone | | | 1 to 5 | member of IPtg |
| Thrifty, Graham | IPtg-SS2 | Pennsylvanian–Permian | sandstone | conglomerate | sd, gr | 5 to 15 | member of IPtg |
| Bunger Limestone | IPbu | Pennsylvanian–Permian | limestone | | | <4 | member of IPtg |
| Gonzales Creek Member | IPgc | Pennsylvanian–Permian | sandstone | shale, mudstone | sd, st, cl | 10 to 50 | member of IPtg |
| Home Creek Limestone | IPhc | Pennsylvanian–Permian | limestone | sandstone, shale, conglomerate | sd, cl, gr | 2 to 145 | |
| Kisinger Sandstone | IPk | Pennsylvanian–Permian | sandstone | conglomerate | sd, gr | <140 | member of IPhc |
| Ranger Limestone | IPr | Pennsylvanian–Permian | limestone | shale | cl | 30 to 60 | |

[1] gr=gravel; sd=sand; st=silt; cl=clay

Site B: Texas 16 between reference markers 450 and 488, Llano and Gillespie Counties, Llano geologic atlas (Barnes, 1981).

| Geologic unit | Symbol | Age | Major lithology | Minor lithology | Constituents | Thickness (ft) | Notes |
|---|---|---|---|---|---|---|---|
| Alluvium | Qal | Quaternary | unconsolidated | | gr, sd, st, cl | <35 | |
| Fort Terrett Member | Kft | Cretaceous | limestone | dolomite | | 150 to 230 | member of Ked |
| Hensell Sand | Kh | Cretaceous | unconsolidated | conglomerate | sd, st, cl, gr | <220 | |
| Hickory Sandstone | Crh | Cambrian | sandstone | | sd, st | 275 to 470 | |
| Younger granitic intrusives | pCy | Precambrian | granite | | | | |
| Town Mountain Granite | pCtm | Precambrian | granite | | | | age 1.0 by |
| Packsaddle Schist | pCps | Precambrian | schist | | | | |
| Valley Spring Gneiss | pCvs | Precambrian | gneiss | | | | |

Site C: Texas 71 between reference markers 528 and 542, Burnet County, Llano geologic atlas (Barnes, 1981).

| Geologic unit | Symbol | Age | Major lithology | Minor lithology | Constituents | Thickness (ft) | Notes |
|---|---|---|---|---|---|---|---|
| Alluvium | Qal | Quaternary | unconsolidated | | sd, st, cl, gr | <35 | |
| Glen Rose Limestone (upper) | Kgru | Cretaceous | limestone | dolomite, marl | | 220 | |
| Glen Rose Limestone (lower) | Kgrl | Cretaceous | limestone | dolomite, marl | | 160 | |
| Hensell Sand | Kh | Cretaceous | unconsolidated | conglomerate | sd, st, cl, gr | <220 | |
| Sycamore Sand | Ksy | Cretaceous | unconsolidated | conglomerate | sd, st, cl, gr | | |
| Marble Falls Limestone | IPmf | Pennsylvanian–Permian | limestone | | | 385 | |
| Honeycut Formation | Oh | Ordovician | limestone | dolomite | | 680 | part of Ellenburger Group |
| Gorman Formation | Og | Ordovician | limestone | dolomite | | 425 to 490 | |

Site D: U.S. 290 between reference markers 536 and 563, Blanco and Hays Counties, Llano (Barnes, 1981) and Austin (Proctor and others, 1974) geologic atlases.

| Geologic unit | Symbol | Age | Major lithology | Minor lithology | Constituents | Thickness (ft) | Notes |
|---|---|---|---|---|---|---|---|
| Alluvium | Qal | Quaternary | unconsolidated | | sd, st, cl, gr | <30 | |
| Fort Terrett Member | Kft | Cretaceous | limestone | dolomite | | 150 to 230 | member of Ked |
| Glen Rose Limestone (upper) | Kgru | Cretaceous | limestone | dolomite, marl | | 220 | |
| Glen Rose Limestone (lower) | Kgrl | Cretaceous | limestone | dolomite, marl | | 160 | |

Site E: Texas 71 between reference markers 590 and 598, Bastrop County, Austin geologic atlas (Proctor and others, 1974).

| Geologic unit | Symbol | Age | Major lithology | Minor lithology | Constituents | Thickness (ft) | Notes |
|---|---|---|---|---|---|---|---|
| Fluviatile terrace | Qt | Quaternary | unconsolidated | | gr, sd, st, cl | | terraces along streams |
| High gravels | Qhg | Quaternary | unconsolidated | | gr | | |
| Calvert Bluff Formation | Ecb | Eocene | mudstone | sandstone, lignite | st, cl, sd | <1000 | part of Wilcox Group |
| Simsboro Formation | Esb | Eocene | unconsolidated | mudstone | sd, cl, gr | <300 | part of Wilcox Group |
| Hooper Formation | Eh | Eocene | mudstone | sandstone | st, cl, sd | <500 | part of Wilcox Group |
| Midway Group | Emi | Eocene | unconsolidated | | cl, st, sd | | |
| Kemp, Corsicana, Marlbrook | Kknm | Cretaceous | unconsolidated | | cl, st | 600 | Kemp Clay, Corsicana Marl, Marlbrook Marl |

Site F: Texas 16 between reference markers 758 and 804, Jim Hogg and Zapata Counties, Laredo (Brewton and others, 1976a) and McAllen–Brownsville geologic atlases (Brewton and others, 1976b).

| Geologic unit | Symbol | Age | Major lithology | Minor lithology | Constituents | Thickness (ft) | Notes |
|---|---|---|---|---|---|---|---|
| Alluvium | Qal | Quaternary | unconsolidated | | cl, st, sd, gr | | floodplain deposits |
| Sand sheet | Qs | Quaternary | unconsolidated | | sd | | eolian deposits |
| Goliad Formation | Pg | Pliocene | clay | sandstone, marl, caliche, limestone, conglomerate | cl, sd, gr | <600 | |
| Catahoula and Frio Formations | MOcf | Miocene–Oligocene | mudstone | claystone, sandstone, tuff, clay | cl, st, sd | | |
| Jackson Group | Ej | Eocene | sandstone | clay | sd, cl | 360 | |
| Yegua Formation | Ey | Eocene | clay | sandstone | cl, sd | 400 | |
| Laredo Formation | El | Eocene | sandstone | clay | sd, cl | 620 | |

# APPENDIX C: FWD DATA FOR STUDY SITES

Site A: Texas 16 between reference markers 220 and 264, Archer and Young Counties, Wichita Falls District.

| County | Geologic[1] atlas sheet | Geologic unit | Elevation (ft) | Reference marker | Normalized FWD deflection (mils) W1 | W2 | W3 | W4 | W5 | W6 | W7 |
|---|---|---|---|---|---|---|---|---|---|---|---|
| Archer | WF-L | IPPm-SS14 | 1105 | 220.0 | 25.33 | 18.34 | 10.43 | 5.66 | 3.36 | 2.27 | 1.68 |
| Archer | WF-L | IPPm-SS14 | 1055 | 220.5 | 8.17 | 5.88 | 3.17 | 1.62 | 0.95 | 0.63 | 0.53 |
| Archer | WF-L | IPPm-SS14 | 1090 | 221.0 | 9.35 | 6.27 | 3.33 | 1.74 | 1.00 | 0.69 | 0.51 |
| Archer | WF-L | IPPm-SS14 | 1060 | 221.5 | 14.08 | 10.52 | 6.96 | 4.33 | 2.68 | 1.78 | 1.41 |
| Archer | WF-L | IPPm | 1020 | 222.0 | 11.46 | 9.58 | 6.54 | 4.42 | 3.15 | 2.25 | 1.52 |
| Archer | WF-L | Qal | 1005 | 222.5 | 26.68 | 17.60 | 9.00 | 3.87 | 1.98 | 1.34 | 1.06 |
| Archer | WF-L | IPPm-SS12 | 1045 | 223.0 | 16.42 | 11.70 | 6.52 | 3.59 | 2.10 | 1.29 | 0.90 |
| Archer | WF-L | | 1040 | 223.5 | 14.74 | 10.20 | 5.49 | 2.62 | 1.34 | 0.87 | 0.61 |
| Archer | WF-L | IPPm-SS12 | 1065 | 224.0 | 11.50 | 8.05 | 4.57 | 2.32 | 1.29 | 0.82 | 0.62 |
| Archer | WF-L | IPPm-SS12 | 1095 | 224.5 | 12.15 | 7.71 | 4.05 | 2.22 | 1.44 | 1.05 | 0.74 |
| Archer | WF-L | IPPm-SS12 | 1060 | 225.0 | 19.51 | 14.23 | 8.68 | 4.63 | 2.54 | 1.54 | 1.12 |
| Archer | WF-L | IPPm-SS11 | 1020 | 225.5 | 13.37 | 9.01 | 5.16 | 3.01 | 1.92 | 1.43 | 1.21 |
| Archer | WF-L | Qal | 1015 | 226.0 | 12.49 | 7.17 | 3.32 | 1.89 | 1.29 | 1.04 | 0.89 |
| Young | WF-L | IPPm | 1018 | 228.0 | 19.59 | 7.75 | 2.18 | 0.82 | 0.59 | 0.50 | 0.38 |
| Young | WF-L | IPPm | 1035 | 228.5 | 37.66 | 22.18 | 11.43 | 6.57 | 4.45 | 3.29 | 2.56 |
| Young | WF-L | IPPm | 1065 | 229.0 | 24.92 | 11.67 | 4.78 | 2.47 | 1.73 | 1.37 | 1.00 |
| Young | WF-L | IPPm | 1065 | 229.5 | 17.95 | 9.17 | 4.54 | 2.56 | 1.67 | 1.18 | 0.90 |
| Young | WF-L | IPPm-SS11 | 1100 | 230.0 | 40.52 | 22.96 | 9.86 | 4.45 | 2.46 | 1.67 | 1.20 |
| Young | WF-L | IPPm-SS11 | 1115 | 230.5 | 29.34 | 16.72 | 8.31 | 4.68 | 3.09 | 2.23 | 1.66 |
| Young | WF-L | IPPm-SS11 | 1100 | 231.0 | 15.33 | 8.94 | 4.26 | 2.11 | 1.24 | 0.86 | 0.64 |
| Young | WF-L | IPPm | 1100 | 231.5 | 32.55 | 16.92 | 7.93 | 4.13 | 2.68 | 1.92 | 1.47 |
| Young | WF-L | IPPm-SS10 | 1105 | 232.0 | 30.63 | 20.12 | 10.95 | 5.92 | 3.55 | 2.48 | 1.94 |
| Young | WF-L | IPPm-SS10 | 1110 | 232.5 | 46.12 | 22.57 | 9.47 | 4.38 | 2.51 | 1.77 | 1.24 |
| Young | WF-L | IPPm-SS10 | 1115 | 233.0 | 27.62 | 13.45 | 5.46 | 2.91 | 2.05 | 1.61 | 1.33 |
| Young | WF-L | IPPm-SS10 | 1150 | 233.5 | 24.42 | 11.05 | 4.19 | 2.10 | 1.40 | 1.05 | 0.75 |
| Young | WF-L | IPPm-SS10 | 1125 | 234.0 | 22.33 | 13.32 | 6.99 | 3.73 | 2.46 | 1.83 | 1.45 |
| Young | WF-L | IPPm-SS10 | 1150 | 234.5 | 19.24 | 9.08 | 3.36 | 1.49 | 1.03 | 0.81 | 0.63 |
| Young | WF-L | IPPm | 1160 | 235.0 | 28.35 | 12.76 | 4.15 | 2.00 | 1.33 | 1.01 | 0.80 |
| Young | WF-L | IPPm-SS11 | 1205 | 235.5 | 28.43 | 18.28 | 8.29 | 3.06 | 1.95 | 1.50 | 1.16 |
| Young | WF-L | IPPm-SS11 | 1265 | 236.0 | 20.45 | 10.23 | 3.67 | 1.50 | 0.94 | 0.73 | 0.60 |
| Young | WF-L | IPPm-SS11 | 1290 | 236.5 | 34.79 | 16.22 | 6.24 | 2.99 | 1.80 | 1.22 | 0.88 |
| Young | WF-L | IPPm-SS11 | 1290 | 237.0 | 24.69 | 14.30 | 6.51 | 2.75 | 1.39 | 0.83 | 0.61 |
| Young | WF-L | IPPm-SS11 | 1290 | 237.5 | 20.89 | 14.05 | 8.08 | 4.59 | 2.93 | 2.02 | 1.54 |
| Young | WF-L | IPPm | 1290 | 238.0 | 11.67 | 8.23 | 5.26 | 3.44 | 2.53 | 1.93 | 1.51 |
| Young | WF-L | IPPm | 1295 | 238.5 | 17.25 | 11.27 | 6.00 | 3.43 | 2.32 | 1.72 | 1.23 |
| Young | WF-L | IPPm | 1295 | 239.0 | 15.59 | 11.30 | 7.25 | 4.58 | 3.09 | 2.21 | 1.70 |
| Young | WF-L | IPPm | 1275 | 239.5 | 8.83 | 6.04 | 3.66 | 2.28 | 1.54 | 1.10 | 0.81 |
| Young | WF-L | IPPm-SS10 | 1275 | 240.0 | 15.31 | 10.23 | 5.42 | 2.54 | 1.28 | 0.84 | 0.57 |
| Young | WF-L | IPPm-SS10 | 1290 | 240.5 | 12.54 | 8.90 | 5.57 | 3.38 | 2.17 | 1.49 | 1.09 |
| Young | WF-L | IPPm | 1260 | 241.0 | 18.66 | 12.29 | 6.59 | 3.65 | 2.26 | 1.57 | 1.20 |
| Young | WF-L | IPtg | 1255 | 241.5 | 15.12 | 10.99 | 6.99 | 4.50 | 3.02 | 2.16 | 1.58 |
| Young | WF-L | IPtg | 1230 | 242.0 | 19.23 | 13.67 | 8.22 | 4.75 | 2.89 | 1.95 | 1.42 |
| Young | WF-L | IPtg | 1210 | 242.5 | 21.75 | 14.50 | 7.75 | 3.83 | 2.33 | 1.57 | 1.25 |
| Young | WF-L | IPtg | 1215 | 243.0 | 15.89 | 12.25 | 8.11 | 5.09 | 3.24 | 2.09 | 1.45 |
| Young | WF-L | IPtg | 1200 | 243.5 | 15.93 | 10.25 | 5.68 | 3.12 | 1.99 | 1.40 | 1.02 |
| Young | WF-L | IPtg | 1200 | 244.0 | 20.79 | 11.47 | 5.95 | 3.46 | 2.32 | 1.64 | 1.29 |
| Young | WF-L | IPtg | 1165 | 244.5 | 12.62 | 6.77 | 3.46 | 2.02 | 1.36 | 1.04 | 0.78 |
| Young | WF-L | IPtg | 1175 | 245.0 | 9.33 | 5.54 | 3.35 | 2.19 | 1.61 | 1.17 | 0.86 |
| Young | WF-L | IPtg | 1190 | 245.5 | 17.12 | 9.83 | 5.23 | 3.11 | 2.09 | 1.48 | 1.10 |
| Young | WF-L | IPi | 1175 | 246.0 | 22.37 | 12.93 | 6.79 | 3.86 | 2.50 | 1.72 | 1.24 |
| Young | WF-L | IPtg | 1190 | 246.5 | 19.38 | 10.00 | 4.70 | 2.62 | 1.90 | 1.50 | 1.23 |
| Young | WF-L | IPtg | 1220 | 247.0 | 13.65 | 5.94 | 2.82 | 1.56 | 1.03 | 0.69 | 0.48 |
| Young | WF-L | IPtg | 1190 | 247.5 | 12.48 | 6.94 | 3.57 | 2.00 | 1.31 | 0.99 | 0.81 |
| Young | WF-L | IPtg | 1130 | 248.0 | 31.28 | 15.19 | 6.53 | 3.73 | 2.64 | 1.94 | 1.55 |
| Young | WF-L | IPtg | 1090 | 248.5 | 17.33 | 9.23 | 4.39 | 2.63 | 1.89 | 1.47 | 1.14 |

[1] WF-L=Wichita Falls–Lawton; ABL=Abilene

| | | | | | | | | | | | |
|---|---|---|---|---|---|---|---|---|---|---|---|
| Young | WF-L | IPtg | 1075 | 249.0 | 9.35 | 5.59 | 3.65 | 2.62 | 1.98 | 1.52 | 1.14 |
| Young | WF-L | IPtg | 1060 | 249.5 | 21.87 | 13.05 | 6.84 | 3.84 | 2.60 | 1.93 | 1.49 |
| Young | WF-L | IPtg | 1060 | 250.0 | 13.67 | 6.50 | 3.85 | 2.87 | 2.15 | 1.65 | 1.25 |
| Young | WF-L | IPtg | 1030 | 250.6 | 6.87 | 5.20 | 3.58 | 2.38 | 1.68 | 1.22 | 0.94 |
| Young | WF-L | IPtg | | 251.0 | 7.55 | 6.39 | 5.12 | 3.87 | 2.85 | 1.99 | 1.28 |
| Young | WF-L | IPtg | | 251.5 | 16.63 | 9.10 | 3.96 | 2.00 | 1.24 | 0.77 | 0.43 |
| Young | WF-L | IPtg-SS2 | | 252.0 | 20.18 | 9.07 | 4.57 | 2.59 | 1.54 | 0.95 | 0.59 |
| Young | WF-L | IPtg-SS2 | | 252.5 | 9.48 | 3.22 | 1.23 | 0.59 | 0.39 | 0.26 | 0.21 |
| Young | WF-L | IPtg-SS2 | 1040 | 253.0 | 8.72 | 3.34 | 1.40 | 0.89 | 0.60 | 0.41 | 0.28 |
| Young | WF-L | IPtg-SS2 | 1065 | 253.5 | 13.65 | 6.36 | 2.92 | 1.57 | 0.88 | 0.57 | 0.33 |
| Young | WF-L | IPtg | 1030 | 254.0 | 19.75 | 11.53 | 5.70 | 3.02 | 1.81 | 1.08 | 0.70 |
| Young | WF-L | IPtg | 1030 | 254.5 | 21.62 | 9.62 | 2.57 | 0.97 | 0.74 | 0.59 | 0.46 |
| Young | WF-L | IPtg | 1080 | 255.0 | 13.48 | 5.02 | 1.65 | 0.96 | 0.71 | 0.57 | 0.42 |
| Young | WF-L | IPtg-SS2 | 1130 | 255.5 | 14.00 | 7.12 | 3.51 | 2.30 | 1.74 | 1.21 | 0.91 |
| Young | WF-L | IPbu | 1150 | 256.0 | 38.96 | 20.79 | 8.88 | 5.15 | 3.49 | 2.61 | 1.84 |
| Young | WF-L | IPgc | 1120 | 256.5 | 26.58 | 13.76 | 5.68 | 3.65 | 2.79 | 2.17 | 1.69 |
| Young | WF-L | IPgc | 1140 | 257.0 | 14.38 | 4.96 | 1.65 | 0.93 | 0.56 | 0.42 | 0.38 |
| Young | WF-L | IPgc | 1170 | 257.5 | 20.77 | 10.53 | 4.18 | 2.20 | 1.40 | 1.08 | 0.76 |
| Young | WF-L | IPtg | 1090 | 258.0 | 25.90 | 12.87 | 6.14 | 3.40 | 2.36 | 1.67 | 1.22 |
| Young | WF-L | IPtg | 1170 | 258.5 | 9.68 | 4.69 | 2.51 | 1.64 | 1.18 | 0.91 | 0.65 |
| Young | WF-L | IPhc | 1050 | 259.0 | 11.33 | 6.32 | 3.00 | 1.94 | 1.46 | 1.16 | 0.95 |
| Young | WF-L | IPhc | 1040 | 259.5 | 12.72 | 4.74 | 2.24 | 1.36 | 0.96 | 0.71 | 0.51 |
| Young | WF-L | IPhc | 1050 | 260.0 | 20.68 | 9.65 | 5.13 | 3.33 | 2.25 | 1.48 | 0.99 |
| Young | WF-L | IPk | 1050 | 260.5 | 16.75 | 5.89 | 2.31 | 1.49 | 1.09 | 0.81 | 0.62 |
| Young | WF-L | IPk | 1060 | 261.0 | 7.21 | 2.86 | 1.36 | 0.96 | 0.72 | 0.53 | 0.36 |
| Young | WF-L | IPhc | 1055 | 261.5 | 8.33 | 3.76 | 2.11 | 1.32 | 1.01 | 0.78 | 0.62 |
| Young | ABL | IPcc | 1045 | 262.0 | 15.67 | 6.98 | 2.87 | 1.61 | 1.19 | 0.92 | 0.69 |
| Young | ABL | IPcc | 1075 | 262.5 | 18.04 | 8.04 | 2.71 | 1.13 | 0.73 | 0.54 | 0.36 |
| Young | ABL | IPcc | 1075 | 263.0 | 11.95 | 7.60 | 4.64 | 2.96 | 2.03 | 1.39 | 0.96 |
| Young | ABL | IPcc | 1095 | 263.5 | 18.83 | 9.69 | 4.02 | 1.75 | 0.91 | 0.54 | 0.34 |
| Young | WF-L | IPr | 1085 | 264.0 | 21.60 | 8.91 | 3.74 | 2.16 | 1.43 | 0.96 | 0.64 |

Site B: Texas 16 between reference markers 450 and 488, Llano and Gillespie Counties, Austin District.

| | Geologic[2] atlas | Geologic | Elevation | Reference | ——— Normalized FWD deflection (mils) ——— | | | | | | |
|---|---|---|---|---|---|---|---|---|---|---|---|
| County | sheet | unit | (ft) | marker | W1 | W2 | W3 | W4 | W5 | W6 | W7 |
| Llano | LLN | pCps | 1065 | 450.0 | 12.46 | 8.53 | 5.12 | 3.10 | 1.96 | 1.28 | 0.87 |
| Llano | LLN | pCps | 1065 | 450.5 | 31.43 | 18.04 | 7.40 | 3.35 | 1.73 | 1.17 | 0.87 |
| Llano | LLN | pCps | 1070 | 451.0 | 31.74 | 14.01 | 4.38 | 2.21 | 1.49 | 1.09 | 0.87 |
| Llano | LLN | pCps | 1080 | 451.5 | 39.21 | 16.94 | 4.41 | 1.45 | 0.71 | 0.59 | 0.40 |
| Llano | LLN | pCy | 1090 | 452.0 | 38.15 | 13.81 | 2.14 | 0.77 | 0.48 | 0.32 | 0.23 |
| Llano | LLN | pCps | 1090 | 452.5 | 43.35 | 21.48 | 7.07 | 3.38 | 2.05 | 1.38 | 1.18 |
| Llano | LLN | pCy | 1130 | 453.0 | 36.55 | 15.32 | 4.43 | 2.10 | 1.39 | 1.07 | 0.83 |
| Llano | LLN | pCps | 1150 | 453.5 | 45.29 | 19.12 | 6.14 | 3.00 | 1.66 | 1.00 | 0.68 |
| Llano | LLN | pCps | 1270 | 456.0 | 58.23 | 30.11 | 12.00 | 6.05 | 3.55 | 2.28 | 1.52 |
| Llano | LLN | pCps | 1310 | 456.5 | 56.29 | 24.43 | 7.57 | 3.87 | 2.24 | 1.53 | 1.12 |
| Llano | LLN | pCps | 1320 | 457.0 | 33.66 | 15.25 | 4.90 | 2.21 | 1.26 | 0.84 | 0.63 |
| Llano | LLN | pCps | 1350 | 457.5 | 49.51 | 21.92 | 7.18 | 3.19 | 1.88 | 1.32 | 0.93 |
| Llano | LLN | pCps | 1390 | 458.0 | 37.32 | 17.49 | 5.60 | 2.87 | 1.78 | 1.24 | 0.91 |
| Llano | LLN | pCvs | 1390 | 458.5 | 46.97 | 23.85 | 8.79 | 4.22 | 2.44 | 1.64 | 1.25 |
| Llano | LLN | pCvs | 1360 | 459.0 | 40.06 | 17.10 | 5.29 | 1.99 | 0.91 | 0.58 | 0.39 |
| Llano | LLN | pCvs | 1310 | 459.5 | 10.83 | 3.63 | 1.46 | 0.91 | 0.57 | 0.41 | 0.28 |
| Llano | LLN | pCvs | 1270 | 460.0 | 40.86 | 18.53 | 5.81 | 3.16 | 2.08 | 1.49 | 1.12 |
| Llano | LLN | pCvs | 1270 | 460.5 | 18.28 | 7.57 | 2.99 | 1.62 | 1.01 | 0.77 | 0.55 |
| Llano | LLN | pCvs | 1230 | 461.0 | 19.85 | 8.65 | 2.98 | 1.71 | 1.19 | 0.94 | 0.71 |
| Llano | LLN | pCvs | 1200 | 461.5 | 36.86 | 15.26 | 4.42 | 2.11 | 1.33 | 0.96 | 0.65 |
| Llano | LLN | pCvs | 1210 | 462.0 | 34.72 | 14.37 | 5.01 | 2.37 | 1.33 | 0.80 | 0.60 |
| Llano | LLN | pCvs | 1160 | 462.5 | 46.25 | 22.70 | 7.47 | 2.74 | 1.27 | 0.76 | 0.65 |

[2] LLN=Llano

| | | | | | | | | | | | |
|---|---|---|---|---|---|---|---|---|---|---|---|
| Llano | LLN | pCtm | 1150 | 463.0 | 46.98 | 18.82 | 5.37 | 2.20 | 1.26 | 0.99 | 0.85 |
| Llano | LLN | pCtm | 1190 | 463.5 | 39.09 | 15.35 | 4.67 | 2.67 | 1.88 | 1.42 | 1.16 |
| Llano | LLN | pCtm | 1220 | 464.0 | 42.91 | 20.81 | 7.61 | 3.82 | 2.28 | 1.55 | 1.14 |
| Llano | LLN | pCtm | 1180 | 464.5 | 32.69 | 12.36 | 4.17 | 2.51 | 1.72 | 1.36 | 1.03 |
| Llano | LLN | pCtm | 1240 | 465.0 | 34.01 | 14.28 | 4.92 | 2.61 | 1.56 | 1.01 | 0.78 |
| Llano | LLN | pCtm | 1270 | 465.5 | 41.81 | 16.03 | 4.88 | 2.76 | 1.72 | 1.26 | 0.93 |
| Llano | LLN | pCtm | 1280 | 466.0 | 21.45 | 7.42 | 2.36 | 1.18 | 0.73 | 0.47 | 0.34 |
| Gillespie | LLN | pCtm | 1340 | 468.0 | 39.17 | 16.64 | 5.42 | 2.44 | 1.51 | 0.94 | 0.67 |
| Gillespie | LLN | pCtm | 1290 | 468.5 | 31.36 | 13.92 | 4.45 | 1.80 | 1.12 | 0.85 | 0.71 |
| Gillespie | LLN | pCtm | 1290 | 469.0 | 26.50 | 10.37 | 3.57 | 1.72 | 1.10 | 0.84 | 0.68 |
| Gillespie | LLN | pCps | 1300 | 469.5 | 19.26 | 6.53 | 2.24 | 1.53 | 1.08 | 0.72 | 0.45 |
| Gillespie | LLN | pCtm | 1330 | 470.0 | 16.39 | 5.49 | 0.85 | 0.80 | 0.70 | 0.47 | 0.35 |
| Gillespie | LLN | pCtm | 1380 | 470.5 | 44.85 | 16.51 | 5.12 | 2.93 | 1.85 | 1.32 | 0.90 |
| Gillespie | LLN | pCtm | 1460 | 471.0 | 23.89 | 9.74 | 3.10 | 1.71 | 1.10 | 0.92 | 0.69 |
| Gillespie | LLN | pCtm | 1580 | 471.5 | 23.51 | 7.78 | 2.32 | 1.38 | 0.93 | 0.63 | 0.46 |
| Gillespie | LLN | pCvs | 1690 | 472.0 | 36.28 | 18.64 | 6.92 | 3.34 | 2.15 | 1.63 | 1.29 |
| Gillespie | LLN | pCvs | 1800 | 472.5 | 61.17 | 28.29 | 8.58 | 3.95 | 2.74 | 2.24 | 1.80 |
| Gillespie | LLN | pCtm | 1770 | 473.0 | 27.74 | 11.29 | 4.15 | 1.98 | 1.23 | 0.93 | 0.73 |
| Gillespie | LLN | Kh | 1820 | 473.5 | 47.20 | 21.55 | 10.07 | 5.92 | 3.80 | 2.65 | 1.86 |
| Gillespie | LLN | Kh | 1760 | 474.0 | 36.24 | 16.40 | 7.54 | 4.17 | 2.40 | 1.40 | 0.89 |
| Gillespie | LLN | Crh | 1745 | 474.5 | 33.14 | 12.79 | 4.04 | 2.31 | 1.49 | 1.16 | 0.91 |
| Gillespie | LLN | Crh | 1730 | 475.0 | 39.57 | 16.30 | 5.90 | 3.11 | 2.03 | 1.49 | 1.21 |
| Gillespie | LLN | Crh | 1730 | 475.5 | 21.58 | 10.67 | 4.36 | 2.57 | 1.87 | 1.47 | 1.12 |
| Gillespie | LLN | Crh | 1760 | 476.0 | 26.84 | 10.50 | 4.25 | 2.50 | 1.65 | 1.24 | 0.96 |
| Gillespie | LLN | Crh | 1750 | 476.5 | 35.63 | 13.85 | 4.38 | 2.15 | 1.38 | 0.96 | 0.73 |
| Gillespie | LLN | Kh | 1800 | 477.0 | 27.70 | 12.07 | 4.16 | 1.90 | 1.18 | 0.80 | 0.63 |
| Gillespie | LLN | Kh | 1840 | 477.5 | 22.95 | 9.56 | 3.95 | 2.29 | 1.52 | 1.12 | 0.86 |
| Gillespie | LLN | Kh | 1850 | 478.0 | 28.62 | 14.55 | 5.75 | 2.94 | 1.91 | 1.49 | 1.16 |
| Gillespie | LLN | Kft | 1880 | 478.5 | 27.32 | 15.08 | 8.06 | 4.84 | 3.08 | 2.09 | 1.53 |
| Gillespie | LLN | Kft | 1920 | 479.0 | 29.93 | 16.09 | 6.39 | 3.00 | 1.48 | 0.80 | 0.51 |
| Gillespie | LLN | Kft | 1930 | 479.5 | 36.32 | 17.93 | 7.75 | 4.81 | 2.89 | 2.29 | 1.67 |
| Gillespie | LLN | Kh | 1840 | 480.0 | 29.34 | 10.74 | 3.69 | 2.39 | 1.96 | 1.61 | 1.22 |
| Gillespie | LLN | Kh | 1780 | 480.5 | 13.87 | 4.71 | 2.46 | 1.72 | 1.32 | 1.14 | 0.94 |
| Gillespie | LLN | Kh | 1780 | 481.0 | 29.94 | 12.65 | 5.53 | 3.10 | 1.98 | 1.43 | 1.03 |
| Gillespie | LLN | Kh | 1720 | 481.5 | 22.77 | 7.80 | 2.34 | 1.21 | 0.67 | 0.48 | 0.39 |
| Gillespie | LLN | Kh | 1710 | 482.0 | 79.12 | 30.76 | 9.31 | 5.08 | 3.09 | 2.25 | 1.75 |
| Gillespie | LLN | Qal | 1660 | 482.5 | 28.21 | 12.73 | 5.24 | 2.80 | 1.91 | 1.46 | 1.18 |
| Gillespie | LLN | Kh | 1660 | 483.0 | 34.69 | 17.41 | 6.17 | 3.10 | 2.06 | 1.64 | 1.36 |
| Gillespie | LLN | Kh | 1640 | 483.5 | 44.70 | 19.70 | 6.83 | 3.58 | 2.23 | 1.54 | 1.13 |
| Gillespie | LLN | Kh | 1650 | 484.0 | 48.20 | 22.38 | 9.02 | 4.92 | 3.00 | 2.08 | 1.73 |
| Gillespie | LLN | Kh | 1690 | 484.5 | 64.28 | 30.17 | 9.12 | 4.59 | 3.11 | 2.52 | 1.96 |
| Gillespie | LLN | Kh | 1770 | 485.0 | 64.20 | 30.43 | 10.53 | 4.84 | 2.80 | 1.93 | 1.38 |
| Gillespie | LLN | Kh | 1780 | 485.5 | 39.42 | 14.31 | 4.55 | 2.66 | 1.78 | 1.37 | 1.07 |
| Gillespie | LLN | Kh | 1720 | 486.0 | 4.67 | 2.11 | 1.30 | 0.90 | 0.72 | 0.59 | 0.45 |
| Gillespie | LLN | Kh | 1710 | 486.5 | 30.38 | 9.87 | 4.08 | 2.73 | 2.04 | 1.60 | 1.33 |
| Gillespie | LLN | Kh | 1710 | 487.0 | 24.12 | 12.16 | 4.09 | 1.76 | 1.12 | 0.87 | 0.69 |
| Gillespie | LLN | Kh | 1690 | 487.5 | 7.49 | 4.23 | 1.92 | 1.14 | 0.77 | 0.55 | 0.42 |

Site C: Texas 71 between reference markers 528 and 542, Burnet County, Austin District.

| County | Geologic[3] atlas sheet | Geologic unit | Elevation (ft) | Reference marker | Normalized FWD deflection (mils) W1 | W2 | W3 | W4 | W5 | W6 | W7 |
|---|---|---|---|---|---|---|---|---|---|---|---|
| Burnet | LLN | Oh | 1120 | 528.0 | 15.79 | 8.66 | 3.68 | 1.86 | 1.15 | 0.81 | 0.56 |
| Burnet | LLN | Oh | 1135 | 528.5 | 18.14 | 10.57 | 4.77 | 2.40 | 1.31 | 0.82 | 0.51 |
| Burnet | LLN | Oh | 1110 | 529.0 | 13.63 | 6.05 | 1.98 | 0.57 | 0.44 | 0.33 | 0.15 |
| Burnet | LLN | Og | 1100 | 529.5 | 16.36 | 9.31 | 3.83 | 1.77 | 0.98 | 0.68 | 0.53 |
| Burnet | LLN | Og | 1085 | 530.0 | 13.48 | 6.68 | 2.43 | 1.17 | 0.75 | 0.61 | 0.45 |
| Burnet | LLN | Oh | 1080 | 530.5 | 14.59 | 7.52 | 2.62 | 0.83 | 0.34 | 0.21 | 0.18 |

[3] LLN=Llano; AUS=Austin

| | | | | | | | | | | | |
|---|---|---|---|---|---|---|---|---|---|---|---|
| Burnet | LLN | Og | 1110 | 531.0 | 11.98 | 4.70 | 1.72 | 1.11 | 0.90 | 0.78 | 0.68 |
| Burnet | LLN | Oh | 1050 | 531.5 | 13.80 | 4.67 | 1.67 | 0.90 | 0.56 | 0.36 | 0.26 |
| Burnet | LLN | Oh | 1035 | 532.0 | 18.22 | 7.42 | 2.84 | 1.63 | 1.05 | 0.73 | 0.48 |
| Burnet | LLN | Oh | 1070 | 532.5 | 15.18 | 5.82 | 1.90 | 0.88 | 0.40 | 0.18 | 0.09 |
| Burnet | LLN | Kh | 1030 | 533.0 | 20.43 | 10.22 | 4.13 | 2.34 | 1.56 | 1.22 | 0.97 |
| Burnet | LLN | Oh | 970 | 533.5 | 20.48 | 9.06 | 3.22 | 1.47 | 0.69 | 0.42 | 0.29 |
| Burnet | LLN | Oh | 950 | 534.0 | 19.20 | 6.88 | 2.22 | 0.88 | 0.50 | 0.30 | 0.15 |
| Burnet | LLN | IPmf | 920 | 534.5 | 20.75 | 10.52 | 5.25 | 3.24 | 2.20 | 1.58 | 1.12 |
| Burnet | LLN | Oh | 960 | 535.0 | 14.35 | 4.24 | 1.69 | 1.23 | 0.99 | 0.83 | 0.70 |
| Burnet | LLN | Oh | 950 | 535.5 | 14.64 | 5.94 | 2.45 | 1.59 | 1.20 | 0.97 | 0.76 |
| Burnet | LLN | Oh | 1000 | 536.0 | 15.08 | 3.93 | 1.47 | 0.90 | 0.53 | 0.33 | 0.18 |
| Burnet | LLN | Oh | 970 | 536.5 | 10.17 | 2.55 | 1.06 | 0.67 | 0.46 | 0.33 | 0.22 |
| Burnet | LLN | Oh | 915 | 537.0 | 16.02 | 8.40 | 3.19 | 1.16 | 0.47 | 0.30 | 0.25 |
| Burnet | LLN | Qal | 880 | 537.5 | 11.43 | 4.75 | 2.25 | 1.33 | 0.80 | 0.49 | 0.30 |
| Burnet | LLN | Ksy | 870 | 538.0 | 27.09 | 13.61 | 6.02 | 3.47 | 1.87 | 1.77 | 1.42 |
| Burnet | LLN | Ksy | 850 | 538.5 | 27.40 | 14.29 | 7.00 | 4.21 | 2.94 | 2.06 | 1.59 |
| Burnet | LLN | Ksy | 820 | 539.0 | 35.96 | 16.85 | 7.51 | 4.34 | 2.83 | 1.93 | 1.50 |
| Burnet | LLN | Qal | 800 | 539.5 | 8.77 | 3.74 | 2.25 | 1.70 | 1.36 | 1.15 | 0.92 |
| Burnet | LLN | Kh | 840 | 540.0 | 11.02 | 3.69 | 1.53 | 0.91 | 0.60 | 0.43 | 0.31 |
| Burnet | LLN | Kh | 870 | 540.5 | 13.97 | 5.78 | 2.81 | 1.72 | 1.14 | 0.81 | 0.58 |
| Burnet | LLN | Kh | 900 | 541.0 | 8.76 | 4.15 | 2.33 | 1.54 | 1.09 | 0.80 | 0.62 |
| Burnet | LLN | Kgrl | 930 | 541.5 | 7.56 | 2.95 | 1.79 | 1.29 | 0.95 | 0.78 | 0.61 |
| Burnet | LLN | Kgru | 1060 | 542.0 | 20.25 | 6.90 | 1.48 | 0.48 | 0.30 | 0.29 | 0.28 |
| Burnet | LLN | Kgru | 1010 | 542.0 | 8.07 | 2.47 | 1.03 | 0.63 | 0.48 | 0.40 | 0.33 |

Site D: U.S. 290 between reference markers 536 and 563, Blanco and Hays Counties, Austin District.

| | Geologic[4] atlas | Geologic | Elevation | Reference | ———— Normalized FWD deflection (mils) ———— | | | | | | |
|---|---|---|---|---|---|---|---|---|---|---|---|
| County | sheet | unit | (ft) | marker | W1 | W2 | W3 | W4 | W5 | W6 | W7 |
| Blanco | LLN | Kgrl | 1260 | 536.0 | 9.26 | 3.56 | 1.21 | 0.74 | 0.52 | 0.40 | 0.34 |
| Blanco | LLN | Kgrl | 1250 | 536.5 | 13.05 | 5.73 | 2.78 | 2.12 | 1.43 | 0.89 | 0.72 |
| Blanco | LLN | Kgrl | 1220 | 537.0 | 9.21 | 3.26 | 1.14 | 0.60 | 0.40 | 0.31 | 0.23 |
| Blanco | LLN | Qal | 1180 | 537.5 | 10.42 | 4.62 | 2.22 | 1.25 | 0.86 | 0.64 | 0.52 |
| Blanco | LLN | Kgrl | 1180 | 538.0 | 11.78 | 4.63 | 1.73 | 1.04 | 0.78 | 0.58 | 0.45 |
| Blanco | LLN | Kgru | 1210 | 538.5 | 6.05 | 3.47 | 2.22 | 1.50 | 1.03 | 0.78 | 0.59 |
| Blanco | LLN | Kgru | 1230 | 539.0 | 11.27 | 5.67 | 2.52 | 1.38 | 0.87 | 0.65 | 0.46 |
| Blanco | LLN | Qal | 1120 | 539.5 | 15.85 | 7.56 | 3.45 | 1.94 | 1.25 | 0.90 | 0.68 |
| Blanco | LLN | Kgru | 1260 | 540.0 | 12.32 | 4.95 | 1.95 | 1.16 | 0.78 | 0.57 | 0.44 |
| Blanco | LLN | Kgrl | 1170 | 540.5 | 14.81 | 7.41 | 2.78 | 1.25 | 0.65 | 0.46 | 0.40 |
| Blanco | LLN | Kgrl | 1160 | 541.0 | 9.66 | 4.09 | 1.31 | 0.41 | 0.13 | 0.06 | 0.05 |
| Blanco | LLN | Kgru | 1220 | 541.5 | 14.78 | 4.86 | 1.60 | 0.94 | 0.71 | 0.56 | 0.49 |
| Blanco | LLN | Kgru | 1325 | 542.5 | 14.18 | 7.05 | 3.33 | 1.83 | 1.14 | 0.78 | 0.57 |
| Blanco | LLN | Kgru | 1330 | 543.0 | 14.27 | 8.08 | 4.27 | 2.55 | 1.67 | 1.20 | 0.84 |
| Blanco | LLN | Kgru | 1330 | 543.5 | 10.80 | 5.45 | 2.27 | 1.11 | 0.63 | 0.39 | 0.25 |
| Blanco | LLN | Kgru | 1360 | 544.0 | 11.26 | 5.10 | 2.14 | 1.20 | 0.81 | 0.65 | 0.48 |
| Hays | LLN | Kgru | 1360 | 546.0 | 9.25 | 4.60 | 1.65 | 0.75 | 0.54 | 0.43 | 0.33 |
| Hays | LLN | Kgru | 1380 | 546.5 | 8.67 | 4.53 | 2.23 | 1.45 | 1.09 | 0.86 | 0.67 |
| Hays | LLN | Kgru | 1340 | 547.0 | 7.09 | 2.69 | 0.70 | 0.34 | 0.26 | 0.21 | 0.18 |
| Hays | LLN | Kgru | 1320 | 547.5 | 9.42 | 4.30 | 1.45 | 0.44 | 0.15 | 0.09 | 0.07 |
| Hays | LLN | Kgru | 1360 | 548.0 | 12.58 | 5.97 | 2.27 | 1.14 | 0.77 | 0.55 | 0.43 |
| Hays | LLN | Kgru | 1300 | 548.5 | 8.74 | 3.91 | 1.28 | 0.60 | 0.43 | 0.34 | 0.30 |
| Hays | LLN | Kgru | 1320 | 549.0 | 9.97 | 5.19 | 2.58 | 1.66 | 1.28 | 1.05 | 0.87 |
| Hays | LLN | Kgru | 1330 | 549.5 | 13.26 | 6.56 | 2.52 | 1.25 | 0.73 | 0.48 | 0.29 |
| Hays | LLN | Kgru | 1300 | 550.0 | 9.04 | 3.39 | 1.22 | 0.63 | 0.47 | 0.29 | 0.22 |
| Hays | LLN | Kgru | 1290 | 550.5 | 12.90 | 7.05 | 2.82 | 1.31 | 0.78 | 0.59 | 0.50 |
| Hays | LLN | Kgru | 1300 | 551.0 | 12.10 | 5.66 | 2.04 | 0.79 | 0.34 | 0.18 | 0.11 |
| Hays | LLN | Kgru | 1280 | 551.5 | 7.44 | 3.29 | 1.28 | 0.76 | 0.54 | 0.43 | 0.36 |
| Hays | LLN | Kgru | 1290 | 552.0 | 15.00 | 7.87 | 3.15 | 1.37 | 0.73 | 0.53 | 0.41 |
| Hays | LLN | Kgru | 1245 | 552.5 | 10.91 | 4.87 | 1.84 | 1.08 | 0.74 | 0.53 | 0.40 |

[4] LLN=Llano; AUS=Austin

| | | | | | | | | | | | |
|---|---|---|---|---|---|---|---|---|---|---|---|
| Hays | LLN | Kgru | 1210 | 553.0 | 11.21 | 6.83 | 3.88 | 2.42 | 1.61 | 1.11 | 0.80 |
| Hays | LLN | Kgru | 1190 | 553.5 | 17.08 | 8.01 | 2.83 | 1.15 | 0.62 | 0.40 | 0.29 |
| Hays | LLN | Kgru | 1200 | 554.0 | 6.76 | 3.25 | 1.31 | 0.58 | 0.30 | 0.18 | 0.14 |
| Hays | LLN | Kgru | 1200 | 554.5 | 4.45 | 2.30 | 1.04 | 0.61 | 0.45 | 0.34 | 0.29 |
| Hays | LLN | Kgru | 1165 | 555.0 | 11.45 | 6.06 | 2.53 | 1.31 | 0.78 | 0.50 | 0.32 |
| Hays | LLN | Kgru | 1155 | 555.5 | 10.88 | 6.81 | 3.48 | 1.84 | 1.15 | 0.78 | 0.55 |
| Hays | LLN | Kgru | 1190 | 556.0 | 10.60 | 5.97 | 2.37 | 0.86 | 0.30 | 0.13 | 0.07 |
| Hays | LLN | Kgru | 1260 | 556.5 | 7.39 | 4.57 | 2.28 | 1.04 | 0.42 | 0.17 | 0.05 |
| Hays | LLN | Kgru | 1240 | 557.0 | 11.08 | 6.77 | 3.21 | 1.60 | 0.91 | 0.73 | 0.59 |
| Hays | LLN | Kgru | 1210 | 557.5 | 9.08 | 4.89 | 1.93 | 0.98 | 0.70 | 0.62 | 0.52 |
| Hays | LLN | Kgru | 1249 | 558.0 | 5.65 | 3.21 | 1.48 | 0.69 | 0.35 | 0.23 | 0.16 |
| Hays | LLN | Kgru | 1245 | 558.5 | 10.94 | 3.95 | 1.55 | 0.85 | 0.49 | 0.33 | 0.25 |
| Hays | LLN | Kgru | 1240 | 559.0 | 18.29 | 9.47 | 3.23 | 1.01 | 0.33 | 0.21 | 0.14 |
| Hays | LLN | Kgru | 1250 | 559.5 | 11.44 | 5.79 | 2.41 | 1.25 | 0.82 | 0.60 | 0.47 |
| Hays | LLN | Kgru | 1240 | 560.0 | 8.42 | 4.53 | 2.01 | 1.06 | 0.68 | 0.51 | 0.40 |
| Hays | LLN | Kft | 1244 | 560.5 | 7.84 | 4.69 | 2.14 | 1.02 | 0.54 | 0.35 | 0.25 |
| Hays | AUS | Kgru | 1195 | 561.0 | 7.86 | 4.17 | 1.57 | 0.78 | 0.56 | 0.46 | 0.42 |
| Hays | AUS | Kgru | 1205 | 561.5 | 5.45 | 3.05 | 1.21 | 0.59 | 0.37 | 0.26 | 0.21 |
| Hays | AUS | Kgru | 1173 | 562.0 | 18.62 | 6.32 | 1.88 | 1.10 | 0.71 | 0.47 | 0.37 |
| Hays | AUS | Kgru | 1180 | 562.5 | 11.59 | 5.44 | 1.81 | 0.98 | 0.71 | 0.56 | 0.45 |

Site E: Texas 71 between reference markers 590 and 598, Bastrop County, Austin District.

| | Geologic[5] atlas | Geologic | Elevation | Reference | Normalized FWD deflection (mils) | | | | | | |
|---|---|---|---|---|---|---|---|---|---|---|---|
| County | sheet | unit | (ft) | marker | W1 | W2 | W3 | W4 | W5 | W6 | W7 |
| Bastrop | AUS | Qt | 415 | 590.0 | 28.96 | 14.45 | 6.49 | 3.37 | 2.21 | 1.76 | 1.50 |
| Bastrop | AUS | Qt | 415 | 590.0 | 13.53 | 9.59 | 6.15 | 4.14 | 2.94 | 2.23 | 1.80 |
| Bastrop | AUS | Kknm | 460 | 590.5 | 22.80 | 14.02 | 8.10 | 5.21 | 3.81 | 3.05 | 2.52 |
| Bastrop | AUS | Kknm | 460 | 590.5 | 22.14 | 15.12 | 9.35 | 5.88 | 3.86 | 2.79 | 2.17 |
| Bastrop | AUS | Qt | 420 | 591.0 | 24.85 | 15.16 | 8.37 | 5.18 | 3.79 | 3.08 | 2.53 |
| Bastrop | AUS | Qt | 420 | 591.0 | 20.77 | 15.41 | 10.14 | 6.80 | 4.62 | 3.36 | 2.63 |
| Bastrop | AUS | Emi | 425 | 591.5 | 13.49 | 8.61 | 5.29 | 3.43 | 2.44 | 1.91 | 1.50 |
| Bastrop | AUS | Emi | 425 | 591.5 | 27.92 | 18.93 | 11.12 | 6.60 | 4.16 | 3.01 | 2.35 |
| Bastrop | AUS | Emi | 460 | 592.0 | 17.07 | 8.89 | 4.48 | 2.84 | 1.99 | 1.57 | 1.27 |
| Bastrop | AUS | Emi | 460 | 592.0 | 18.57 | 13.17 | 8.50 | 5.53 | 3.65 | 2.57 | 1.89 |
| Bastrop | AUS | Emi | 450 | 592.5 | 38.57 | 23.67 | 10.95 | 5.29 | 3.13 | 2.42 | 1.99 |
| Bastrop | AUS | Emi | 450 | 592.5 | 32.51 | 20.93 | 12.19 | 7.33 | 4.57 | 3.03 | 2.24 |
| Bastrop | AUS | Eh | 541 | 593.0 | 20.99 | 9.68 | 4.42 | 2.69 | 2.01 | 1.53 | 1.35 |
| Bastrop | AUS | Eh | 541 | 593.0 | 34.65 | 23.83 | 14.35 | 9.07 | 6.04 | 4.52 | 3.49 |
| Bastrop | AUS | Qhg | 568 | 593.5 | 17.01 | 8.06 | 4.08 | 2.65 | 1.95 | 1.57 | 1.28 |
| Bastrop | AUS | Qhg | 568 | 593.5 | 26.98 | 17.51 | 9.69 | 5.43 | 3.39 | 2.47 | 1.97 |
| Bastrop | AUS | Eh | 520 | 594.0 | 18.60 | 8.63 | 3.91 | 2.28 | 1.60 | 1.28 | 1.07 |
| Bastrop | AUS | Eh | 520 | 594.0 | 35.57 | 22.93 | 12.87 | 7.03 | 4.02 | 2.69 | 2.07 |
| Bastrop | AUS | Eh | 530 | 594.5 | 18.18 | 7.24 | 2.72 | 1.48 | 0.96 | 0.68 | 0.51 |
| Bastrop | AUS | Eh | 530 | 594.5 | 21.29 | 14.27 | 8.59 | 5.28 | 3.50 | 2.56 | 2.04 |
| Bastrop | AUS | Qhg | 560 | 595.0 | 23.25 | 8.24 | 2.98 | 1.57 | 1.14 | 1.01 | 0.88 |
| Bastrop | AUS | Qhg | 560 | 595.0 | 15.93 | 9.33 | 4.58 | 2.41 | 1.31 | 0.85 | 0.63 |
| Bastrop | AUS | Esb | 525 | 595.5 | 17.78 | 5.65 | 2.38 | 1.66 | 1.31 | 1.06 | 0.87 |
| Bastrop | AUS | Esb | 525 | 595.5 | 14.86 | 9.28 | 5.15 | 3.01 | 1.88 | 1.35 | 1.03 |
| Bastrop | AUS | Esb | 510 | 596.0 | 13.91 | 5.70 | 3.12 | 2.17 | 1.71 | 1.40 | 1.18 |
| Bastrop | AUS | Esb | 510 | 596.0 | 22.18 | 11.24 | 4.45 | 2.39 | 1.70 | 1.39 | 1.19 |
| Bastrop | AUS | Esb | 510 | 596.5 | 20.73 | 11.03 | 5.16 | 2.66 | 1.58 | 1.18 | 0.95 |
| Bastrop | AUS | Esb | 510 | 596.5 | 14.05 | 6.67 | 2.80 | 1.69 | 1.33 | 1.15 | 0.94 |
| Bastrop | AUS | Esb | 475 | 597.0 | 23.91 | 13.69 | 7.15 | 4.17 | 2.74 | 2.01 | 1.53 |
| Bastrop | AUS | Esb | 475 | 597.0 | 18.56 | 9.54 | 3.97 | 2.20 | 1.59 | 1.27 | 1.00 |
| Bastrop | AUS | Ecb | 430 | 597.5 | 14.57 | 8.22 | 3.76 | 1.79 | 0.95 | 0.61 | 0.47 |
| Bastrop | AUS | Ecb | 430 | 597.5 | 16.65 | 7.08 | 2.20 | 0.78 | 0.46 | 0.40 | 0.32 |
| Bastrop | AUS | Ecb | 430 | 598.0 | 13.50 | 5.11 | 3.11 | 2.13 | 1.53 | 1.15 | 0.90 |
| Bastrop | AUS | Ecb | 430 | 598.0 | 18.05 | 9.53 | 4.16 | 2.13 | 1.30 | 0.93 | 0.72 |

[5] AUS=Austin

Site F: Texas 16 between reference markers 758 and 804, Jim Hogg and Zapata Counties, Pharr District.

| County | Geologic[6] atlas sheet | Geologic unit | Elevation (ft) | Reference marker | Normalized FWD deflection (mils) W1 | W2 | W3 | W4 | W5 | W6 | W7 |
|---|---|---|---|---|---|---|---|---|---|---|---|
| Jim Hogg | LAR | Pg | 593 | 758.0 | 37.85 | 14.47 | 5.15 | 2.57 | 1.59 | 1.05 | 0.78 |
| Jim Hogg | LAR | Pg | 592 | 758.5 | 24.45 | 11.79 | 5.81 | 3.32 | 2.15 | 1.48 | 1.11 |
| Jim Hogg | LAR | Qs | 608 | 759.0 | 38.91 | 14.74 | 4.64 | 2.24 | 1.64 | 1.33 | 1.09 |
| Jim Hogg | LAR | Pg | 636 | 759.5 | 51.71 | 19.96 | 6.92 | 3.26 | 1.86 | 1.26 | 0.96 |
| Jim Hogg | LAR | Pg | 625 | 760.0 | 39.73 | 15.63 | 4.82 | 2.22 | 1.62 | 1.33 | 1.18 |
| Jim Hogg | LAR | Pg | 637 | 760.5 | 37.81 | 14.09 | 4.05 | 2.12 | 1.48 | 1.22 | 0.97 |
| Jim Hogg | LAR | Pg | 650 | 761.0 | 31.37 | 13.54 | 4.92 | 2.31 | 1.45 | 1.30 | 1.09 |
| Jim Hogg | LAR | Pg | 645 | 761.5 | 36.29 | 12.99 | 3.43 | 1.49 | 1.15 | 0.93 | 0.84 |
| Jim Hogg | LAR | Qs | 635 | 762.0 | 19.07 | 9.90 | 4.55 | 2.46 | 1.63 | 1.17 | 0.91 |
| Jim Hogg | LAR | Qs | 642 | 762.5 | 24.18 | 7.68 | 2.27 | 1.38 | 1.03 | 0.80 | 0.67 |
| Jim Hogg | LAR | Pg | 655 | 763.0 | 35.43 | 13.87 | 5.57 | 3.15 | 2.10 | 1.61 | 1.19 |
| Jim Hogg | LAR | Pg | 650 | 763.5 | 23.62 | 6.90 | 1.58 | 1.00 | 0.79 | 0.61 | 0.46 |
| Jim Hogg | LAR | Qs | 660 | 764.0 | 19.36 | 8.80 | 3.45 | 1.67 | 1.04 | 0.81 | 0.66 |
| Jim Hogg | LAR | Qs | 658 | 764.5 | 39.10 | 15.82 | 5.38 | 2.45 | 1.59 | 1.20 | 0.94 |
| Jim Hogg | LAR | Pg | 660 | 765.0 | 29.49 | 11.74 | 4.31 | 2.41 | 1.70 | 1.17 | 0.88 |
| Jim Hogg | LAR | Pg | 665 | 765.5 | 31.38 | 13.88 | 4.52 | 2.45 | 1.70 | 1.24 | 0.86 |
| Jim Hogg | LAR | Pg | 665 | 766.0 | 21.16 | 6.08 | 2.56 | 2.12 | 1.81 | 1.59 | 1.33 |
| Jim Hogg | LAR | Qs | 670 | 766.5 | 38.57 | 19.34 | 8.20 | 4.47 | 2.77 | 1.92 | 1.51 |
| Jim Hogg | LAR | Qs | 690 | 767.0 | 31.61 | 12.30 | 5.50 | 2.50 | 1.16 | 0.93 | 0.83 |
| Jim Hogg | LAR | Pg | 695 | 767.5 | 25.50 | 10.83 | 3.60 | 1.93 | 1.38 | 1.21 | 0.95 |
| Jim Hogg | LAR | Pg | 712 | 768.0 | 23.23 | 11.74 | 5.09 | 2.55 | 1.68 | 1.29 | 1.10 |
| Jim Hogg | LAR | Pg | 710 | 768.5 | 32.57 | 13.57 | 3.73 | 1.80 | 1.27 | 0.94 | 0.75 |
| Jim Hogg | LAR | Pg | 720 | 769.0 | 37.11 | 13.49 | 4.82 | 2.61 | 1.68 | 1.47 | 1.11 |
| Jim Hogg | LAR | Pg | 720 | 769.5 | 26.14 | 9.57 | 2.92 | 1.59 | 1.20 | 0.91 | 0.82 |
| Jim Hogg | LAR | Pg | 725 | 770.0 | 33.35 | 14.45 | 4.74 | 2.44 | 1.66 | 1.34 | 1.11 |
| Jim Hogg | LAR | Pg | 710 | 770.5 | 41.36 | 15.86 | 5.58 | 3.26 | 2.35 | 1.85 | 1.38 |
| Jim Hogg | LAR | Pg | 732 | 771.0 | 22.65 | 8.66 | 3.11 | 1.30 | 0.87 | 0.71 | 0.62 |
| Jim Hogg | LAR | Pg | 730 | 771.5 | 24.15 | 8.81 | 2.49 | 1.33 | 0.96 | 0.83 | 0.69 |
| Jim Hogg | LAR | Pg | 730 | 772.0 | 35.89 | 14.72 | 6.60 | 4.25 | 3.20 | 2.57 | 2.08 |
| Jim Hogg | LAR | Pg | 750 | 772.5 | 34.49 | 10.92 | 2.44 | 1.28 | 1.01 | 0.77 | 0.66 |
| Jim Hogg | LAR | Pg | 750 | 773.0 | 31.19 | 15.46 | 6.31 | 3.22 | 2.50 | 1.95 | 1.72 |
| Jim Hogg | LAR | MOcf | 710 | 773.5 | 50.12 | 22.56 | 5.80 | 2.42 | 1.47 | 1.24 | 0.85 |
| Jim Hogg | LAR | MOcf | 690 | 774.0 | 41.04 | 16.33 | 5.31 | 2.97 | 2.09 | 1.57 | 1.32 |
| Jim Hogg | LAR | MOcf | 680 | 774.5 | 36.20 | 12.46 | 4.09 | 2.38 | 1.83 | 1.51 | 1.28 |
| Jim Hogg | LAR | MOcf | 673 | 775.0 | 38.67 | 16.60 | 6.77 | 4.25 | 3.25 | 2.56 | 2.05 |
| Jim Hogg | LAR | MOcf | 660 | 775.5 | 39.51 | 14.45 | 4.83 | 3.18 | 2.47 | 1.97 | 1.64 |
| Jim Hogg | LAR | MOcf | 630 | 776.0 | 50.34 | 23.38 | 10.57 | 6.47 | 4.60 | 3.49 | 2.61 |
| Jim Hogg | LAR | MOcf | 625 | 776.5 | 33.67 | 13.31 | 5.57 | 3.46 | 2.51 | 2.05 | 1.69 |
| Jim Hogg | LAR | MOcf | 615 | 777.0 | 48.38 | 20.65 | 7.48 | 4.42 | 3.19 | 2.45 | 2.01 |
| Jim Hogg | LAR | MOcf | 605 | 778.0 | 43.69 | 17.36 | 6.38 | 4.05 | 3.03 | 2.16 | 1.89 |
| Jim Hogg | LAR | MOcf | 590 | 778.5 | 33.57 | 10.41 | 3.06 | 1.97 | 1.60 | 1.25 | 1.09 |
| Zapata | LAR | MOcf | 580 | 780.0 | 53.23 | 23.18 | 7.54 | 3.91 | 2.76 | 2.00 | 1.74 |
| Zapata | LAR | MOcf | 550 | 780.5 | 32.88 | 14.92 | 5.58 | 3.41 | 2.50 | 2.04 | 1.79 |
| Zapata | LAR | Ej | 540 | 781.0 | 42.57 | 18.45 | 6.54 | 4.81 | 3.67 | 2.76 | 1.91 |
| Zapata | LAR | Ej | 525 | 781.5 | 77.57 | 30.89 | 8.40 | 4.16 | 2.97 | 2.08 | 1.55 |
| Zapata | LAR | Ej | 510 | 782.0 | 70.54 | 29.08 | 10.78 | 5.77 | 4.03 | 3.23 | 2.38 |
| Zapata | LAR | Ej | 495 | 782.5 | 47.39 | 16.21 | 5.24 | 3.06 | 2.19 | 1.62 | 1.43 |
| Zapata | LAR | Ej | 490 | 783.0 | 81.08 | 26.87 | 7.44 | 4.75 | 3.48 | 2.80 | 2.29 |
| Zapata | LAR | Ej | 480 | 783.5 | 68.91 | 29.00 | 10.06 | 5.55 | 3.85 | 3.01 | 2.31 |
| Zapata | LAR | Ej | 495 | 784.0 | 84.44 | 36.97 | 13.51 | 6.92 | 4.80 | 3.53 | 2.59 |
| Zapata | LAR | Ej | 530 | 784.5 | 46.79 | 18.27 | 6.75 | 4.15 | 2.88 | 2.09 | 1.69 |
| Zapata | LAR | Ej | 505 | 785.0 | 32.03 | 11.43 | 3.89 | 2.07 | 1.58 | 1.23 | 1.04 |

[6] LAR=Laredo; MC-B=McAllen–Brownsville

| | | | | | | | | | | | |
|---|---|---|---|---|---|---|---|---|---|---|---|
| Zapata | LAR | Ej | 505 | 785.5 | 45.01 | 17.81 | 5.75 | 3.62 | 2.69 | 2.08 | 1.72 |
| Zapata | LAR | Ej | 490 | 786.0 | 66.59 | 33.35 | 12.03 | 6.26 | 4.38 | 3.09 | 2.57 |
| Zapata | LAR | Ej | 500 | 786.5 | 49.23 | 15.99 | 5.73 | 3.80 | 2.49 | 2.24 | 1.78 |
| Zapata | LAR | Ej | 505 | 787.0 | 78.71 | 35.22 | 11.19 | 5.85 | 4.01 | 3.14 | 2.41 |
| Zapata | LAR | Ej | 503 | 787.5 | 28.59 | 13.50 | 5.41 | 3.02 | 2.77 | 1.89 | 1.62 |
| Zapata | LAR | Ej | 495 | 788.0 | 52.83 | 28.17 | 11.11 | 6.42 | 4.06 | 3.17 | 2.69 |
| Zapata | LAR | Ej | 485 | 788.5 | 25.85 | 13.09 | 3.68 | 3.08 | 2.59 | 2.46 | 1.55 |
| Zapata | LAR | Ej | 465 | 789.0 | 46.81 | 19.35 | 6.97 | 3.54 | 2.36 | 1.84 | 1.52 |
| Zapata | LAR | Ej | 475 | 789.5 | 54.11 | 24.58 | 7.49 | 3.49 | 2.55 | 1.65 | 1.42 |
| Zapata | LAR | Ej | 490 | 790.0 | 27.40 | 16.09 | 7.66 | 4.01 | 2.68 | 2.01 | 1.52 |
| Zapata | LAR | Ej | 475 | 790.5 | 21.71 | 13.43 | 6.70 | 3.84 | 2.63 | 1.92 | 1.58 |
| Zapata | LAR | Ej | 465 | 791.0 | 22.71 | 13.64 | 6.63 | 3.67 | 2.48 | 1.83 | 1.45 |
| Zapata | LAR | Ej | 455 | 791.5 | 20.10 | 14.18 | 8.23 | 4.90 | 3.10 | 2.17 | 1.72 |
| Zapata | LAR | Ej | 450 | 792.0 | 41.24 | 21.83 | 10.30 | 5.39 | 3.48 | 2.51 | 1.72 |
| Zapata | MC-B | Ej | 450 | 792.5 | 22.81 | 14.24 | 6.61 | 3.59 | 2.45 | 1.88 | 1.49 |
| Zapata | MC-B | Ej | 420 | 793.0 | 15.03 | 9.83 | 5.76 | 3.30 | 1.99 | 1.35 | 1.07 |
| Zapata | MC-B | Ej | 420 | 793.5 | 14.21 | 8.23 | 4.06 | 2.56 | 1.89 | 1.48 | 1.05 |
| Zapata | MC-B | Ej | 400 | 794.0 | 21.40 | 12.58 | 5.53 | 3.21 | 2.40 | 1.94 | 1.58 |
| Zapata | MC-B | Ej | 380 | 794.5 | 12.71 | 7.17 | 2.96 | 1.57 | 1.13 | 0.95 | 0.81 |
| Zapata | MC-B | Ej | 365 | 795.0 | 23.47 | 13.56 | 6.84 | 4.30 | 3.39 | 2.70 | 1.82 |
| Zapata | MC-B | Qal | 335 | 795.5 | 17.41 | 11.65 | 6.69 | 4.07 | 2.71 | 1.95 | 1.55 |
| Zapata | MC-B | Qal | 340 | 796.0 | 29.66 | 17.75 | 8.60 | 4.93 | 3.39 | 2.51 | 2.01 |
| Zapata | MC-B | Ej | 365 | 796.5 | 25.95 | 15.55 | 8.60 | 5.44 | 3.86 | 2.91 | 2.37 |
| Zapata | MC-B | Ej | 380 | 797.0 | 25.58 | 16.25 | 7.79 | 4.23 | 2.86 | 2.07 | 1.69 |
| Zapata | MC-B | Qs | 390 | 797.5 | 27.27 | 18.08 | 9.81 | 5.29 | 3.33 | 2.55 | 2.08 |
| Zapata | MC-B | Ey | 380 | 798.0 | 28.26 | 17.52 | 8.40 | 4.54 | 2.90 | 2.08 | 1.65 |
| Zapata | MC-B | Qs | 350 | 798.5 | 7.83 | 4.30 | 2.42 | 1.70 | 1.30 | 1.04 | 0.89 |
| Zapata | MC-B | Qs | 340 | 799.0 | 12.83 | 8.76 | 4.99 | 3.05 | 2.28 | 1.68 | 1.24 |
| Zapata | MC-B | Qs | 335 | 799.5 | 13.96 | 9.51 | 5.74 | 3.20 | 2.00 | 1.41 | 1.04 |
| Zapata | MC-B | Qs | 335 | 800.0 | 22.40 | 15.69 | 8.51 | 4.85 | 3.21 | 2.38 | 1.87 |
| Zapata | MC-B | Qs | 360 | 800.5 | 10.09 | 5.70 | 2.75 | 1.78 | 1.27 | 0.95 | 0.75 |
| Zapata | MC-B | Qs | 410 | 801.0 | 6.66 | 4.00 | 2.41 | 1.68 | 1.27 | 0.93 | 0.72 |
| Zapata | MC-B | Ey | 390 | 801.5 | 9.53 | 5.60 | 3.25 | 2.19 | 1.66 | 1.33 | 1.10 |
| Zapata | MC-B | El | 385 | 802.0 | 11.47 | 7.06 | 3.64 | 2.08 | 1.39 | 1.02 | 0.85 |
| Zapata | MC-B | El | 390 | 802.5 | 11.97 | 7.84 | 4.30 | 2.65 | 1.89 | 1.52 | 1.23 |
| Zapata | MC-B | El | 380 | 803.0 | 21.66 | 15.13 | 8.17 | 4.29 | 2.38 | 1.41 | 1.06 |
| Zapata | MC-B | El | 370 | 803.5 | 40.87 | 26.44 | 13.63 | 7.83 | 5.14 | 3.83 | 3.00 |